Three-phase Resonant DC-link Converter

Munk-Nielsen, Stig

Publication date:
1997

Document Version
Publisher's PDF, also known as Version of record

Three Phase Resonant DC Link Converters

Analysis, Realization and Test

Ph.D. Thesis, report no. 2/2

by
Stig Munk-Nielsen
April 1997

AALBORG UNIVERSITY
INSTITUTE OF ENERGY TECHNOLOGY

DEPARTMENT OF ELECTRICAL ENERGY
CONVERSION , DENMARK

Three Phase Resonant DC Link Converters
Analysis, Realization and Test

ISBN 87-89179-16-1 (kpl.)

Published by Instituite of Energy Technology
Aalborg University

Printed by Kopicentralen, Aalborg University

Distribution Institute of Energy Technology
Aalborg University
Pontoppidansstræde 101
DK-9220 Aalborg Øst

Phone: +45 96 35 80 80
Fax: +45 98 15 14 11

Abstract

The purpose of the project is to develop a three-phase resonant converter suitable for standard speed drives. The motivation for working with resonant converters is found in the problems of the standard converter type used today.

In standard converter type Pulse Width Modulated-Voltage Source Inverter, PWM-VSI, the switches are subject to high current and voltage stress during switching, which causes losses. The fast switching of modern switches reduces switching losses. Unfortunately this produces increased dv/dt and the size of the input/output filters of the PWM-VSI must be increased. The high speed of the switches cannot be fully utilized.

By using a parallel resonant converter the switching happens at low or zero voltage which reduces switch losses. The dv/dt is controlled by the resonant circuit, and it is therefore reduced significantly. The perspective using a resonant converter is high switching frequency combined with a high converter efficiency and low dv/dt.

In the first report several resonant converters are investigated to find a resonant converter that can compete with the standard PWM-VSI converter. Four converters were selected for the theoretical analysis, and the converters are simulated. An evaluation of the resonant converters is made, and one converter is selected for realization.

In the second report the realization of the selected resonant converter is described. This includes analysis, design and test of the converter.

A new control principle, using no additional power electric components, is eliminating the high voltage peaks associated with the resonant circuit. The resonant link voltage peaks are limited below 2.1 times the DC link voltages.

A new principle eliminating former resonant converter stability problems are proposed, implemented and tested. A resonant converter efficiency of 97 [%] was measured. The low dv/dt of the converter makes it possible to drive long cables without filtering. A successful test with a 300 [m] long cable and an induction machine load was carried out.

It is concluded that a stable, high efficiency and high switching frequency three phase parallel resonant converter is realized.

Preface

This report is the second of two reports which are the basis in my attempt to obtain the Ph.D. degree. The reports are a part of the project named 'Resonans Konverter for Elektrisk Energi-omformning' initiated February 1, 1993 and ended April 7, 1997.

The project is financed by the 'Danish Technical Research Council' and also in part by the foundation 'Det Obelske Familiefond'. The project is carried out at Aalborg University, Institute of Energy Technology (IET).

During writing several people have contributed to the report. Four supervisors followed the project and they have made an invaluable contribution, they are Head of Institute, Associate Professor John K. Pedersen and Associate Professor, Ph.D. Frede Blaabjerg from the Institute of Energy Technology, IET and Ph.D. Paul Thøgersen and B.Sc. Ulrik Jæger from Danfoss Drives A/S. I would also like to thank Danfoss A/S who supported the project by a VLT 3008 frequency converter.

I stayed four memorable months in Aachen at 'Institut für Stromrichtertechnik und Elektriche Antribe', where Oscar Apeldoorn and Franz-F. Protiwa were a great source of inspiration, and I thank them and people at ISEA for the very pleasant visit.

At Aalborg University, I would like to thank all the people at IET. In particular all the Ph.D. students and research assistants for interesting discussions, and Birthe Johansen for general help with the text editing. Technician Walter Neumayer has done a lot of laboratory work. During the last phase student Jacob Buck was helping in the laboratory. A special thanks to Ph.D. Peter Nielsen, now employed by Danfoss, for interesting discussions and pleasant company.

Aalborg University April 1997

Stig Munk-Nielsen
M.Sc. EE.

Table of Contents

1

Introduction

In this chapter a recapitulation of the expected resonant converter properties is done. After that the aim of the report is described. Finally, the report structure is presented.

1.1 Recapitulation of expected resonant converter properties

The perspective of using the parallel resonant converter is low switching loss and low dv/dt in the output voltage. The importance of the two converter properties is discussed in the first report 'Three-Phase Resonant DC link Converters (Analysis and Simulation)'.

A significant drawback of the parallel resonant converter is the high link voltage peak /1/. In the first report a solution of this problem was a major issue. After study and comparison of several resonant converters the RDCLVPC converter was selected for realization. The converter is shown in Fig.1.1.

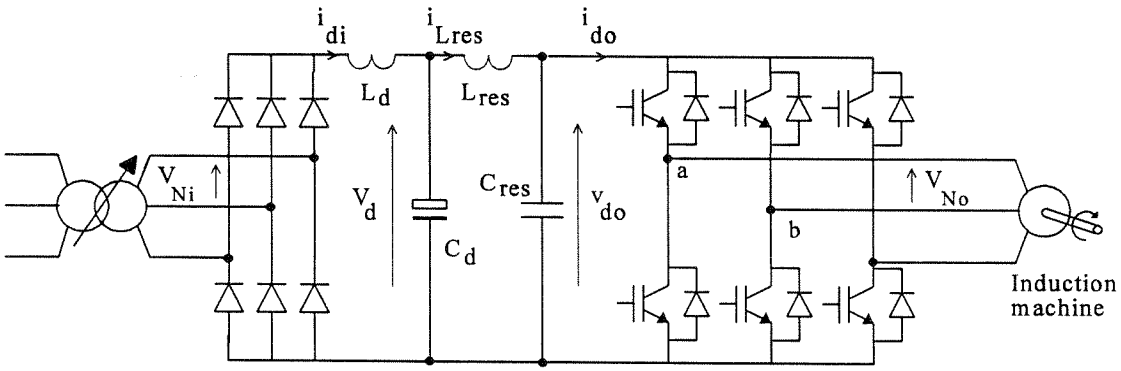

Fig. 1.1 Overall diagram of resonant converter worked with in this report

The RDCLVPC converter is able to control the voltage peak of v_{do} down to twice the DC link voltage without an additional clamp circuit and therefore there are used a minimum number of power electronic components. This is a new approach and it is described in /12/.

It is shown that the output voltage performance of the simulated RDCLVPC converter is almost identical to the RDCL converter proposed in /1/. The output voltage quality, with a resonant frequency of 50 [kHz], was similar to that of the PWM-VSI, with a switching frequency of 5 [kHz]. At a low modulation index the resonant converter is inferior. The results are concordant with results presented in /5/,/6/.

1.2 Aim of the report

In this second report analysis and the realization of the RDCLVPC converter is described, and experimental tests are carried out.

The aim is to realize a RDCLVPC converter and secondly measure the performance of the selected resonant converter. Since the RDCLVPC converter is an extension of the RDCL converter, the RDCL converter is also described.

There are several sub-aims of the report:

In the first report the link voltage peak control, VPC, principle is derived using idealized conditions. To improve the VPC control the influence of the converter loss elements and DC link current changes is incorporated in this report.

To build a converter which is able to opeate stable at higher DC link voltages than 500 [V].

Measuring the efficiency of the RDCLVPC and RDCL converter.

Test the resonant converter ability to drive a long cable and a motor.

1.3 Structure of the report

In the realization of the resonant converter there are three steps. The purpose of this structure is to split the realization of the converter into modules. This approach is useful when debugging the system. The same structure is used in the report. Chapter 3, chapter 4, and chapter 5 describes each one of the three realization stages for the resonant converter.
Fig. 1.2 illustrates the stages.

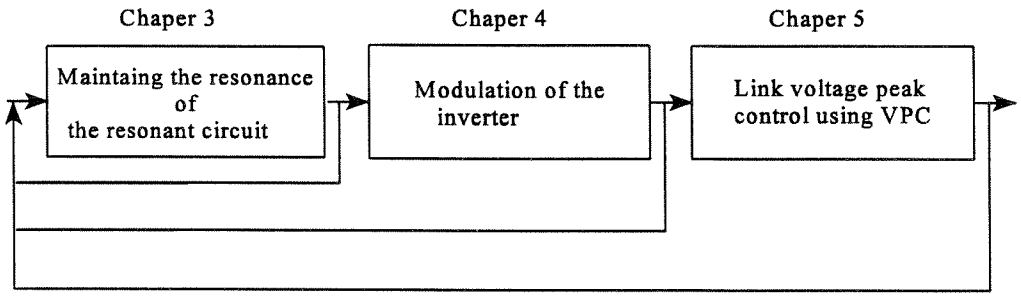

Fig. 1.2 Design stages of the RDCLVPC converter

In Fig. 1.2 there is a feed back from each of the realization stages, showing that the design of the converter had to be modified more than once to fulfill the aims of the project.

Chapter 2.

Converter specifications are given, and the presentation of the RDCLVPC converter is made, focusing on the proposed Voltage Peak Control, VPC. A selection of resonant circuit component values is done.

Chapter 3.

The implementation of the first loop shown in Fig. 1.2 is presented. The purpose is to maintain the resonance of the converter. Due to the need of high bandwidth this loop is realized in hardware. The resonant frequency of the converter is 41 [kHz].

Chapter 4.

Open loop control of the electrical machine is desired and varius modulators is analysed and one is selected. The modulator is implemented in software due to the great flexibility of software compared with hardware.

Chapter 5.

The VPC control strategy is able to limit the resonant peak voltage. The efficiency of the VPC is dependent on several parameters eg. link component loss and load current. Some parameters are changing dynamically, and this must be taken into account. A matematical model of the resonant converter is made and used to improve the resonant link voltage control.

Chapter 6.

Measured current and voltage curves of the realized RDCLVPC and RDCL converters are shown. The resonant converter efficiency is measured. A measurement of the loss distribution is made. Test of the resonant converter ability to drive a long cable and a motor is done.

Chapter 7.

Conclusions of the realization and tests of the resonant converters are summarised.

1.4 Conclusion

In this chapter a link to the work in the first report in the Ph.D. thesis is made. This second report is built on top of the results obtained in the first report. The first report focused on evaluation of results presented in litterature as well as analysis and simulation of converters. A new link voltage principle was proposed /12/ and a converter using this principle will now be realized. This second report concentrates on converter analysis, realization and experimental test.

2

Introduction to the RDCLVPC converter

In this chapter converter specifications are given, then a presentation of the RDCLVPC converter is made, focusing on the proposed Voltage Peak Control, VPC. A selection of resonant circuit component values is done and the VPC strategy ability to control the link voltage peak, with the selected resonant circuit components, is investigated.

2.1 Converter and load specifications

The power rating of the resonant converter is selected to be 9,7 [kVA] and the line voltage is 400 [V]. Key specifications are:

- DC link voltage V_d = 550 [V]
- Output phase current I_{NO} = 14 [A]
- Output phase-phase voltage V_{NO} = 400 [V]
- Output power S_{NO} = 9.7 [kVA]

The load used is an induction machine, MT 100 Lb 28-4 from ABB

- Phase current I_{NO} = 6.9 [A]
- Phase-phase voltage V_{NO} = 400 [V]
- Output power P_{NO} = 3.0 [kW] with load $\cos(\phi)$=0.8
- Speed n = 1430 [rmp]

Though this report two different DC link voltages a voltage of 300 [V] and one of 500 [V] for experimental test of the resonant converter is used. The hardware of the resonant converter changed during the development time and at first operation above 300 [V] was unstable. The problems and there solutions are going to be described. At the end there was no problems using a DC voltage of 500 [V] or higher. During the test is used a three phase transformator, in order to obtain galvanic isolation and a vario-transformer. In this setup the voltage was limitated to 500 [V] in order to maintain the voltage constant at all loads.

The IGBT used in the RDCLVPC converter must have a blocking voltage level that ensures a safety margin. The maximum peak voltage is ideally twice the DC link voltage. The DC link voltage changes due to line voltage variations and load changes including breaking energy. The selected IGBT module, MG30V2YS40, is a dual pack modul. For an ambient temperature of 25 [°] the characterisitics are:

- Collector-emitter voltage V_{ce} = 1700 [V]
- Collector current I_c = 30 [A]
- Saturation voltage V_{ce_sat} = 3.2 [V]

The IGBT's used are of NPT type.

2.2 Description of the RDCLVPC converter

A high level drawing of a VSI-PWM and the RDCLVPC converter are shown in Fig 2.1.

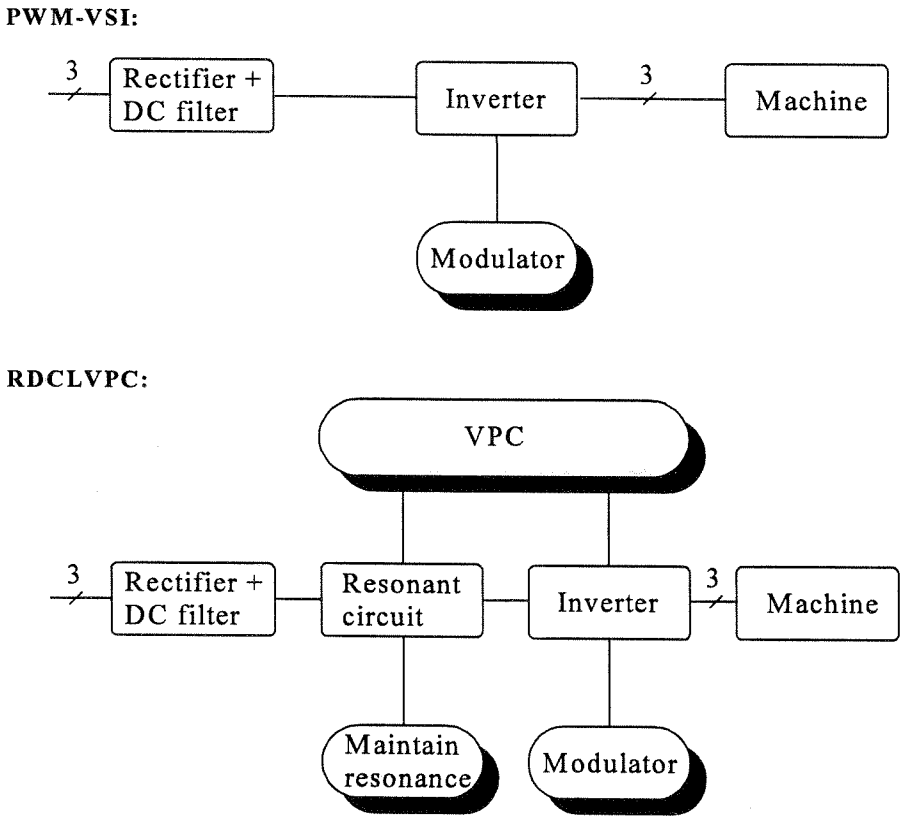

Fig. 2.1 Principal drawing of PWM-VSI and Resonant DC link converter, RDCLVPC

The PWM-VSI and RDCLVPC are shown to summarize the differences. In the main power flow path (square boxes) of the RDCLVPC is a resonant circuit. The basic function of the resonant circuit is to convert the input DC voltage into a sinusoidal AC voltage superimposed a DC voltage. Ideally the output voltage of the resonant circuit is oscillating between zero and twice the input DC voltage at a frequency typical around 1000 times the input line frequency. By turning the inverter switches off and on at zero, or low, voltage the switching losses are reduced compared with switching losses in the PWM-VSI.

Another alternative to reduce the switching losses in the PWM-VSI is by a snubber circuit, which is robust and simple to realize. Snubber circuits are designed to dissipate switching power in a resistor and the total losses are increased. The resonant circuit is ideally a non-dissipative circuit and therefore an interesting alternative to snubber circuits.

Using a resonant circuit introduces two major technical problems which must be overcome:

1: The voltage peaks of the resonant circuit depend on the link current and peak values significant above twice the DC voltage occur. The output voltage of the resonant circuit must be made undependable of the link current.

2: Maintain the resonance of the resonant link circuit even during transient error conditions must be possible. A robust resonance cycle is required.

Chapter three deal with the second problem and this is not discussed further in this chapter.

To solve the first problem the VPC strategy is proposed in the first Ph.D report. A detailed discussion in carried out in chapter 5, but the operation of the proposed VPC strategy is heavily influenced by the selection of the resonant circuit. The VPC strategy is therefore recapitulated here and a investigation of the resonant circuit values influence is done.

The resonant circuit consist of a inductor and capacitor in a low pass filter coupling. Shown in Fig. 2.2 is a equivalent circuit of the resonant converter.

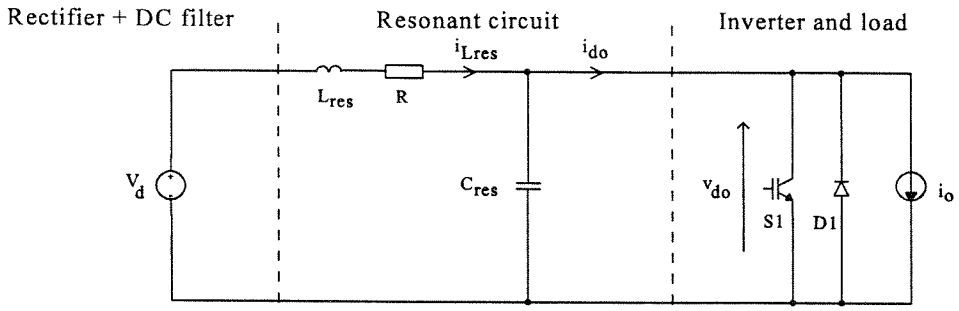

Fig. 2.2 Equivalent circuit of resonant converter.

A voltage peak higher than $2V_d$ is generated if the resonant inductor is suddenly discharged and the inductor discharge through the resonant capacitor. This situation is shown in Fig. 2.3a. A IGBT in the inverter is turning off and the link current abruptly changes amplitude. The following charge of the resonant capacitor is responsible for the high voltage peak. The high voltage peak can be prevented. By turning the IGBT off a short time before the zero DC link voltage condition the charge of the capacitor can be controlled. Turning the IGBT off at a link voltage level of ΔV_{do} causes the next resonant voltage peak to be twice the DC link voltage. The principle is illustrated in Fig 2.3b.

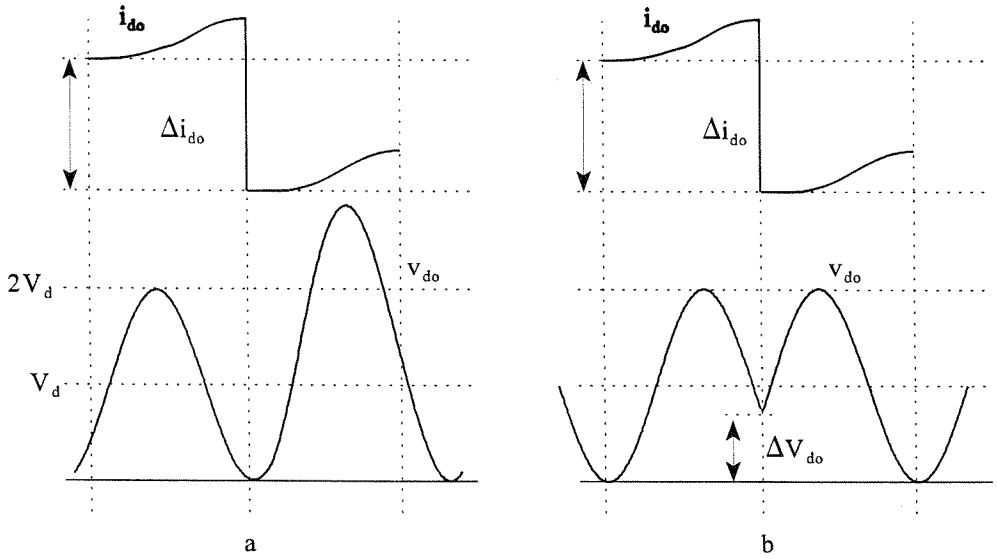

Fig. 2.3 DC link current, i_{do}, and link voltage, v_{do}.
a: resonant transition with no voltage control.
b: when the link voltage peak is controlled by VPC.

The VPC strategy used to control the resonant DC link voltage is derived in /12/, the strategy can be formulated in a simple eq. (2.1).

$$\Delta V_{do} = V_d \left(1 - \cos\left(\text{asin}\left(\frac{\Delta i_{do} Z_{res}}{2V_d}\right)\right)\right) \qquad \textbf{(2.1)}$$

V_d : DC link voltage.
Z_{res} : Resonant impedance = $\sqrt{L_{res}/C_{res}}$.
Δi_{do} : link current change.

The ΔV_{do} is the resonant voltage level where the DC link current must change, to make the next resonant voltage peak twice the DC link voltage.

2.3 Selection of resonant circuit component values

A first step in selection of resonant circuit component values L_{res} and C_{res} is to choose the resonant frequency, f_{res}. In the first report /12/ the resonant frequency was chosen to be 50 [kHz], because the resonant converter output voltage quality then is close to the 5 [kHz] PWM-VSI output voltage quality. A higher frequency increases the output voltage quality, but the demand to the bandwidth of the control circuit and inverter switches get also higher. The resonant frequency of 50 [kHz] is an initial selection, and experience will show if it has to be changed.

Selection of a resonant impedance is a difficult task. It is important that the resonant circuit eliminate the lossy switching of the PWM-VSI. However, the resonant circuit is not loss less and the switching loss of the inverter switches is also not loss less.
It is shown in /1/ that using an ideal circuit there is an optimum value of Z_{res}.

Design step 1 /1/:
An equation for Z_{res} which minimize resonant link loss, is derived in quite a similar way presented in /1/. The current through the resonant inductor in Fig. 2.2 assuming a idealized circuit is

$$i_{Lres} = I_{do} + \frac{V_d}{Z_{res}} \sin\left(2\pi \frac{1}{T_{res}} t\right) \qquad \textbf{(2.2)}$$

where
f_{res} : natural resonant frequency
I_{do} : average of DC link current i_{do}.
T_{res} : $1/f_{res}$

The average power dissipated in the resonant circuit is:

$$P = \frac{1}{T_{res}} \int_0^{T_{res}} R\, i_{Lres}^2 \, dt \qquad \textbf{(2.3)}$$

after integration and using Q = Z/R, R is equivalent resonant resistance, the equation for P is

$$P = \frac{Z_{res} I_{do}^2}{Q} + \frac{1}{2}\frac{V_d^2}{Z_{res} Q} \qquad \textbf{(2.4)}$$

It is conclude there is an optimum value of Z_{res} giving the lowest power dissipated in R. As expected the power losses decreases with a higher Q value. Since it is difficult to calculate the value of the equivalent resistor R, the Q factor is often determined by experiment. The process of designing the resonant inductor is therefore iterative. It is not within the scope of this report to design an optimum resonant circuit, the inductor is designed by F.F. Protiwa from University of Aachen.

The optimum value of Z_{res} is determined from eq. 2.4 to be

$$Z_{optimal} = \frac{1}{\sqrt{2}}\frac{V_d}{I_{do}} \qquad \textbf{(2.5.a)}$$

and the average link current, I_{do} is

$$I_{do} = \sqrt{3}\frac{V_{NO}}{V_d} I_{NO} \cos(\phi) \qquad \textbf{(2.5.b)}$$

The optimal impedance at a nominal load is $Z_{optimal} = 32$ [Ω] and this value is a minimum value because the I_{do} is a maximum value at nominal load current.

Design step 2:

Investigating the influence of resonant link impedance on the VPC strategy.

Using the voltage peak control, VPC, there is a restricted operation area in which control of the resonant link voltage peak is possible. The maximum link current change allowed is $\Delta i_{do} \leq 2V_d/Z_{res}$, the maximum ΔV_{do} is V_d.

It is decided that there should be a maximum limit of ΔV_{do} at normal operation. It must be ensured that for any Δi_{do} inside the normal operation area the limit of ΔV_{do} is not exceeded.

The maximum value of ΔV_{do} is a function of Δi_{do}, Z and V_d, refer to (2.1). The maximum value of ΔV_{do} should no be to high, since the inverter switches turn-off at this voltage. It is investigated if a limit of ΔV_{do} in the area of 100 [V].. 300 [V] is possible having a $Z_{res} = 32$ [Ω] and using the converter specifications shown in section 2.1.

The value of Δi_{do} is dependent on phase current level, switching strategy and load cos(ϕ). The link current change definition is

$$\Delta i_{do} = i_{o_{old}} - i_o \qquad \textbf{(2.6)}$$

and the link current is determined by the switching vector and the three phase currents

$$i_o = i_a s_a + i_b s_b + i_c s_c \qquad \textbf{(2.7)}$$

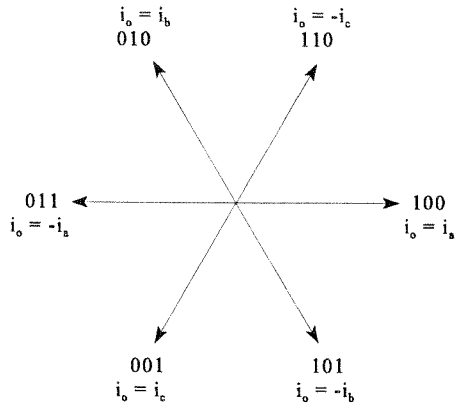

Fig. 2.3 Switching vector's in the complex plane.

The relationship between switching vector, phase current and link current, i_o, is shown in Fig. 2.3. There are six active switch vectors shown Fig. 2.3 and two zero vectors '000' and '111', which is not shown. The maximum Δi_{do} from a sequence of two vectors, beginning or ending with a zero vector is $\Delta i_{do}=\pm\sqrt{2}I_{NO}$. But a change between two active vectors can generate larger Δi_{do}.

From Fig. 2.3 is seen that a switch vector jump of 180 [°] generate a $\Delta i_{do} = i_a + i_a$, with the sequence '100' → '011'.

A general equation describing the Δi_{do} as function of the angle between switch vectors can be found in the following way.

In Fig. 2.4 are the possible states of the link current shown for every one of the active vectors, during 7/6 of a fundamental period. If the sequence '001' → '110' is used in the first 1/6 period, the link current would jump between the two thick lines. The maximum link current change Δi_{do}, is $2i_{c\_peak}$ This is the same result obtained earlier in the complex plane.

Jumping from one switch vector to another generate a Δi_{do} equal to the difference between two sinusoidal curves with a phase shift of α_s. The inverter limits the α_s values to $\alpha_s = \pm 60$ [°] or $\alpha_s = \pm 120$ [°] or $\alpha_s = \pm 180$ [°] or zero. The Δi_{do} is

$$\Delta i_{do} = \sqrt{2} I_{NO} \sin(\omega t) - \sqrt{2} I_{NO} \sin(\omega t - \alpha_s) \qquad \textbf{(2.8)}$$

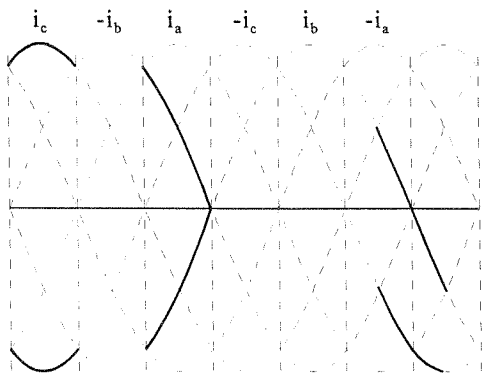

Fig. 2.4 Possible link current values assuming sinusoidal phase currents.

This is rewritten to

$$\Delta i_{do} = \sqrt{2} I_{NO} \cos(\omega t - \frac{\alpha_s}{2}) \sin(\frac{\alpha_s}{2}) \quad \textbf{(2.9)}$$

At steady state operation assuming sinusoidal phase current the maximum of Δi_{do} is

$$\Delta i_{do_{max}} = \sqrt{2} I_{NO} \sin(\frac{\alpha_s}{2}) \quad \textbf{(2.10)}$$

The Δi_{do} as function of Branch Switch Over, BSO is shown in Table 2.1. It is noticed that at 1 BSO is $\alpha_s = \pm$ 60 [°], at 2 BSO is $\alpha_s = \pm$ 120 [°] and at 3 BSO is $\alpha_s = \pm$ 180 [°].

Number of Branch Switch Over	1 BSO	2 BSO	3 BSO
$\frac{\Delta i_{do_{max}}}{\sqrt{2} I_{NO}}$	±1.0	$\pm\sqrt{3}$	±2.0

Table 2.1 Link current stress as a function of Branch Switch Over's.

The link current stress is reduced if the modulator restricts the switchings to changes between adjacent switching vectors that only generate one branch switch over. The eq. (2.10) can also be derived from the vectors shown in the complex plane Fig. 2.3. The result shown in Table 2.1 can also be found just by looking at Fig. 2.4. The thick lines in Fig. 2.4 show the results in Table 2.1.

The starting point of deriveing (2.10) was to the fact that the VPC strategy introduce a number of switchings at a voltage level of ΔV_{do}. The voltage level is dependend on Δi_{do}, Z_{res} and V_d, it is investigated if the selected converter data enables the VPC strategy to work at a low maximum value of ΔV_{do}.

With (2.10) and (2.1) it is now possible to calculate Z_{res} as function of ΔV_{do} and phase current I_{NO} and DC link voltage V_d. Assuming one BSO operation Z_{res} is:

$$Z_{res} = \sqrt{2} \frac{V_d}{I_{NO}} \sin(\text{acos}(1 - \frac{\Delta V_{max}}{V_d})) \quad \textbf{(2.11)}$$

where:

ΔV_{max} : maximum switching voltage of the inverter switches.

The Z_{res} impedance is calculated for values of I_{NO}=10 [A]..60 [A] and shown in Fig. 2.5.a. Three limits of ΔV_{do} were tried.

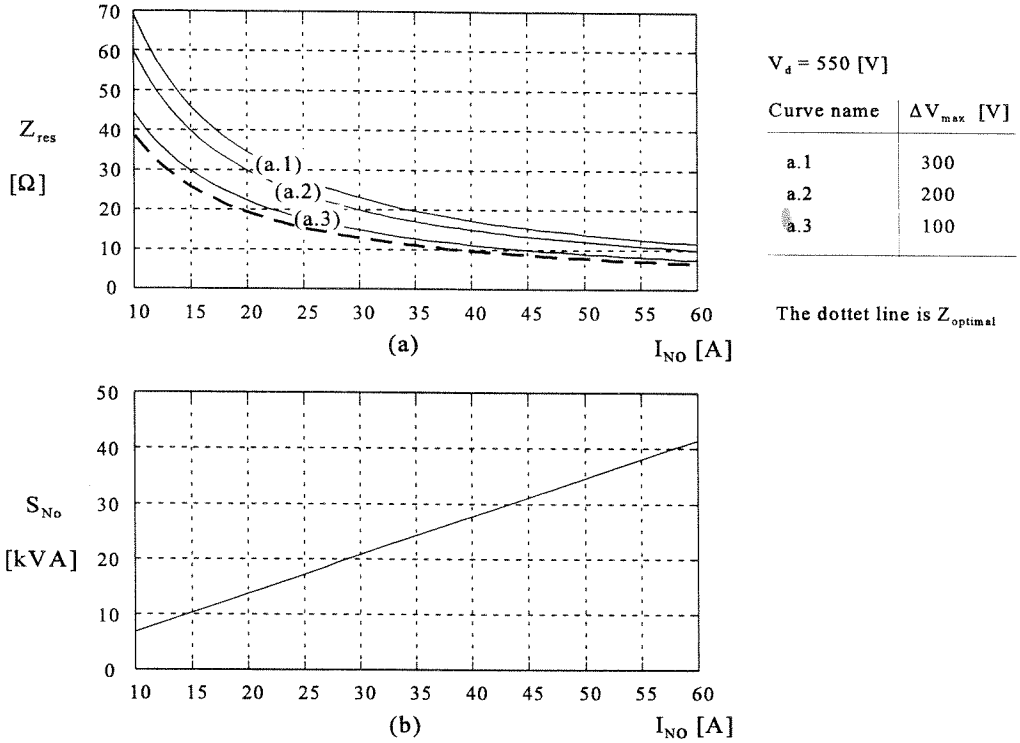

Fig. 2.5 **a)** The full lines are Z_{res} versus nominal phase current I_{NO}. The dotted line is $Z_{optimal}$ versus I_{NO}.

b) Apparent converter output power versus I_{NO}.

Previous in design step 1 there is found an optimal value of Z_{res}, eqn. (2.5) this value is plotted as an dotted line in Fig. 2.5.a.

The optimal value of Z_{res} is close to the Z_{res} values calculated under the assumption of a certain maximum turn-off voltage ΔV_{max}. This show that the application of the VPC strategy is realistic.

In Fig. 2.5.b is the apparent power plotted as function of nominal phase current I_{NO} in order to give an impression of apparent converter power and Z_{res}.

The investigation shows that a limit of ΔV_{do} in the area of 100 [V].. 300 [V] is not execced having a Z_{res} = 32 [Ω] at I_{NO} = 14 [A] and the converter specification showed in paragraph 2.1.

Resonant link component values:

The actual resonant inductor and resonant capacitor value used in the RDCLVPC is shown in Table 2.2. The values are based on experiment's. The Q value is equal to Z/R where R is the serial equivalent resistor of the resonant circuit. In R is included resistance in resonant inductor, resonant capacitor and DC link capacitor.

L_{res}	C_{res}	f_{res}	Q	Z_{res}
153 [μH]	100 [nF]	41 [kHz]	120	39 [Ω]

Table 2.2 Actual used resonant link circuit values in the three phase converter.

2.4 Conclusion

The Resonant DC Link Voltage Peak Controlled, RDCLVPC Converter is presented which is the introduction to a more deep description of the three main functions: maintaining the resonance, the modulation and the VPC control strategy.

A selection of resonant components is made based on design equations found in literature, the link current stress is investigated and it is concluded that jumps between active voltage vectors should only happen between adjacent active vectors in order to reduce link current stress.

Investigation of the VPC strategy ability to control the resonant link voltage is carried out. The VPC strategy has a limited operation range determined by DC link voltage, impedance and link current change values. In the reality the number of factors increases beyond the three mentioned, but that will be discussed later. Here is shown that the VPC strategy is able to control the resonant link voltage peak, and it is shown that for a fixed value of link voltage of 550 [V] and a maximum turn-off voltage of $\Delta V_d = 100$ [V] is the resonant impedance close to the optimum resonant impedance calculated in the design equation.

The conclusion is that the VPC strategy can control the resonant link voltage peak in the investigated converter power range of 7 [kVA] to 45 [kVA].

3

Maintaining the resonant link cycle of the RDCLVPC

In this chapter it is described how the resonance of the resonant circuit is kept on. At first sight the problem appears simple, after sometime one realizes this is wrong. The maintaining of the resonance is a key problem that must be solved. Proper operation of the resonance ensures zero or low voltage switching of the inverter switches. During a design procedure there are several things to consider:

1) How to initiate the resonance. This can be done in a rough or gentile way as described later.

2) The resonance must be error tolerant, this mean if an error occurs and the resonance is prevented to complete, the resonant circuit control must be able of restoring the resonance in the next resonant cycle. It is not acceptable that the whole converter stops because of electrical noise.

3) The resonant circuit stores reactive power and to keep resonant circuit losses low the level of reactive power must be kept at a low level.

4) Finally, the circuit that controls the resonance should be able of operating the converter at higher DC link voltages as 500 [V].

There are presented two methods. The first is published in patents and papers /1/,/25/. The principle of the method is simple, this is an advantage but realizing it is not without problems, unfortunate there are problems obtaining the four points mentioned above. The method is known as the short circuit method. The second method is proposed on the experience of working with the first described method. It is a bit more complex to describe theoretically than the short circuit method and it requires apparently a few extra components. Realizing the circuit takes a bit of work but compared with the short circuit method it is much simpler. There is worked approximately half a year with the short circuit method and with the second method it took only one week from idea to realization.

3.1 Short circuit method

The resonance is maintained by a short circuit interval of the inverter bridge, the short circuit interval ensures sufficient energy storage in the resonant inductor to overcome the circuit losses and therefore ensures the link voltage resonate to zero voltage next time interval.

The circuit that maintains the resonant cycle is shown in Fig. 3.1. When v_{do} reaches zero, the signal called ZVSI is generated. This signal triggers the beginning of the short circuit interval and this signal also triggers the read out of a new switch vector to the inverter. A link current measurement is used to detect when to turn-off the short circuit.

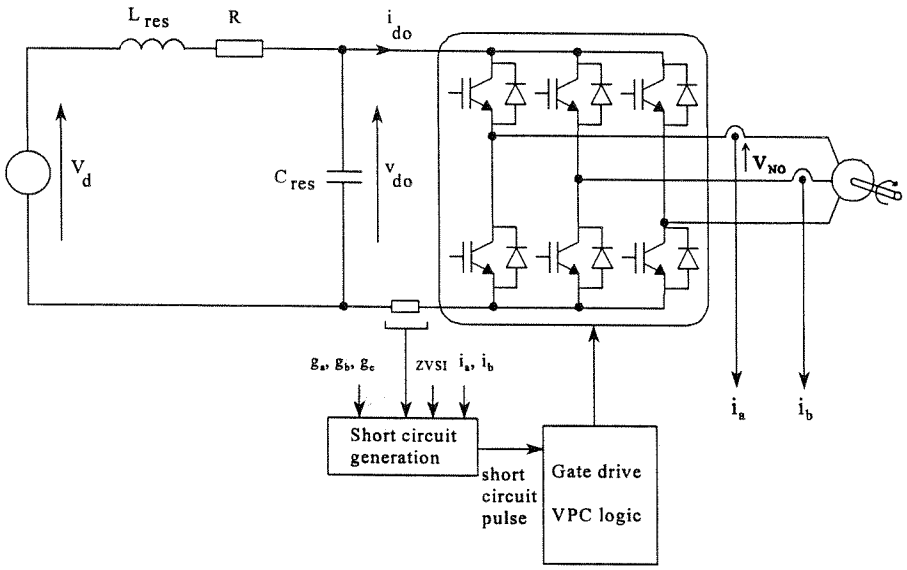

Fig. 3.1 The function of the 'Short circuit generation' box discussed.

The short circuit of the inverter bridge is done to ensure an increase of energy in the resonant inductor. A short circuit of the inverter is also used to start the resonance. Before the start up the resonant link voltage v_{do} is equal to the DC link voltage V_d. The inverter bridge is then short circuited, and the energy of the resonant capacitor is dissipated in the inverter switches and stray components. The switches are stressed, but since the short circuit duration is short, below 5 [μs], the switches are not destroyed.

To maintain the resonance is it necessary to compensate the energy change that decreases the resonant link energy, during a resonant cycle. If an energy compensation is not done, the resonant voltage does not oscillate back to zero. Several major loss elements are present in a resonant circuit, where the most significant are the serial resistance of the resonant inductor, the resonant capacitor and the DC-voltage capacitor. The total resistive losses are determined from an experiment /26/ where a measurement of succeeding resonant voltage amplitudes is used to determine the quality factor, Q. With the knowledge of Z_{res} the equivalent serial resistor is $R = Z_{res}/Q$. To compensate the losses in R the inverter bridge is short circuited during the zero voltage interval. The stored energy in the resonant inductor compensates the energy dissipation in R. In /27/ an equation is found which describes the level of current in L_{res} needed to overcome the resistor losses.

$$\Delta I_{Lres} = \sqrt{\frac{R\left(\frac{V_d}{Z_{res}}\right)^2}{f_{res}\, L_{res}}} \qquad (3.1)$$

3.2 Realization of the short circuit method

The short circuit of the resonant inverter is done by turning all the inverter switches on when the resonant link voltage v_{do} reaches zero voltage. During the first part of the short circuit period L_{res} is properly discharged and the antiparallel diode conducts. An equivalent circuit is shown in Fig. 3.2. After the resonant inductor is discharged, the current flow turns and a charging of the resonant inductor begin. The short circuit lasts until inductor current has increased to $\Delta I_{Lres} + i_o$. Since the beginning of the zero period is easily to detect, turning the short circuit on is straightforward, but the turn-off is more difficult.

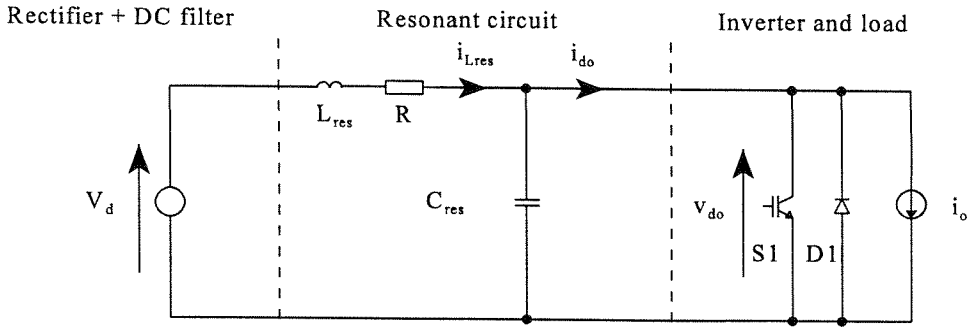

Fig. 3.2 Equivalent circuit of the resonant converter.

Several methods can be used to decide when to turn the short circuit off. A measurement of the resonant inductor current is the most direct way, but a high speed low inductance current shunt, is needed. In /13/ a method is using the on-state IGBT voltage drop and from this determine how long the IGBT's should be conducting is suggested. Implementing the method is relatively simple, but the accuracy of the method is not good due to the on-state voltage dependency on conducted current. With further investigations and improvements the method could be useful and preferable.

It is decided to use a direct current measurement method. The advantage of this method is better accuracy, but the implementation is quite complex. The short circuit turn-off can be determined by a measurement of the L_{res} current or link current, i_{do}. It seems natural to measure the inductor current i_{Lres} directly, but it was decided to use the current measurement in a protection circuit. A L_{res} current measurement is not as fast as an i_{do} current measurement since the resonant capacitor current is omitted. A measurement of the resonant link current i_{do} was selected to be used in the turn-off circuit.

The link current i_{do} is measured using a shunt resistor. During the short circuit period the current must increase to $i_{do} = \Delta I_{Lres} + i_o$. Notice, during a short circuit the inductor current i_{Lres} is identical to i_{do}. The value of i_o is determined from the switch vector and phase current value. The i_o is calculated using eq. (2.7). The bandwidth of the short circuit electronics must be high. Input and output from the short circuit generator are shown in Fig. 3.3.

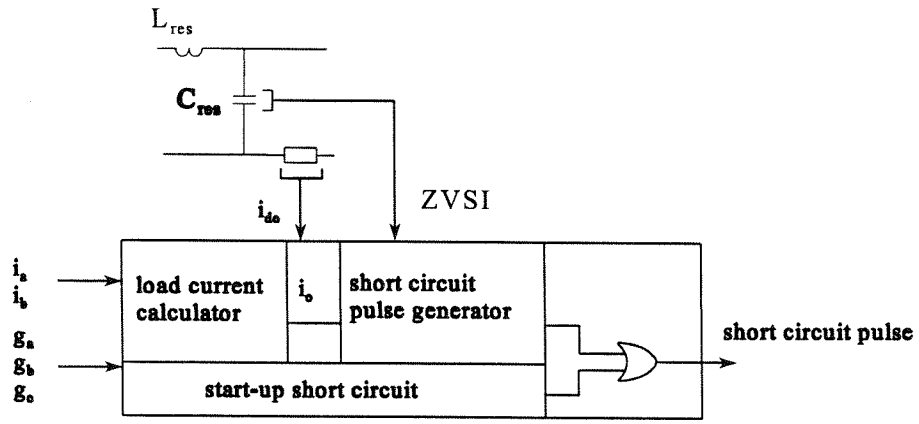

Fig. 3.3 A detailed view of the box named 'Short circuit generation' in Fig. 2.1.

The load current calculator circuit is shown in Fig. 3.4. It is working by converting two-phase currents into the six possible i_o current values, earlier shown in Fig. 2.4. By using a multiplexer controlled by the switch vector $S = [g_a\ g_b\ g_c]$, one of the six values is selected. The phase currents are measured using standard LEM hall-effect sensors. The six possible i_o current values are calculated using standard LM324 o-amps. The multiplexer and the o-amp, which works as a voltage follower, must be fast.

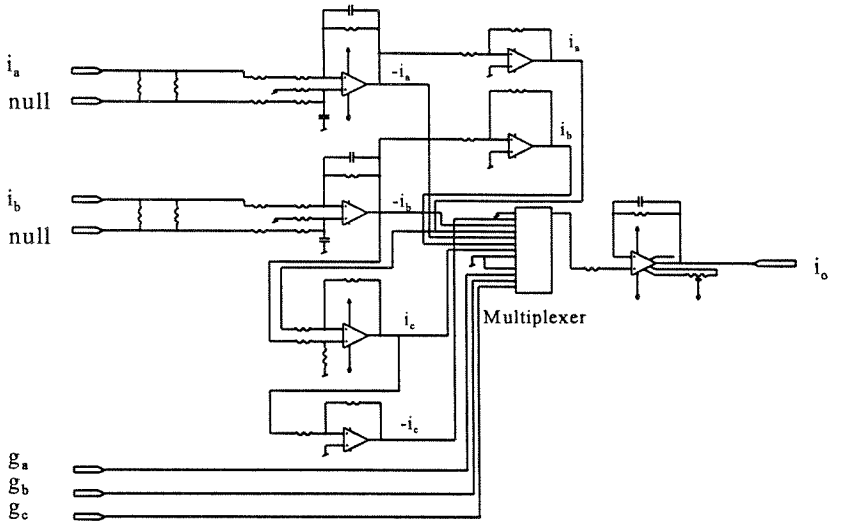

Fig. 3.4 Load current, i_o calculator

The short circuit pulse generator generating the short circuit pulse is shown in Fig. 3.5. From the zero voltage interval a pulse called ZVSI is generated. This pulse initiates the short circuit pulse, short_ZVS to a logic high state. Using two high speed o-amp's, Δi_{Lres} is calculated. After that Δi_{Lres} is compared with a reference value, ΔI_{Lres}. When Δi_{Lres} is increased beyond the reference value, ΔI_{Lres}, the short circuit is turned off.

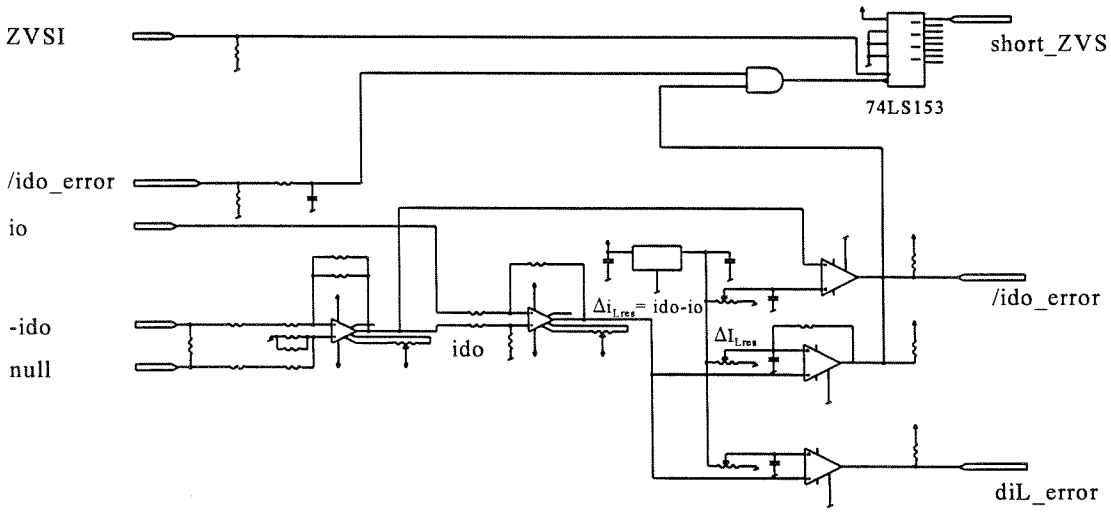

Fig. 3.5 Generation of short circuit signal short_ZVS.

The delay in the turn-off circuit cannot be ignored. The delay includes delays from the

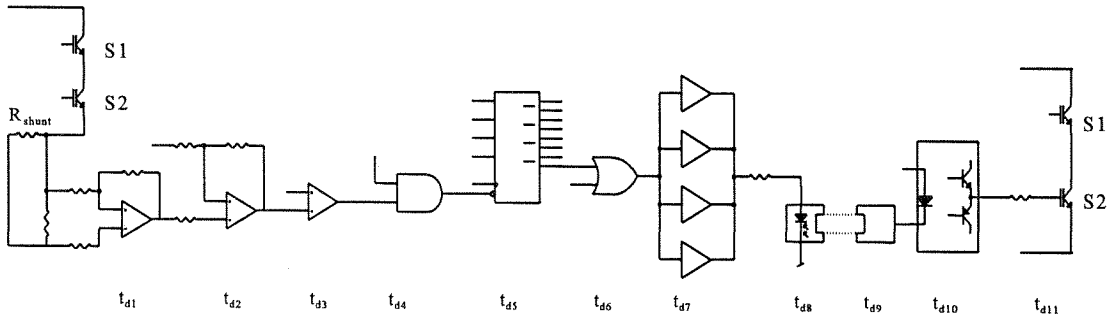

Fig. 3.6 Time delay in the short circuit control.

measurement of i_{do} to the IGBT collector current begins to decrease at turn-off. The delay is measured to $t_{delay} = 900$ [ns]@20[°C]. This value is dependent on many components and is a highly nonlinear value. The major single component delay is in the IGBT. In Table 3.1 the single delay values are shown. The values are found in data-sheets except for the IGBT where the delay, t_{d11}, was measured.

t_{d1}	t_{d2}	t_{d3}	t_{d4}	t_{d5}	t_{d6}	t_{d7}	t_{d8}	t_{d9}	t_{d10}	t_{d11}	$\Sigma=t_{delay}$
100	100	80	10	15	10	10	50	50	150	400	975 [ns]

Table. 3.1 Distribution of the total delay time t_{delay}, the optocupler, and the IGBT has the largest delay.The unit is [ns].

The theoretical ΔI_{Lres} must be compensated for the delay.
The current rate during the short circuit is V_d/L_{res} and the compensated ΔI_{Lres} is

$$\Delta I_{Lres} = \sqrt{\frac{R\left(\frac{V_d}{Z_{res}}\right)^2}{f_{res}\, L_{res}}} - \frac{V_d}{L_{res}} t_{delay} \qquad (3.2)$$

In the realized resonant converter the value of ΔI_{Lres} from eq. (3.2) is negative, the minimum possible reference current value is zero, and the short circuit interval is therefore increased. Consequently, the resonant inductor is charged beyond the level that compensates the resonant link losses.

Increased resonant inductor energy extends the zero voltage interval since the antiparallel diodes clamp the link voltage to zero until the resonant inductor is discharged and the current stress and link voltage peak increase. One problem is the delay time increases with the higher values of V_d.

The short circuit generation unit was first tested with a zero phase current reference and i_o was therefore zero. During the test a number of bugs were discovered and removed. After that, the test was carried out with a non-zero phase current reference and a particular problem arises. With i_o having a non-zero value the resonance of the converter would stop after some time of running. One way of partly solving the problem was to increase the reference ΔI_{Lres} value. But then the resonant voltage peak increases substantially beyond twice V_d, and the current stress and

the zero voltage period increase. The disadvantage of increasing ΔI_{Lres} is not acceptable.

The situation that causes the problem of loosing the converter resonance is discussed in the following paragraph.

An example where the resonant voltage does not resonate to zero is shown in Fig. 3.7. First thing to notice is that Δi_{Lres} is positive and higher than the reference ΔI_{Lres}. This is explained by looking at the measured link current i_{do} and the i_o current. The current i_o is determined using the circuit in Fig. 3.4. The circuit is quite fast and a change of switch vector state would result in a new value of i_o after a few tenth of nano seconds. The switch vector only changes when the resonant link voltage, v_{do} reaches zero. The change of the switch vector is triggered by the signal ZVSI.

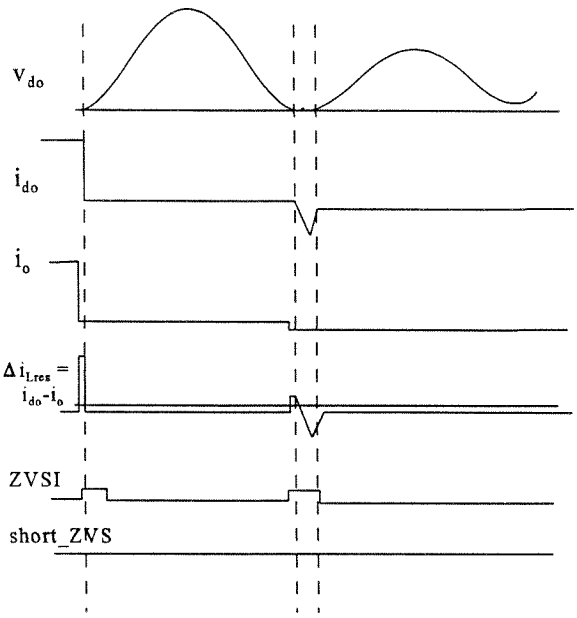

Fig. 3.7 A situation where the zero voltage interval is lost.

The change of i_o always happens before i_{do} changes, because the IGBT has a delay of several hundreds of nanoseconds. This is the explanation of Δi_{Lres} becoming positive in Fig. 3.7. Since Δi_{Lres} is positive, the inverter switches are not short circuited, which is seen on the short_ZVS signal that stays low. A positive Δi_{Lres} which is higher than the reference value of Δi_{Lres} indicates that there is enough energy in the resonant inductor at the beginning of a resonant period to ensure a zero voltage interval at the end of the resonant period. This is clearly seen in the left side resonant pulse shown in Fig. 3.7 But in the following resonant period there is a problem because v_{do} does not reach zero. Since the most left side link current changes in Fig. 3.7 leaves a relatively large amount of energy in the resonant inductor, the anti-parallel diodes begin to conduct at next zero voltage interval. This is unfortunately since the resonant inductor discharges totally, and there should be a short circuit period to charge the resonant inductor. The reason this does not happen is that Δi_{Lres} is positive when the short circuit should commence. As consequence there is no short circuit period. The problem is solved by turning the short circuit on always when a ZVSI signal is detected. The short circuit is turned on for a few hundred nanoseconds. This increases the link peak voltage and current stress, but it works better than an increase of ΔI_{Lres}.

The problem is explained more efficiently by a phase plane plots in Fig. 3.8. In Fig. 3.8.a there is no problem of maintaining the resonance $\Delta i_{o1} < \Delta i_{o2}$:

Going from i_{o1} to i_{o2} the energy of the resonant circuit increases, and the radius of the polar plot circles enhance. This is not explained in detail yet, but in chapter 5 a mathematical explanation is presented. Looking at Fig. 3.8 at the point marked 1. This is the initial conditions for the resonant period by going from i_{o2} to i_{o3}. At mark 1 there is initial conditions show that there is some initial energy in the resonant circuit. This energy is assumed lager than necessary to compensate the ohmic losses.

In Fig. 3.8.b there is also two step changes of i_{do}, but now $\Delta i_{o1} > \Delta i_{o2}$:

Going from i_{o1} to i_{o2} increases the energy of the resonant circuit, and the radius of the polar plot circles enhance as before. Going from i_{o2} to i_{o3} an unfortunate situation occurs. Measurements

of i_{do} and i_o shows that Δi_{Lres} is larger than ΔI_{Lres} just before the current change happens, therefore no short circuit is started. However there is not accounted for the stored resonant circuit energy, obtained going from i_{o1} to i_{o2}.

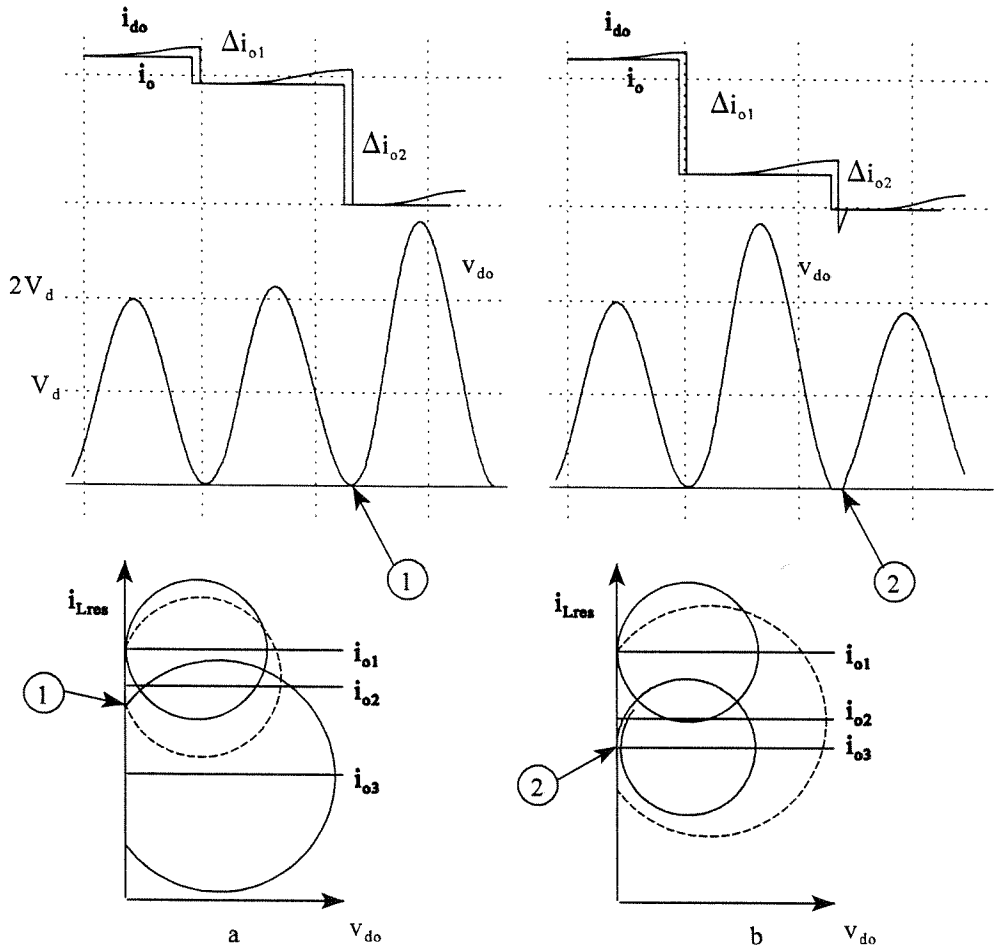

Fig. 3.8 Demonstrating the circumstances where the resonant circuit oscillation is lost.
a: There is sufficient energy to sustain the resonance.
b: At mark 2 control of the resonance is lost.

When the voltage v_{do} resonant down to zero voltage the stored energy in the resonant inductor is transferred to the V_d source. The initial condition for the current step from i_{o2} to i_{o3} is shown at mark 2. There is no energy stored in the resonant inductor, since the initial inductor current (i_{Lres}-i_{o3}) is zero. The following resonance period is not going to oscillate v_{do} to zero voltage since there is not enough energy to overcome the ohmic losses.

3.3 A laboratory test of the short circuit method

A lot of time is spent in the laboratory to realize the short circuit method, particular time consuming was the debugging of the circuit. It was made difficult due to the strong influence of

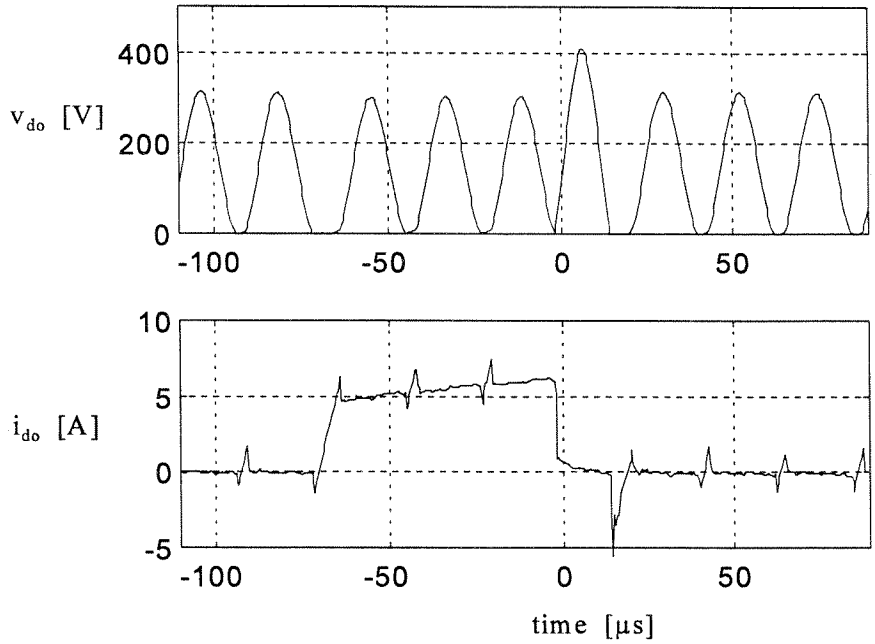

Fig. 3.9 Measured resonant link voltage and current. The resonance is maintained by the short circuit method.

factors as time delay, link current state changes, DC voltage and electrical noise. The resonant converter was able to operate at DC link voltages up to 300 [V], but it then becomes unstable and the converter had to be restarted.

In Fig. 3.9 link current and resonant voltage is shown for a DC link voltage of 150 [V]. Notice the period of the short circuit interval is adjusted fine to operation conditions. The initial inductor current is kept close to 1.5 [A], a lower initial current was tried but the instability of the converter increased. The short circuit time is then approximately 1.6 [μs] and this is close to the minimum short circuit time. An increase in the DC link voltage therefore increases the initial resonant inductor current. The problem is that the inductor current is increased beyond what is necessary and reactive losses therefore increases.

Based on laboratory experience the following is concluded about the short circuit method:

1) Start of the resonant link is done by a direct short circuit of the fully charged resonant capacitor. At higher DC link voltage the inverter switch stress increases.

2) If an error occurs and the resonant voltage, v_{do} do not resonate down below 15 [V] the short circuit does not start, and the resonance terminates. The converter must be restarted. Among other, this make the converter operation un-robust.

3) There is a minimum short-circuit time that already increases the initial resonant inductor current beyond required value at $V_d = 150$ [V]. With increased reactive power flow and losses as consequence.

4) The circuit builded in the laboratory was not able to operate stable for DC voltage above 300 [V].

Beside the four points another drawback is the requirement of two phase current and one link current measurement.

3.4 A non-short circuit method

Transferring energy to the resonant circuit is necessary in order to compensate for loss elements. In the short circuit method this was done at the beginning of the resonant period. Another method is to transfer the energy inductively which can be done by a secondary winding on the resonant coil and it is then a transformer. The secondary side energy source is a current generator that produces a puls train with a frequency of the resonant circuit. The principal of the idea is shown in Fig. 3.10.

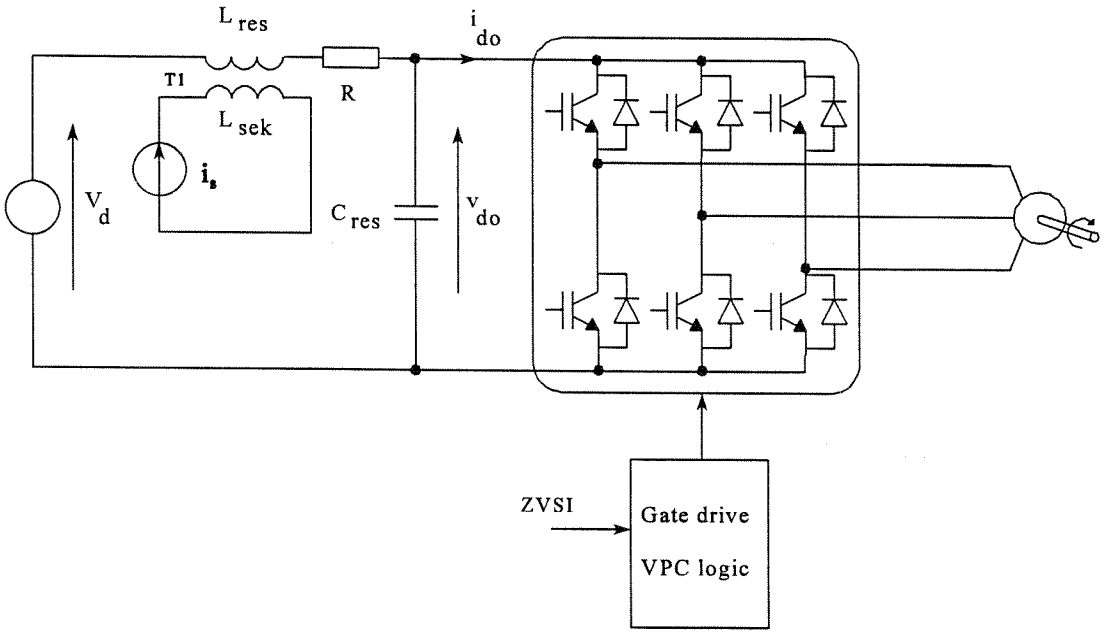

Fig. 3.10 Non-short circuit method to maintain the resonance. Using a transformer and current generator i_s.

Inductive energy transfer is widely used. Here a current source supplies the resonant circuit with energy. The basic principle of the current source resonant converters are described in /28/ using a parallel resonant circuit. The key waveforms are shown in Fig. 3.11.

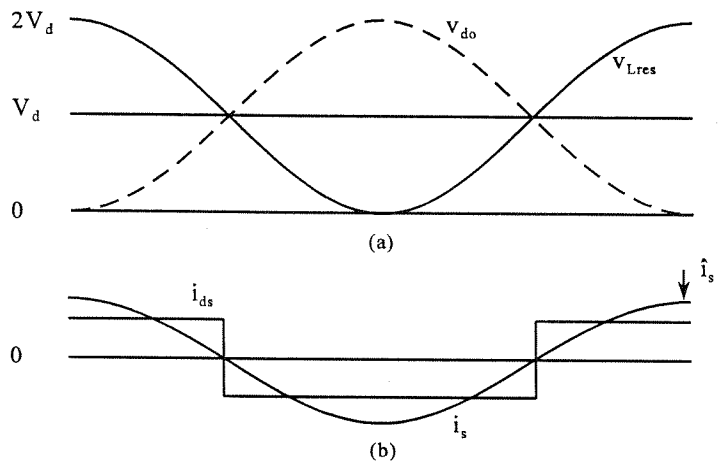

Fig. 3.11 Idealized resonant converter waveforms
a) Primary voltage, v_{do} and secondary voltage, v_{Lres}.
b) Secondary current, i_{ds}, fundamental current, $\hat{I}_s$.

The current source is typically a square wave, since this is the easiest to produce. The current i_{ds} is shown in Fig. 3.11 and it is in phase with v_{Lsek}. The advantage of zero-phase displacement is the transition of current happens at zero voltage. Current source switches therefore have low switching losses. A phase displacement of current and voltage is not desirable here. An example of a current generator i_{ds} is shown in Fig. 3.12.

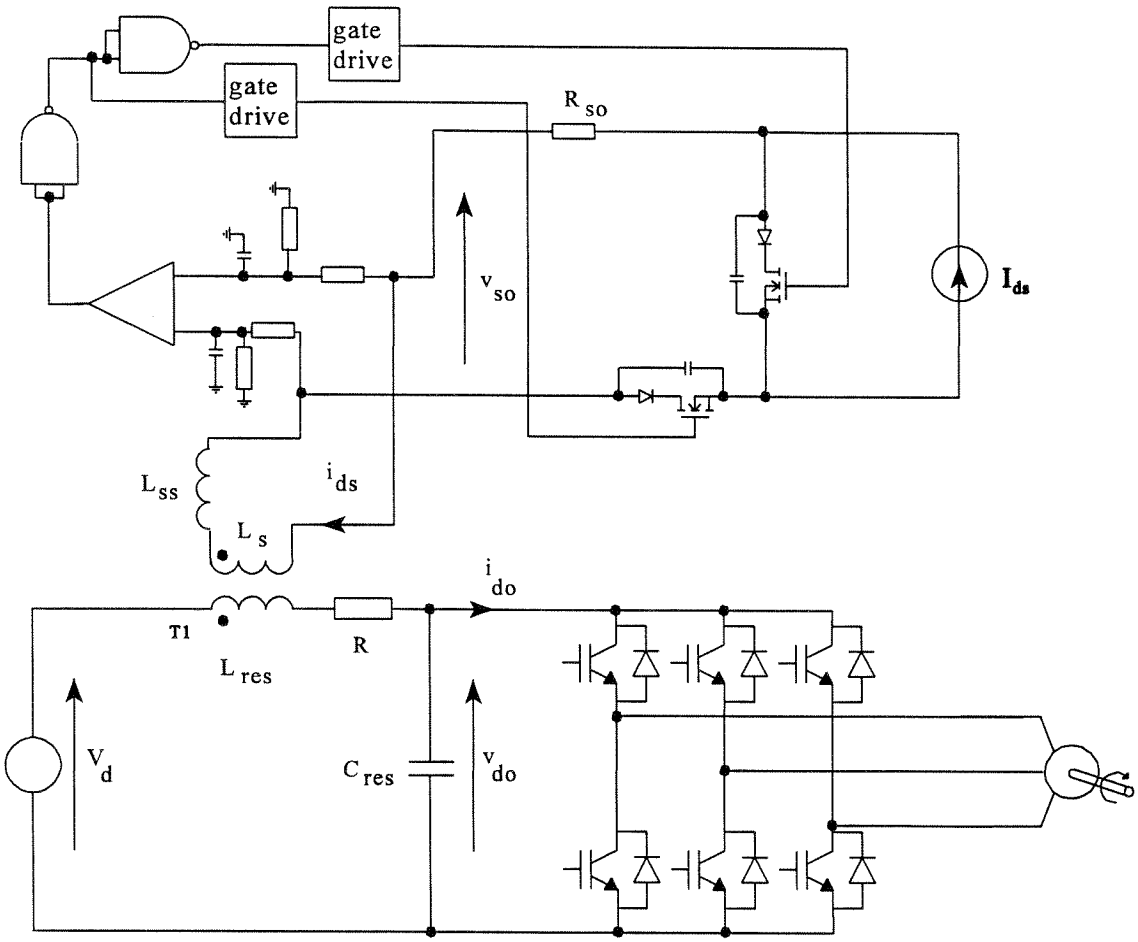

Fig. 3.12 A circuit to maintain resonance using inductively energy transfer to compensate ohmic losses.

Notice the control of the two switches is simple e.g. no dead-time is required. The gate control of the switches is obtained by a simple comparator that detects the sign of the secondary voltage of v_{so}, and the switches are controlled directly from this signal.

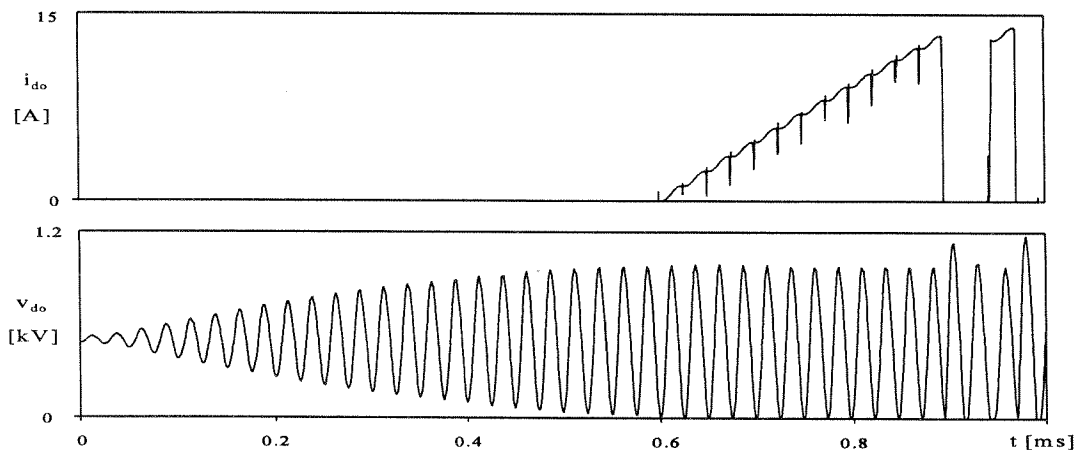

Fig. 3.13 Start of resonant oscillation with the non shortening method.

In Fig. 3.13 a simulation shows how the energizing circuit is working. At the beginning the voltage v_{do} is a DC voltage equal to V_d, the current converter is started and energy is transferred to the resonant circuit and the amplitude of the oscillation increases. The oscillation amplitude increases until the v_{do} reaches zero voltage, the antiparallel diodes begin to conduct and clamp the voltage. In Fig. 3.14 a zoom of the resonant converter waveform is shown.

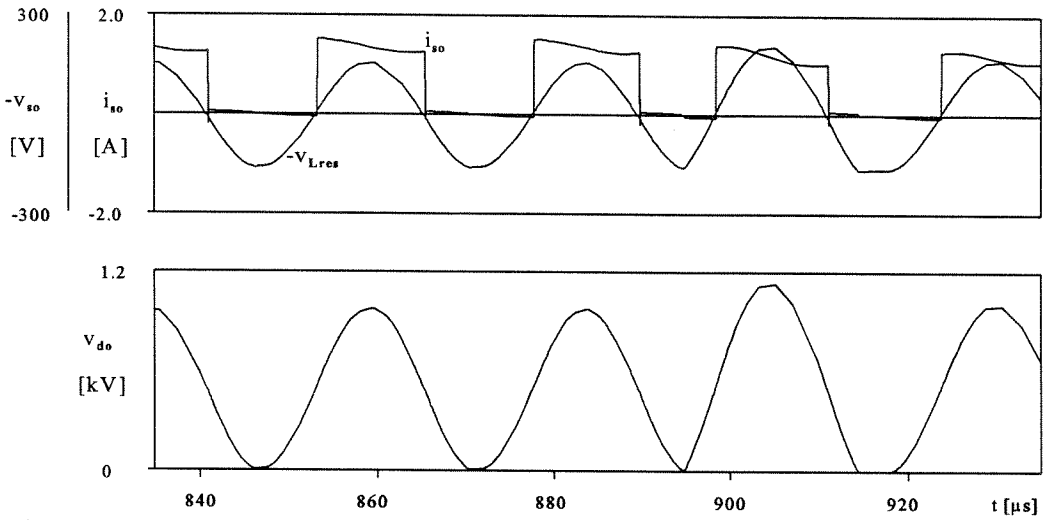

Fig. 3.14 Zoom of resonant converter waveforms with the non shortening method.

If there is excessive energy in the resonant circuit, it is transferred to the voltage source V_d during the conducting interval of the antiparallel diodes. If a disturbance occurs that prevent the voltage v_{do} to reach zero the current generator will continue to supply the resonant circuit with energy and eventually the voltage reaches zero. This way of energizing the resonant circuit makes the resonance very robust. The amount of energy transferred from the current source to the resonant circuit is determined by the current amplitude.

The necessary current amplitude to overcome the losses in the resonant circuit must be calculated. To do this a model of the resonant converter is used and it is shown in Fig. 3.15. From the model the required amplitude of i_s can be calculated using Laplace transformation. To simplify the task, i_s is not modelled as a square wave, but as a cos function. This make sense since energy is transferred by the fundamental of the square wave.

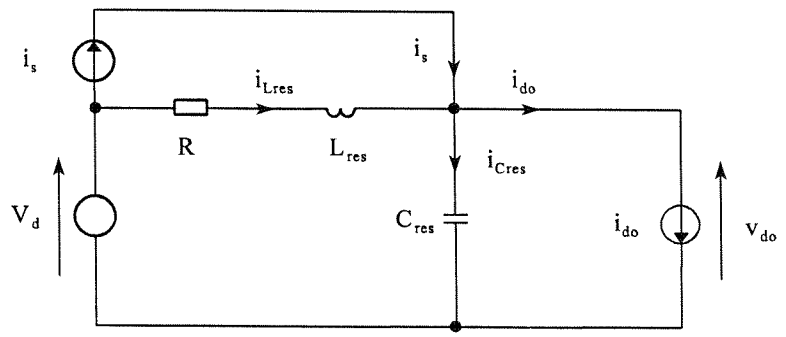

Fig. 3.15 Equvivalent circuit of resonant converter and non-short circuit energizing method

The equations of the circuit shown in Fig. 3.15 is shown in App. A. The whole solution equation is quite long and not repeated her, but a 'light' version of the equations is shown. The equation is close to the real solution assuming R << Z, and $i_{Lres(o)} = i_{do}$ and $v_{do} = 0$, and this can be applied here.

$$i_{Lres} = \frac{V_d}{Z} e^{-\alpha t} \sin(\omega t) + \frac{1}{2} \hat{i}_s \omega t \sin(\omega t) \quad \textbf{(3.3)}$$

$$v_{do} = V_d (1 - e^{-\alpha t} \cos(\omega t)) + \frac{1}{2} \hat{i}_s \omega Z t \cos(\omega t) \quad \textbf{(3.4)}$$

$$i_s = \hat{i}_s \cos(\omega t) \quad \textbf{(3.5)}$$

If a Taylor expansion of $e^{-\alpha t} = 1 - \alpha t$ is used, it is observed that a value calculated using eq. 3.6 compensate the losses of the resonant circuit. It is also noticed that the calculated amplitude of i_s compensates the loss in the resonant circuit in such a way the wave form of i_{Lres} and v_{do} is very close to those of the loss free resonant circuit. This is not the case using the short circuit method where the voltage and current wave forms are distorted noticeably.

$$\hat{i}_s = R \frac{V_d}{Z^2} \quad \textbf{(3.6)}$$

In Fig. 3.16 is shown the waveforms of i_{Lres} and v_{do} using the short circuit method and the non-short circuit method. Two plots are shown on Fig. 3.16 for every v_{do}, i_{Lres}. The one is an ideal curve calculated using a loss less circuit, another for the lossy circuit where the energy loss compensation is used. At Fig. 3.16.a is the short circuit method used, it over comes the resonant circuit losses using an initial resonant inductor current calculated using eq. 3.1. The initial conditions are $i_{Lres(0)} - i_o = \Delta i_{Lres}$ and $v_{do} = 0$. They cause a phase displacement between the ideal curve form and the compensated curve. There is an amplitude difference, largest at the beginning of the resonant period and almost zero at the end of the resonant period. This is seen from the phase plane plot. Simulation shows that an increase of the initial current Δi_{Lres} with 50 % has a significant influence on the wave forms including an increased difference in amplitude.

In Fig. 3.16.b the non-short circuit method is used to energize the resonant circuit. There is no phase displacement and the current waveform are plotted very close to those of the loss less resonant circuit. The losses of the resonant circuit are compensated in such a way the resonant circuit behaves as it is loss less. A 50 % increase of i_s current do not cause a significant phase shift and the amplitude is only distorted a little. In the simulation the values in Table 3.2 were used.

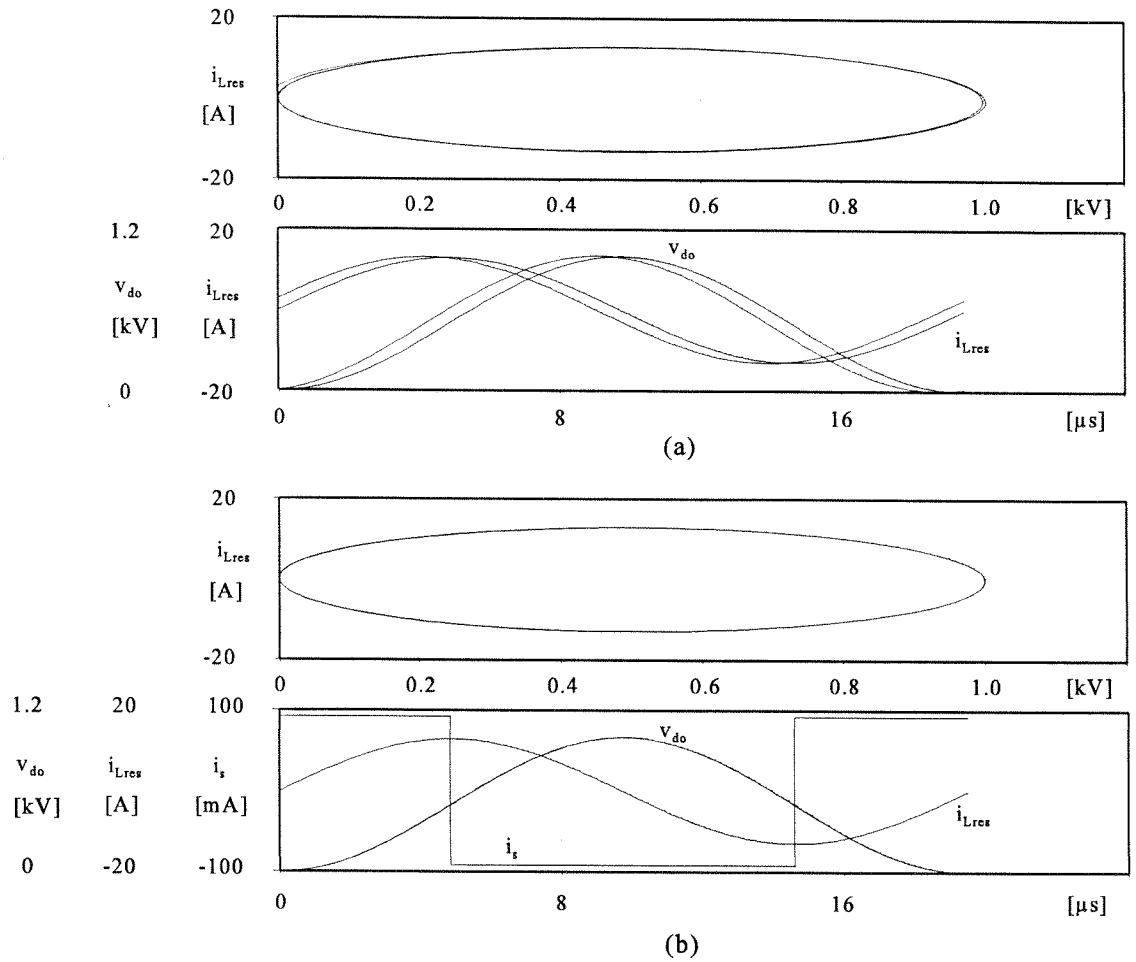

Fig. 3.16 a) Short circuit method
b) Non-short circuit method

In Table 3.2 two current equations are shown in the non-short circuit method box. The amplitude of i_s is in the case of a sinusoidal current source and i_{ds} is used for square wave currents. If the i_{ds} current is bi-directional the equation in Table. 3.2 is used, if only a positive pulse can be generated by the current generator, then i_{ds} must be multiplied by two. This is the case of the current generator shown Fig. 3.12.

Vd = 500 [V] L = 150 [µs] C = 100 [ns] Z = 38.7 [Ω] f_{res} = 41.09 [kHz] R = 0.35 [Ω]	
short circuit method	non-short circuit method
$\Delta i_{Lres} = \sqrt{\frac{R(\frac{V_d}{Z_{res}})^2}{f_{res} L_{res}}}$	$\hat{i}_s = R\frac{V_d}{Z_{res}^2}d$ $i_{ds} = \hat{i}_s \frac{\pi}{4}$
Δi_{Lres} = 3.1 [A]	i_{ds} = 91.6e-3 [A]

Table 3.2 Calculation of initial current using the short circuit method and current amplitude using non-short circuit method.

How much power is it necessary to transfer to the resonant circuit ?. This is simply calculated assuming the wave forms shown in Fig. 3.11.

The power P_1 transferred from the current source I_s is

$$P_1 = \frac{\hat{i}_s}{\sqrt{2}} \frac{\hat{v}_{Lres}}{\sqrt{2}} \tag{3.7}$$

Assuming a loss less circuit. The required power P_2 to compensate resistive losses is

$$P_2 = (\frac{V_d}{Z\sqrt{2}})^2 R \tag{3.8}$$

The amplitude of v_{Lres} is V_d and the amplitude of i_s is the only unknown. It is already calculated by Laplace calculation, in this way the amplitude of i_s is found more easily. Using $P_1 = P_2$ the amplitude of i_s is derived.

$$\hat{i}_s = R \frac{V_d}{Z^2} \tag{3.9}$$

An equation identical to eq. 3.6 is obtained. The requirement of the current source in Fig. 3.11 is

$$I_{ds} = 2V_d \frac{R}{Z^2} \frac{\pi}{4} \frac{N1}{N2} \tag{3.10}$$

where:

N1 : primary winding number
N2 : secondary winding number

3.5 A laboratory test of the non-short circuit method

About one week was used to build the circuit that maintains the resonance and it was working right from the beginning. Since there were problems with the short circuit method at DC link voltages above 300 [V] the converter was first tested at 300 [V] level, then a 500 [V] level was used. A stable converter operation was a fact, using the non-short circuit method. To obtain the stabile converter operation the current source amplitude in the circuit that maintains the resonance had to be increased significant beyond the theoretical value.

The current I_{ds} and P_{ds} are calculated using eq. 3.10 and eq. 3.8:

I_{ds} = 0.6 [A]
P_{ds} = 29 [W]

where

R = 0.35 [Ω]
Z = 38.7 [Ω]
N1/N2 = 3.1
V_d = 500 [V]

In the laboratory experiment was used an I_{ds} of 3.0 [A], to obtain stable converter operation. Using this current, the delivered power from the current source is 154 [W], which is significant higher than the calculated 29 [W].

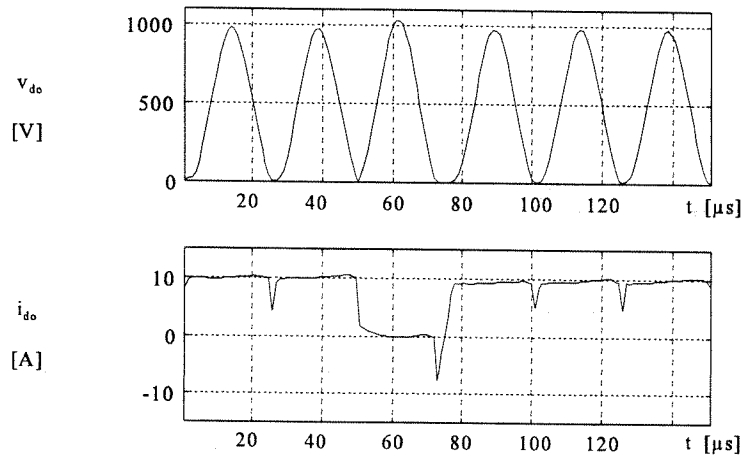

Fig. 3.17 Measured link voltage and link current using the non-short circuit method.

Looking at Fig. 3.17 it is seen that a substantial amount of energy is stored in the resonant inductor at the end of a resonant period, the energy is transferred to the DC link voltage capacitor during the antiparallel diode conducting interval. The initial current is approximate 6 [A] the total power transferred to the DC capacitor is

$$P_{DC} = f_{res} \frac{1}{2} L_{res} \Delta I^2 \qquad \textbf{(3.11)}$$

P_{DC} is calculated to be P_{DC} = 111 [W] using ΔI = 6 [A] and the parameters in table 3.2.

Based on simulation and laboratory experience the following is concluded about the non-short circuit method:

1) The start of the resonance is done without current stress of the inverter switches, or any excessive stress at all.

2) If an error occurs and the resonant voltage, v_{do} does not resonate below 15 [V] the resonance is not terminated, the energy transfer to the resonant circuit is continued and the converter operation is not affected. This make the converter operation robust.

3) There is a required amount of energy needed to compensate the losses of the resonant circuit, the amount of energy actually transferred to the resonant circuit is approximately 5 times the minimum required value. With an increase reactive power flow and losses as consequence.

4) The resonant converter is operated at DC link voltage of 500 [V] and there is no reason why this should not be increased.

Another advantage of the method is that no phase current or link current measurement is required. This is another reason to the stable converter operation. The only drawback is the need of a current source able of deliver approximately 150 [W]. Simulation and theoretical analysis show the current source only needs to deliver 29 [W].

3.6 Conclusion

Two circuits that maintain the resonance of the RDCLVPC converter are presented. Simulation and experimental results show how they work and perform.

The gained experience is summarized in Table 3.3

Parameter\Method	**Short circuit**	**Non-short circuit**
Stress on converter at start up of the resonance	High stress on inverter switches	No excessive stress on any components
Error tolerant resonance	No	Yes
Reactive power level relative theoretical level	increased	increased
Converter operation possible at high DC link voltage > 500 [V]	No or very difficult	Yes
Method dependent on measurement of link voltage or current.	Yes	No
Realization	Complex	Simple

Table 3.3 Comparison of different methods to maintain the resonant link cycle of the RDCLVPC

It concluded that the non-short circuit method possesses many advantages over the short circuit method. The implemented non-short circuit works well but the amount of power supplied to the resonant circuit should be decreased from 150 [W] to a value closer to the theoretical 29 [W].

4

Resonant converter modulators

In this chapter is dealt with modulators that are suitable for resonant converters. There is a lot of knowledge available due to the work of D. Divan /1/,/5/,/15/ and his fellow reachers at University of Wisconsin and A. Mertens /6/,/16/ from University of Aachen just to mention a few. Many modulators are proposed in the litterature and here is selected a few that are proven to be suitable in voltage control. An in dept discussion of the modulators is made, in order to obtain an understanding of the various types of modulators. The selected modulators are voltage controlled. With an induction machine load, voltage control is relative simple compared to current control, and open loop speed control with voltage/frequency control is used.

The design of a modulator is often based on a wish of low content of harmonics in current and voltage, another approach of designing the modulator is using the ideal trajectory of the machine stator flux as reference, as proposed in /17/,/19/,/29/ they design pulse width modulators. Here the design method is applied on the resonant converter.

Three modulators are investigated:

- Sigma Delta Modulator, SDM /1/,/5/
- Space Vector Sigma Delta Modulator, SVSDM /5/,/6/,/15/,/16/
- Stator Flux orientated Discrete Pulse Modulator, SFDPM

The three modulator's performances are compared by simulation, in a system as shown in Fig. 4.1.

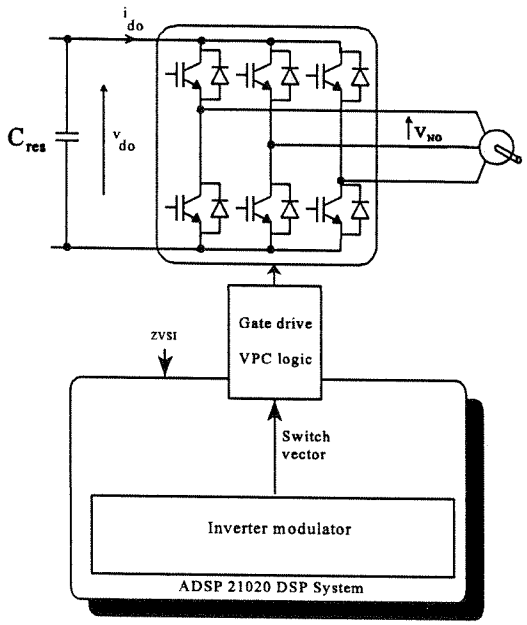

Fig. 4.1 The inverter modulator is at focus in this chapter.

4.1 Voltage/frequency control

Open loop speed control of induction machines is often done by a Voltage/frequency control /20/,/22/ because of its simplicity. This type of control is described in its most basic form.

In eq. (4.1) from /22/ is shown that electrical torque produced by the induction machine in steady state, disregarding stator resistor and for a small value of ω_r is:

$$m_{el} = \left(\frac{V_{phase}}{\omega_s} \right)^2 k\ p\ \omega_r \qquad (4.1)$$

where: m_{el} electrical machine torque
ω_s synchronous speed equal to $2\pi f_{ref}$
V_{phase} phase voltage effective value
ω_m rotor speed
ω_r relative rotor angular frequency equal to $\omega_s - p\omega_m$ or slip speed $\omega_r = s\omega_s$, s= slip.
k konstant
p number of pole pair

If V_{phase}/ω_s is held constant there is a close to linear relation ship between ω and the developed electrical torque. Using (4.1) the relation between the rotor speed and synchronous speed is:

$$\omega_m = \frac{1}{p}\omega_s - \frac{1}{k_1} m_{el} \qquad (4.2)$$

The value of constant k_1 could apparently, with advantage, be increased at lower speed where there the inverter is able to deliver an increased voltage, V_{phase}. The torque influence on the rotor speed could be reduced. But this is not possible for longer periods due to thermal limitations. At low speed the fan is almost without influence and the machine heats up, mainly because of copper losses. The m_{el}/k_1 influence is disregarded here.

4.2 Voltage controlled modulators

A conventional open loop voltage/frequency speed control using a voltage controlled modulator is shown in Fig. 4.2.

Various types of modulators are used in open loop voltage/frequency speed control. For discrete pulse modulator the voltage controlled sigma delta modulator is a good choice in induction machine control /3/. The sigma delta modulator, as shown in Fig. 4.3., is a single-phase voltage modulator. One disadvantage as with all single-phase modulators is that they do no utilize that there are three phases to be controlled. They cannot be expected to be the optimal solution in three-phase systems.

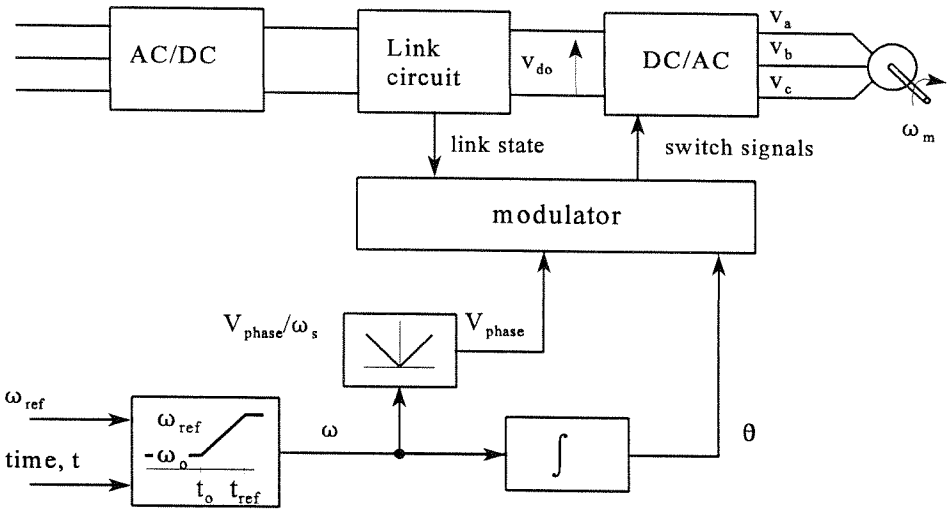

Fig. 4.2 Conventional open loop voltage/frequency speed control of induction machine using a voltage controlled modulator

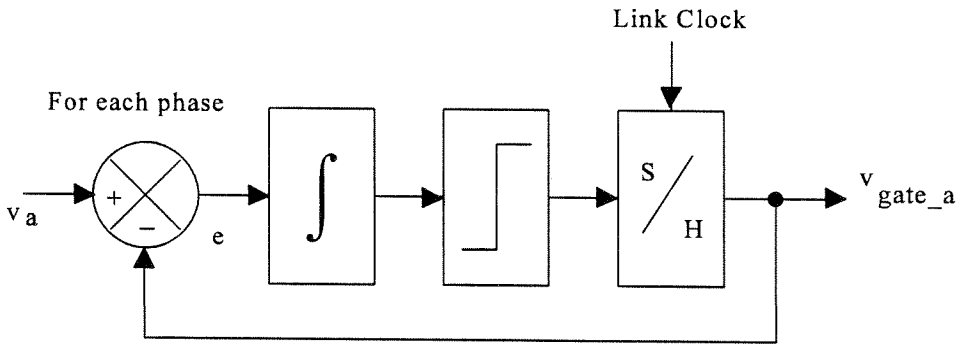

Fig. 4.3 Single phase Sigma Delta Modulator, SDM.

A possibility to improve the modulator performance could be to design a modulator using space vectors. This is done with success in PWM systems. Since the use of voltage space vectors is a success in PWM-VSI, a discussion of space vectors is made, and then a discrete pulse modulation, DPM, strategy using the space vectors is designed. The design specifications of a particular PWM strategy are used in a design of a DPM.

4.3 Instant and average space voltage vector

The voltage space vector $\mathbf{v}_s$ obtained by Park transformation to the stator-fixed system of coordinates (α,β) is

$$\mathbf{v}_s = \frac{2}{3}(v_{ax} + \mathbf{a}\, v_{bx} + \mathbf{a}^2 v_{cx}) = v_{s\alpha} + j v_{s\beta} = \hat{v}_s e^{(j\theta_s)} \qquad \textbf{(4.3)}$$

where v_{ax},v_{bx},v_{cx} eg. are branch voltages or phase voltages.
$\mathbf{a}$,$\mathbf{a}^2$ is complex operators: $e^{j2\pi/3}$, $e^{j4\pi/3}$.

In a short form eq. 4.3 is written

$$\mathbf{v}_s = \mathbf{M}\,\mathbf{v}_x \tag{4.4}$$

where

$$\mathbf{M} = \begin{bmatrix} 1 & \mathbf{a} & \mathbf{a}^2 \end{bmatrix} \tag{4.5}$$

$$\mathbf{v}_x = \begin{bmatrix} v_{ax} \\ v_{bx} \\ v_{cx} \end{bmatrix} \tag{4.6}$$

Using Eq. 4.3 it is assumed the zero-sequence component is zero, which is obtained for balanced loads. The induction machine is assumed to be a balanced load in this case.

There is a free choice of x-indices on v_{ax},v_{bx},v_{cx} there are three voltages that can be used resulting in the same voltage space vector, v_s. This is shown in Fig. 4.4

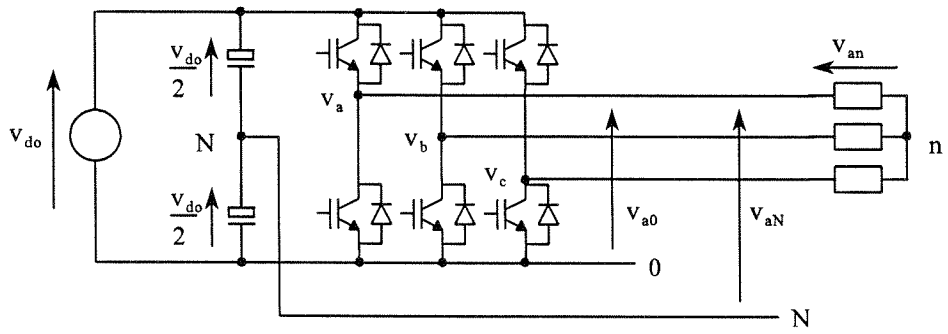

Fig. 4.4 Definition of branch voltages and phase voltage.

$$\mathbf{v}_n = \frac{2}{3}(v_{an} + \mathbf{a}\,v_{bn} + \mathbf{a}^2 v_{cn}) \tag{4.7}$$

$$\mathbf{v}_0 = \frac{2}{3}(v_{a0} + \mathbf{a}\,v_{b0} + \mathbf{a}^2 v_{c0}) \tag{4.8}$$

$$\mathbf{v}_N = \frac{2}{3}(v_{aN} + \mathbf{a}\,v_{bN} + \mathbf{a}^2 v_{cN}) \tag{4.9}$$

$$\mathbf{v}_s = \mathbf{v}_n = \mathbf{v}_0 = \mathbf{v}_N \tag{4.10}$$

$\mathbf{v}_s$ describes the instant state of the inverter bridge. There are seven possible values of $\mathbf{v}_s$, six determined by the active switch vectors and one determined by the two zero switch vectors. The eight switch vectors are shown in Fig. 2.3.

The input to a modulator can e.q. be a voltage or a current or a flux vector. Here is the voltage modulator considered.

The modulator input voltage vector at a given time instant should be reproduced on the inverter output during the time a switching period lasts. This is the average voltage vector $\mathbf{v}_{ave}$ generated by a switching sequence. There is a delay between the input voltage vector and the $\mathbf{v}_{ave}$ equal to the switching frequency. The $\mathbf{v}_{ave}$ expressed by the voltage vector sequence and the time duration of each voltage vector, is shown in eq. (4.11)

$$\mathbf{v}_{ave} = \frac{t_0}{T_{sw}}\mathbf{v}_{s0} + \frac{t_1}{T_{sw}}\mathbf{v}_{s1} + \frac{t_2}{T_{sw}}\mathbf{v}_{s2} + \frac{t_3}{T_{sw}}\mathbf{v}_{s3} = \frac{t_1}{T_{sw}}\mathbf{v}_{s1} + \frac{t_2}{T_{sw}}\mathbf{v}_{s2} \qquad \textbf{(4.11)}$$

where $\mathbf{v}_{s0}$ is vector 000
$\mathbf{v}_{s1}$ is vector 100
$\mathbf{v}_{s2}$ is vector 110
$\mathbf{v}_{s3}$ is vector 111
'0' = 0
'1' = V_d
T_{sw}= switching period time
hence 000 = [0 0 0] and so on.

The average vector $\mathbf{v}_{ave}$ can be placed everywhere inside the sector, distended by switch vector 100 and 110, by proper adjustment of t_1 and t_2. Using eq. (4.11) is obtained

$$t_1 = \frac{3}{2}T_{sw}\frac{\hat{v}_{avg}}{V_d}\left(\cos\theta_{avg} - \frac{1}{\sqrt{3}}\sin\theta_{avg}\right) \qquad \textbf{(4.12)}$$

$$t_2 = \sqrt{3}\,T_{sw}\frac{\hat{v}_{avg}}{V_d}\sin\theta_{avg} \qquad \textbf{(4.13)}$$

where $\hat{v}_{avg}$ length of $\mathbf{v}_{avg}$
θ_{avg} angle of $\mathbf{v}_{avg}$

The maximum average value obtainable, assuming linear modulation, is for the condition

$$T_{sw} = t_1 + t_2 \qquad \textbf{(4.14)}$$

Using eq. 4.12. to eq. 4.14 the average amplitude as function of θ_{avg} is found.

$$\hat{v}_{avg}(\theta_{avg}) = \frac{V_d}{\frac{3}{2}\cos\theta_{avg} + \frac{\sqrt{3}}{2}\sin\theta_{avg}} \qquad \textbf{(4.15)}$$

Maximum average amplitude is for θ_{avg} = 30 [°]. The maximum length of the average voltage vector found eq.4.15 is

$$\hat{v}_{avg\_MAX} = \frac{V_d}{\sqrt{3}} = \frac{2}{\sqrt{3}}\frac{V_d}{2} \sim 1.155\frac{V_d}{2} \tag{4.16}$$

The maximum phase voltage amplitude is obtained for a modulation index m of m=1. Overmodulation is not considered.

$$m = \frac{\hat{v}_{ref}}{\hat{v}_{avg\_MAX}} \qquad m = [0..1] \tag{4.17}$$

where $\hat{v}_{ref}$ is reference phase voltage amplitude.

It is noticed that the scale factor of $^2/_3$ in eq. (4.3) adjusts the length of the average voltage vector such that it equals the amplitude of the phase voltage.

4.4 Space Vector Sigma Delta Modulator (SVSDM)

The sigma delta modulator shown Fig. 4.3 is a single phase modulator, it is able to control an inverter branch and with three of them the inverter can produce a three phase voltage output. The output of the inverter using sigma delta modulator is a fundamental voltage and harmonic voltages. The fundamental voltage must produce a phase voltage amplitude at maximum linear modulation index m of

$$\hat{v}_{xn} = \frac{V_d}{\sqrt{3}} \tag{4.18}$$

If eq. 4.18 is not full filled the gain of the inverter is less than one. The average value of the output voltage v_{xN} from the inverter is limited to the average value of one resonant pulse.

$$v_{xN} = [\frac{V_d}{2}, -\frac{V_d}{2}] \tag{4.19}$$

To maximize the fundamental amplitude of v_{xn}, a third harmonic with an amplitude of 1/6 is used /18/. The input voltage to the modulator is then given by $\mathbf{v_N}$:

$$\mathbf{v_N} = m\frac{2}{\sqrt{3}}\begin{bmatrix} \cos\theta - \frac{1}{6}\cos 3\theta \\ \cos(\theta - \frac{2}{3}\pi) - \frac{1}{6}\cos 3(\theta - \frac{2}{3}\pi) \\ \cos(\theta - \frac{4}{3}\pi) - \frac{1}{6}\cos 3(\theta - \frac{4}{3}\pi) \end{bmatrix} \tag{4.20}$$

where v_N input to modulator [-1..1]
θ angle of input voltage
m modulation index [0..1]

The feed back to the sigma delta modulator can be the branch state, which is

$$\mathbf{s_N} = \begin{bmatrix} s_{aN} \\ s_{bN} \\ s_{cN} \end{bmatrix} \qquad s_{xN} = [-1, 1] \tag{4.21}$$

or the phase state, which is

$$\mathbf{s_n} = \begin{bmatrix} s_{an} \\ s_{bn} \\ s_{cn} \end{bmatrix} \qquad s_{xn} = [-\frac{4}{3}, -\frac{2}{3}, 0, \frac{2}{3}, \frac{4}{3}] \tag{4.22}$$

The five different states of s_{xn} is explained in the following paragraph. It could seem more natural to use the branch v_{xN} or phase voltage v_{xn} as feed back to the modulator, but here it is assumed that the branch switching state s_{xN} is proportional to branch voltage v_{xN}.

Assuming a balanced load the phase voltage is expressed by the branch potentials in the following way:

$$v_{an} = \frac{2}{3}v_{aN} - \frac{1}{3}v_{bN} - \frac{1}{3}v_{cN} \tag{4.23}$$

$$v_{bn} = -\frac{1}{3}v_{aN} + \frac{2}{3}v_{bN} - \frac{1}{3}v_{cN} \tag{4.24}$$

$$v_{cn} = -\frac{1}{3}v_{aN} - \frac{1}{3}v_{bN} + \frac{2}{3}v_{cN} \tag{4.25}$$

From eq. 4.23 to eq. 4.25 a table of possible switching states are calculated and the sum of the switching states are shown in Table 4.1

s_{aN}	-1	1	-1	1	1	-1	1	-1
s_{bN}	-1	1	1	-1	1	-1	-1	1
s_{cN}	-1	1	1	-1	-1	1	1	-1
$\sum s_{xN}$	-3	3	1	-1	1	-1	1	-1
s_{an}	0	0	$-4/3$	$4/3$	$2/3$	$-2/3$	$2/3$	$-2/3$
s_{bn}	0	0	$2/3$	$-2/3$	$2/3$	$-2/3$	$-4/3$	$4/3$
s_{cn}	0	0	$2/3$	$-2/3$	$-4/3$	$4/3$	$2/3$	$-2/3$
$\sum s_{xn}$	0	0	0	0	0	0	0	0

Table 4.1 Branch s_{xN} and phase s_{xn} switching states.

In Fig. 4.5 is one branch of two sigma delta modulators shown.

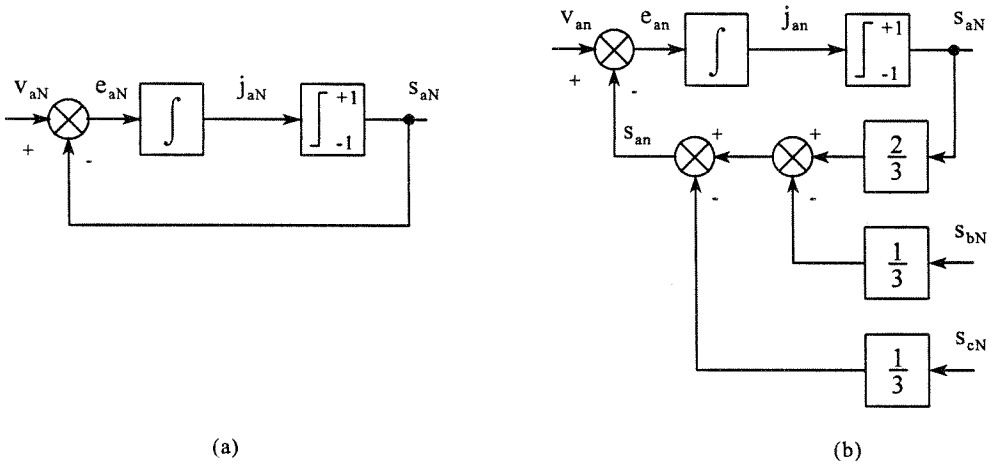

Fig. 4.5 a) Sigma delta modulator with branch state feed back
b) Sigma delta modulator with phase state feed back

If the sum of signals into to the comparator's shown on Fig. 4.5 equal zero, this causes only generation of active vectors. Therefore, if the sum of j_{xN} or j_{xn} is zero none zero voltage vector is generated. From Table 4.1one find that the sum of j_{xN} is not zero, and therefore the modulator generates zero voltage vectors. The modulator branches are operated independent of each other.

If the phase state feed back is used eq.4.26 governs

$$j_{an} + j_{bn} + j_{cn} = 0 \qquad \textbf{(4.26)}$$

and the modulator do not produce zero voltage vectors. However, is the three reference voltage zero or in phase, the integrated error is zero on all three phases, and zero voltage vectors are generated.

An important analysis of the delta modulators is made by /16/. A connection matrix C to transform the branch voltages to phase voltages is used. This is the same transformation shown in (4.23 - 4.25) and the reason for doing this is found in a statement from paper /16/ 'Since the distortion currents are governed by the phase voltages, it can be more efficient to directly control these voltages'. The phase voltage v_{xn} is closer to the sinusoidal voltage v_{xn} than brach voltage v_{xN} to v_{xN}. Therefore the error is smaller using $\mathbf{e_n} = C(\mathbf{v_N}-\mathbf{s_N})$ than using $\mathbf{e_N} = \mathbf{v_N}-\mathbf{s_N}$.

The connection matrix C eliminates multiple of the third harmonic, the addition of the third harmonic in eq. 4.20 is therefore without influence, but the multiplication of 2/sqrt(3) must still be used to obtain the unity inverter gain. The connection matrix is also used here, and the three phase sigma delta modulator is shown Fig. 4.6.

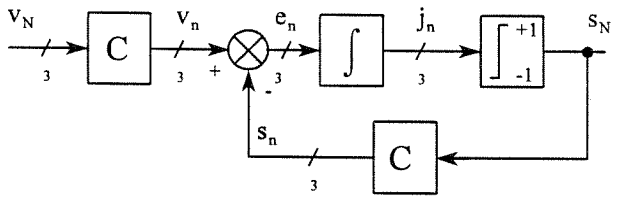

Fig. 4.6 Three phase sigma delta modulator with branch state feed-back

In /15/,/16/ a space vector sigma delta modulator is shown and it is reproduced in Fig. 4.7.

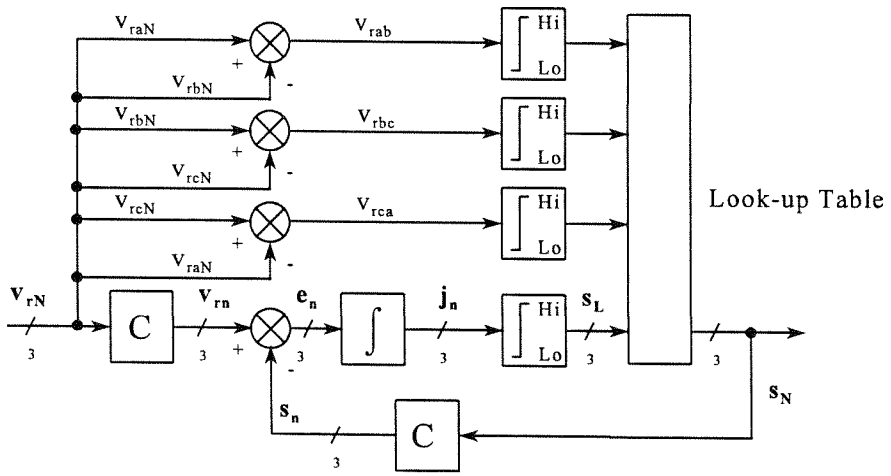

Fig. 4.7 Space vector sigma delta modulator for a three-phase inverter.

The purpose of the look up table is to reduce the number of 'random' switching. It is stated in /16/ 'that RMS ripple current can be reduced if only those switching space-vectors are used which are situated right next to the voltage reference space-vector **A**'. A consequence of this is reduced link current stress which is discussed in details in chapter 2.

The construction of the look up table is discussed in the following text. Input to the look up table are six states, generated by 2 x 3 comparators. Fig. 4.8 shows the three comparators that has $\mathbf{j}_n$ as input.

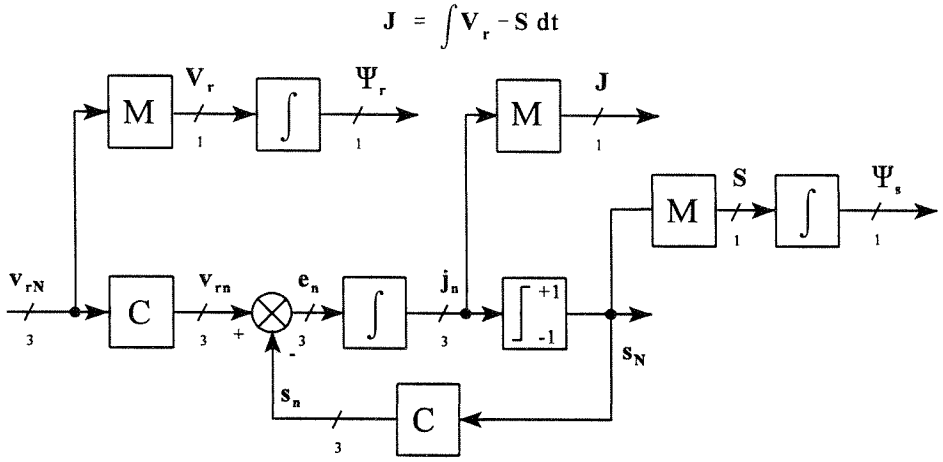

Fig. 4.8 Space vector sigma delta modulator.

The integral of $\mathbf{V}_r$, in Fig. 4.8 represents the reference stator flux Ψ and the integral of $\mathbf{S}$ represent the stator flux Ψ_s of the induction machine. Please disregard the vectors do not has the 'true' length, the syntax is thereby made simpler. The integral of the error $\mathbf{e}_n$ is $\mathbf{j}_n$, when it is transformed to the stationary reference frame which is equal to:

$$\mathbf{J} = \int (V_r - S)\, dt \tag{4.27}$$

$$\mathbf{J} = \int \mathbf{V}_r\, dt - \int \mathbf{S}\, dt \tag{4.28}$$

$$\mathbf{J} = \Delta\Psi = \Psi_r - \Psi_s \tag{4.29}$$

With this interperation the flux path's are drawn in Fig. 4.9

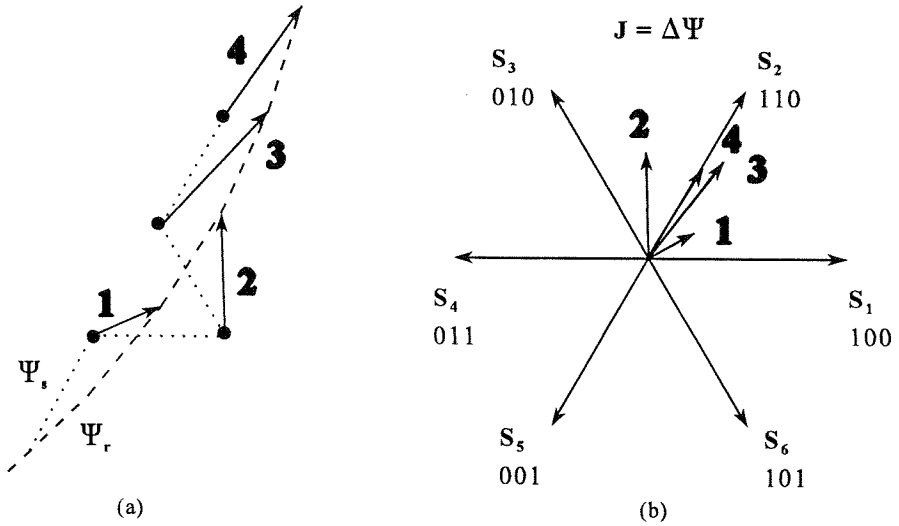

Fig. 4.9 a) Reference flux path Ψ_r = dashed line, stator flux path Ψ_s = dotted line, flux error **J** = full line.

b) Flux error **J** in four cases 1,2,3,4, six switching vectors S_1-S_6.

The direction of **J** determine the selection of the next switch vector, this is illustrated in Fig. 4.9. The flux error **J** with label nr. 1 is positioned nearest to switch vector S_1 therfore S_1 is selected as next switching vector, flux error **J** with label nr. 2 is positioned nearest to switch vector S_3 and so on. By doing so, the modulator selects the active switch vector that causes the smallest error. Switch vector S_1 is selected if the angle of **J** is between -30 [°] and +30 [°]. Switch vector S_2 is selected if the angle of **J** is between +30 [°] and 90 [°]. This divide the switch vector star shown Fig. 4.9 into six sectors, in each sector is one of the active vectors located in the middle. The modulator only selects between the active vectors, at least in most cases as discussed earlier. This is not optimal, since the error **J** sometimes are closer to one of the zero voltage vectors. The flux error **J** label nr. 1 is a case where a zero voltage vector might have been a better selection. To make this judgement the length of **J** must be known and furthermore a more precise definition of a 'good selection' must be used. This is discussed later. In Fig. 4.9 the modulator produce a switch sequence of:

$$S_1 \rightarrow S_3 \rightarrow S_2 \rightarrow S_2 \qquad \textbf{(4.30)}$$

Earlier in chapter 2 is discussed that 2 BSO as generated by $S_1 \rightarrow S_3$ should be avoided. The considerations behind the strategy in /16/ are stated in Table 4.2.

Consideration No. 1	The best selection of switch vector S_x is the vector located next to reference vector V_r. Since this generates the smallest ripple current.
Consideration No. 2	If the error vector **J** causes selection of a switch vector located more than 60 [°] away from the adjacent vectors of V_r, then the adjacent vector of V_r is selected
Consideration No. 3	If the error vector **J** causes selection of a switch vector located more than 120 [°] away from the adjacent vectors of V_r a zero vector is selected.

Table 4.2 Switch vector selection critia for space vector sigma delta modulation .

One switch vector star is divided into six sectors, the number of the sector determine where the reference vector $\mathbf{V}_r$ is located. Another switch vector star is divided into sectors that determine where the error vector **J** is located. This is shown in Fig. 4.10. If **J** is inside area A then switch vector $\mathbf{S}_1$ is selected. If **J** is inside area B switch vector $\mathbf{S}_2$ is selected. **J** is inside area C switch vector $\mathbf{S}_2$ is selected and so on.

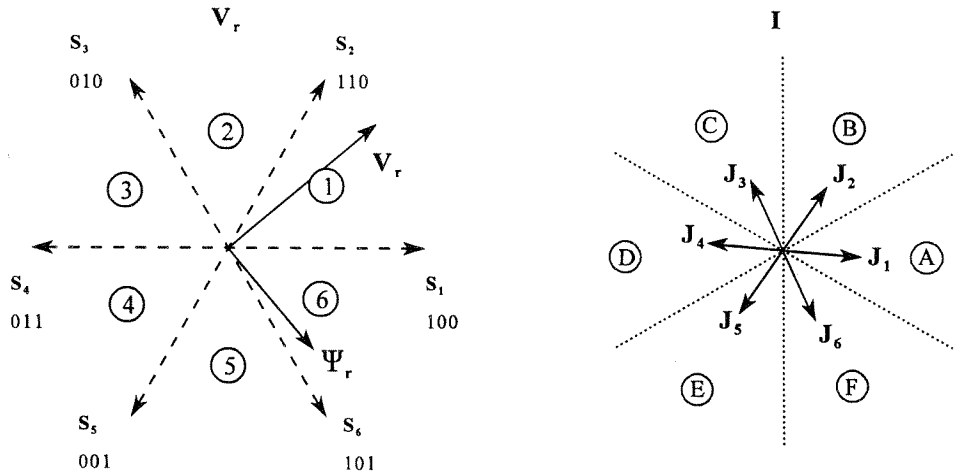

Fig. 4.10 The sector 1..6 determine where the reference vector, $\mathbf{V}_r$ is located and sector A..F determine where the integral of the error **J** is located

Based on Fig. 4.10 and selection criteria in Table 4.2 a look up table is made and its content is shown in Table 4.3. The table is identical to the one in /16/.

V_r \ J	A	B	C	D	E	F
1	S_1	S_2	S_2	S_7	S_7	S_1
2	S_2	S_2	S_3	S_3	S_0	S_0
3	S_7	S_3	S_3	S_4	S_4	S_7
4	S_0	S_0	S_4	S_4	S_5	S_5
5	S_6	S_7	S_7	S_5	S_5	S_6
6	S_1	S_1	S_0	S_0	S_6	S_6

Table 4.3 Switching table for space vector sigma delta modulator, proposed in /16/.

It is stated earlier that the selection of switch vector $\mathbf{S}_L$ Next in Fig. 4.7 it is determined by the angle of error **J**, where $\mathbf{S}_L = \mathbf{M}s_L$, $\mathbf{J} = \mathbf{M}\mathbf{j}$, M is from eq.(4.5). This is discussed in the following paragraph.

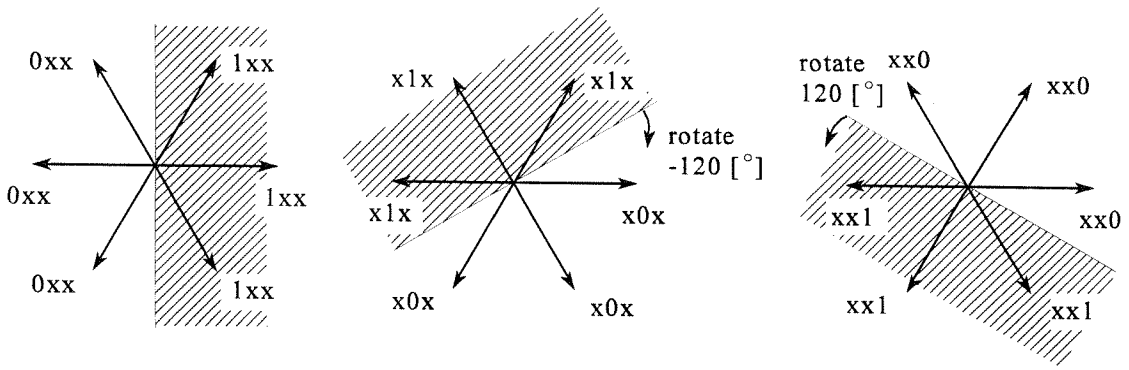

Fig. 4.11 Transformation from αβ coordinate system to three phase system.

If phase a is discussed first, and one look at Fig. 4.11 which shows the complex plane (αβ), where **J** is located. The transformation from (αβ) coordinate system to three phase system is done by taking the real part of **J**. Then the sign of signal determines the comparator output state.

$$s_{aN} = \text{sign}(\text{Re}(\mathbf{J})) \tag{4.32}$$

Phase b is obtained by rotating the **J** vector -120 [°] and then take the real part. Phase c is obtained by rotating the **J** vector 120 [°] and then take the real part. The switching stage calculation is shown eq. 30 and eq 31.

$$s_{bN} = \text{sign}(\text{Re}(\mathbf{a}^2\mathbf{J})) \tag{4.33}$$

$$s_{cN} = \text{sign}(\text{Re}(\mathbf{a}\mathbf{J})) \tag{4.34}$$

It is concluded that the comparator in the three phase domain selects the switch vector located inside the sector A,B,C,D,E,F as shown in Fig.4.10 where input vector **J.**

This also explains why the phase-phase voltages is a good input to the three comparator shown Fig. 4.7. In the complex (αβ) domain the phase-phase voltage vector is turned + 30 [°] as shown Fig. 4.12, with the phase-phase reference voltage as input to the comparators and they select the sector where the reference voltage vector $\mathbf{V}_r$ is located. The sector is represented by a three bit binary number.

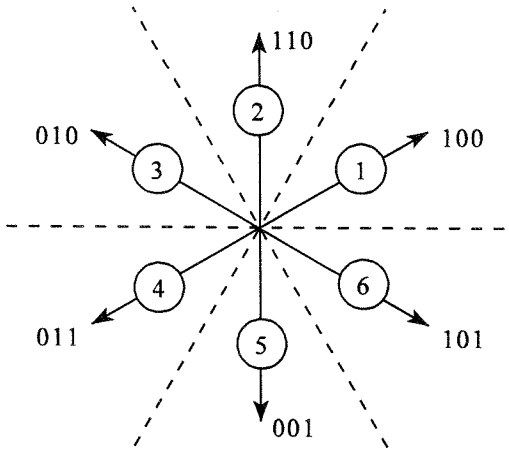

Fig. 4.12 Selection of reference voltage location based on line voltages

Finally is discussed if the implementation of the modulator in a digital system should be made in the complex domain or in the three phase domain. The implementation that require least computational power could be preferred. The input to the modulator is a three phase signal, as the one in eq. 4.20.

	Complex domain	Three phase domain
Transformation	$E_{re} = \frac{2}{3}(v_{raN} - s_{aN}) + \frac{1}{3}(s_{bN} - v_{rbN} + s_{cN} - v_{rcN})$ $E_{im} = v_{bN} - s_{bN} + s_{cN} - v_{cN}$	$s_{an} = s_{aN} + s_{aN} - s_{bN} - s_{cN}$ $s_{bn} = s_{bN} + s_{bN} - s_{aN} - s_{cN}$ $s_{cn} = s_{cN} + s_{cN} - s_{aN} - s_{bN}$
Calculation of error **J**,j	$J_{re} = J_{re} + E_{re}$ $J_{im} = J_{im} + E_{im}$	$e_{an} = v_{ran} - s_{an}$ $e_{bn} = v_{rbn} - s_{bn}$ $j_{an} = j_{an} + e_{an}$ $j_{bn} = j_{bn} + e_{bn}$
Reverse transformation	$s_{aN} = \text{sign}(J_{re})$ $s_{bN} = \text{sign}(J_{im} - J_{re})$ $s_{cN} = \text{sign}(-J_{im} - J_{re})$	$s_{aN} = \text{sign}(j_{an})$ $s_{bN} = \text{sign}(j_{bn})$ $s_{cN} = \text{sign}(-j_{an} - j_{bn})$
* operations	2	0
+ operations	13	15

Table 4.4 Comparison of SVSDM implemented in αβ coordinate system and SVSDM implemented in three phase system.

Comparing the number of operations by implementing the modulator in αβ coordinate or three phase domain, they are equal. The three phase domain implementations has the advantage of avoiding multiplications. The reason why the two ways of implementation is quite similar is that $s_{an} + s_{bn} + s_{cn}$ is equal to zero in the three phase system.

4.5 Stator Flux oriented Discrete Pulse Modulator (SFDPM)

With the use of space vectors many new PWM modulation strategies have emerged. The common factor of most of them, if not all of them, is that they use the same values of t_1 and t_2 shown eq. 4.11 to eq. 4.13, and active vectors for a particular value of θ_{ave}, to generate a desired average voltage value. The difference of the modulation strategies is the way the zero voltage vectors are placed relative to the active voltage vectors in the switching period.

In /17/,/19/ a PWM strategy is described where the electrical torque ripple is minimized. This is done by centering the two active voltage vectors in the switch period. The considerations behind the torque ripple and noise minimization are stated in short form in Table 4.2.

Consideration No. 1	The angle difference of the stator flux vector and reference stator flux causes the torque ripple.
Consideration No. 2	The magnitude difference of stator flux vector and reference stator flux causes acoustic noise.

Table 4.5 Design considerations for modulation strategies minimizing the torque ripple and noise.

The strategy in /17/,/29/ is denoted Stator Flux oriented asynchronous Vector Modulation, SFAVM.

In resonant converters using DPM there are many modulation strategies based on sinusoidal voltage or current references. Many of the modulation strategies are in nature single-phase modulation strategies. It is assumed a better modulator is obtained if the modulator is designed specific for a three phase system.

Another basic problem of many sinusoidal modulators is that they do not take into account that the inverter is only able to produce 8 voltage vectors. If for example the modulation strategy is derived in the vector plane, the limitation of having only 8 voltage vectors available can be utilized in the best possible way.

From the above discussion it seems natural to design a space vector modulation strategy in a stator-fixed system of coordinates (α,β). The strategy should minimize the torque and the noise of the electrical machine. Therefore the design specifications shown in Table 4.5 are used.

Stator flux trajectory:

The modulation strategy should in steady state control the stator flux vector to be as close as possible to a circle. The reference flux vector in steady state is /17/,/29/.

$$\Psi_{ref} = \frac{\hat{u}_{ref}}{j\omega} e^{j\omega t} \qquad (4.35)$$

where $\hat{u}_{ref}$ is reference phase voltage amplitude

ω is reference angular frequency $\omega = 2\pi f_{ref}$,

The stator flux vector is a function of the stator voltage vector. The stator resistance in the induction machine is disregarded.

$$\Psi_s = \int_{t_0}^{t_0+T} v_s \, dt + \Psi_{s\,t_0} \qquad (4.36)$$

At every time instant t_0 the flux Ψ_s can be controlled into 6 directions by the six active vectors or it can remain in a fixed position by using one of the two zero vectors. This is shown in Fig. 4.13.

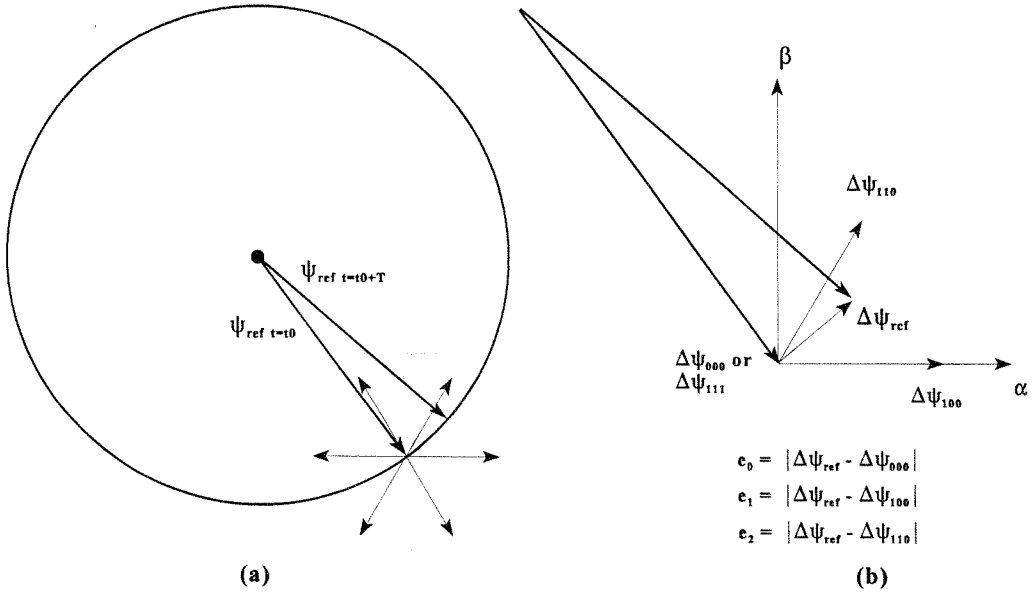

Fig. 4.13 a) The reference stator flux vector trajectory and two stator flux vectors are shown at time instant t_0 and t_0+T. The six possible directions of flux changes are shown.
b) A zoom of a. Only the four stator flux changes that can cause a minimum flux error for the reference flux vector at the time instant t_0+T are shown.

The optimal flux trajectory is obtained by selecting the stator voltage vector that generates the lowest value of three errors e_0, e_1, e_2, shown in Fig. 4.13.

From Fig. 4.14 is seen that the stator flux oriented discrete pulse modulation generates vector changes with more than one branch switch-over. It is checked that there is no zero voltage vector between '110' and '011'.

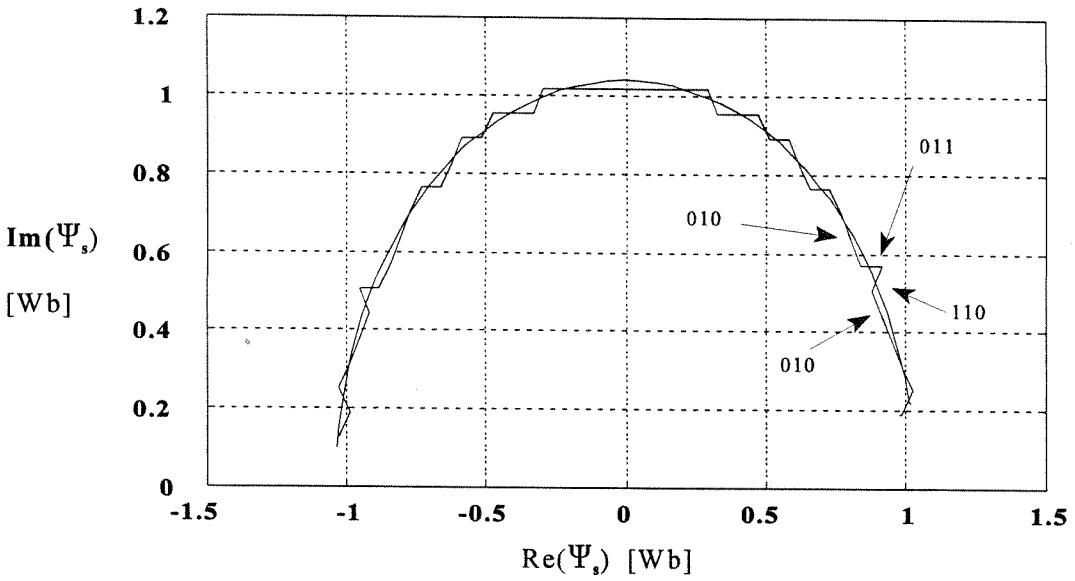

Fig. 4.14 Stator flux oriented discrete pulse modulation, SFDPM. Ψ_s is the trajectory of integrated branch voltage. The reference flux, Ψ_{ref}, is also shown.

In chapter 2. was shown that the link current stress increases with the number of branch switch-over's between active vectors, and a restriction to one BSO is preferable. This is called adjacent control. The influence of adjacent control on the inverter output is shown in Fig. 4.15.

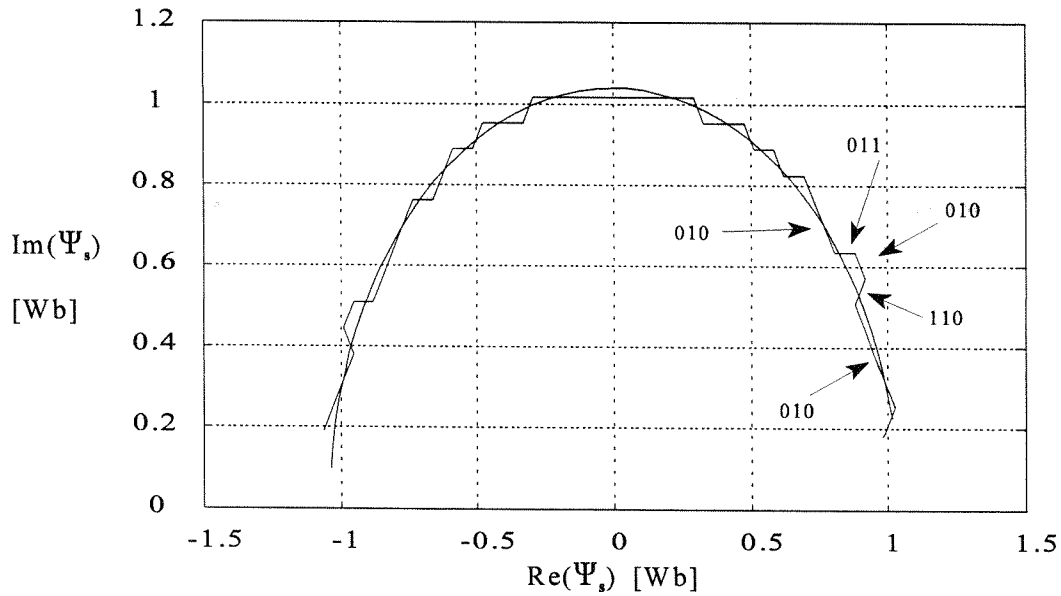

Fig. 4.15 Stator flux discrete pulse modulation, SFDPM, with adjacent state control.

The adjacent control increases the amplitude and angle error of the modulator. This is shown clearly in the time domain on Fig. 4.16.

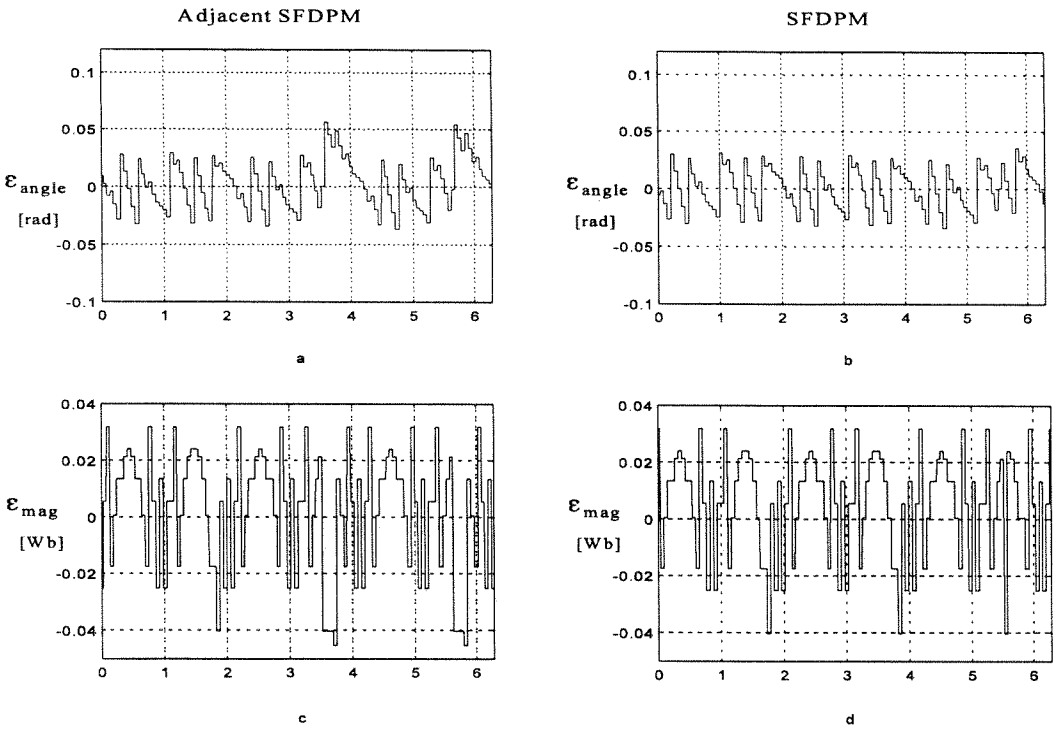

Fig. 4.16 SFDPM with adjacent control and without adjacent control. A whole fundamental period is shown, f_{res} = 45 [Hz]. The x axis are in [rad].
a,b : Angle error $e_{angle} = \theta_{ref} - \theta_s$.
c,d : Amplitude error $e_{mag} = |\Psi_{ref}| - |\Psi_s|$

The peak-peak value of the error using the adjacent control is increased. According to Table 4.5 this increases the torque ripple of induction machines.

4.6 Comparison of SDM, SVSDM and SFDPM control

The three modulators are simulated in a Matlab program. A system consist of constant Voltage/frequency control, modulator, resonant inverter and load. The link voltage of the RDCLI is modelled by eq. 4.37.

$$v_{do} = V_d(1 - \cos(2\pi f_{res} t)) \qquad \textbf{(4.37)}$$

where
V_d : DC-link voltage, V_d = 500 [V]
f_{res} : resonant link frequency, f_{res} = 41 [kHz]

The load is an ABB induction machine MT100LB28-4. Both a and b and parameters used are shown in App. B. The simulated system is shown in Fig. 4.17.

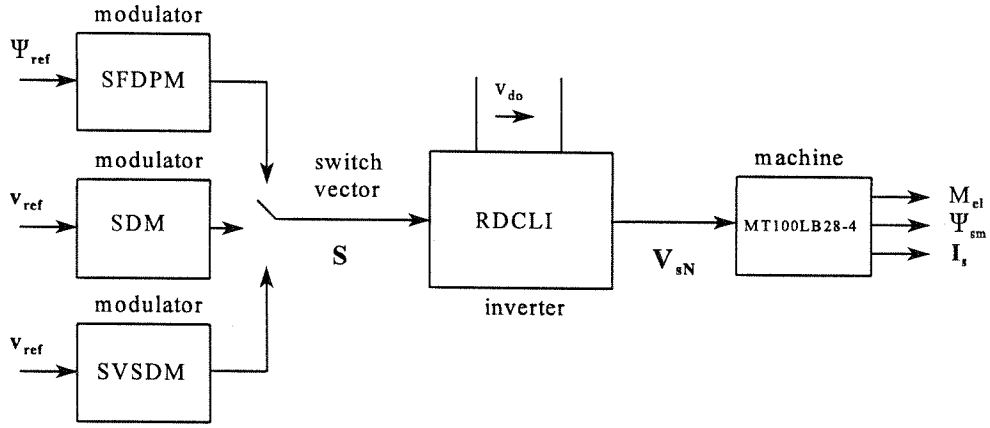

Fig. 4.17 The simulation system used for evaluation of three modulation strategies.

The nominal voltage of the machine is 400 [V], and the nominal frequency is $f_N = 50$ [Hz]. The flux amplitude of the reference flux is 0.92 [Wb]. This is calculated from eq. 4.35 using the phase-phase voltage value $V_d = 500$ [V] and a $f_1 = 50$ [Hz].

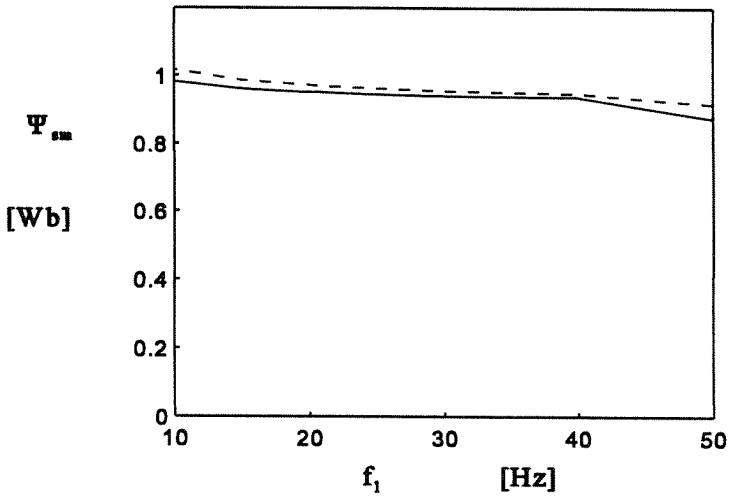

Fig. 4.18 Induction machine flux, using an open loop Voltage/frequency control.
Full line: Torque load = 21.0 [Nm]
Dotted line: Torque load = 1.8 [Nm]

The machine is loaded with a simple load. The amplitude of the machine flux Ψ_{sm} is shown in Fig.4.18. The stator resistor voltage drop is compensated by a compensation current, related to the load torque of the machine. Eg. for $M_{load} = 20$ [Nm], $I_{comp} = 7.1$ [A]. $V_{comp} = R_s I_{comp}$. This is not very accurate, but it is simple and therefore used.

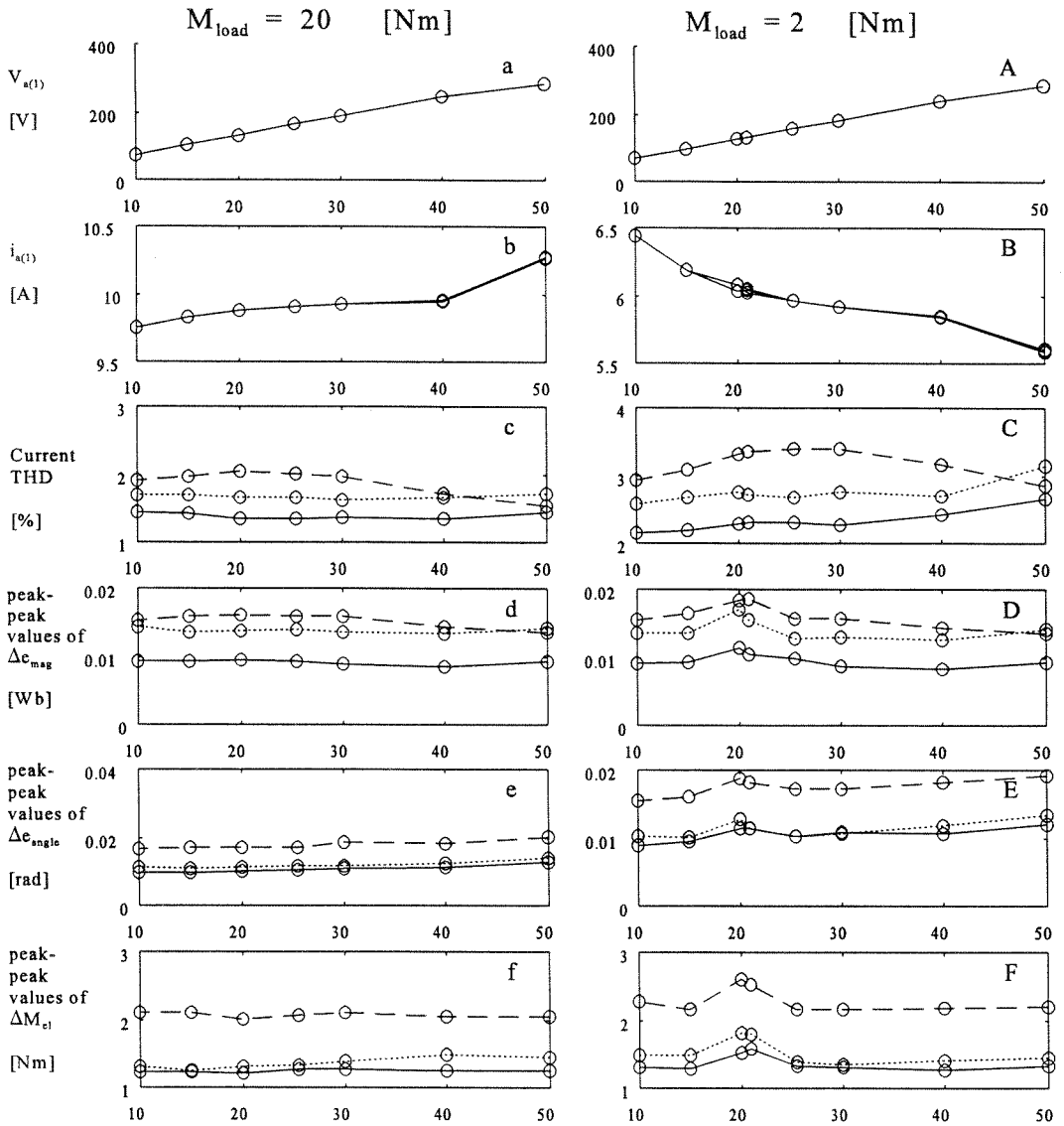

Fig. 4.19 The dashed lines are SDM, dotted lines are SVSDM and full line are SFDPM results. At the x-axis reference frequency in [Hz] is shown.

a,A : Fundamental of phase voltage $\hat{v}_{an}$ of the modulators,
b,B : Fundamental of phase current $\hat{i}_{an}$ of the modulators,
c,C : THD of phase current harmonics to $2f_{res,}$
d,D : Peak-peak values of magnitude error $\Delta e_{mag} = |\Psi_{sm}|-|\Psi_r|$,
e,E : Peak-peak values of angle error $\Delta e_{angle} = \theta_{sm} - \theta_r$,
f,F : Peak-peak values of torque $\Delta e_M = M_{el}$.

The THD is defined as follows:

$$THD = \frac{\sqrt{\sum_{h=2}^{2f_{res}/f_1} i_h^2}}{i_1} \qquad \textbf{(4.38)}$$

The torque ripple is related to the angle error which is seen from Fig. 4.19 e,f and E,F. Just as interesting, it look as current THD is related to the amplitude error of the flux, this is seen form

4.19 c,d and C,D.

The number of simulations is increased and simulation of torque ripple and THD is made for the following operation points:

f_1	[Hz]	= [50	40	30	25.5	21	20	15	10];
M_{load}	[Nm]	= [21.0	19.0	15.9	1.9	10.9	7.9	5.8	1.8];

and the stator voltage drop is compensated by $R_s I_{comp}$.

I_{comp} = f(Mload)= [7.1	6.4	5.7	5.7	5.7	4.9	4.2	3.5];	

By testing three different modulators a total of 192=3x8x8 simulations was made. A simulation speed, real time ratio of 600 was accomplished. The program extract all relevant data and save them automatically. The programme was running approximately 24h and the simulation was finished.

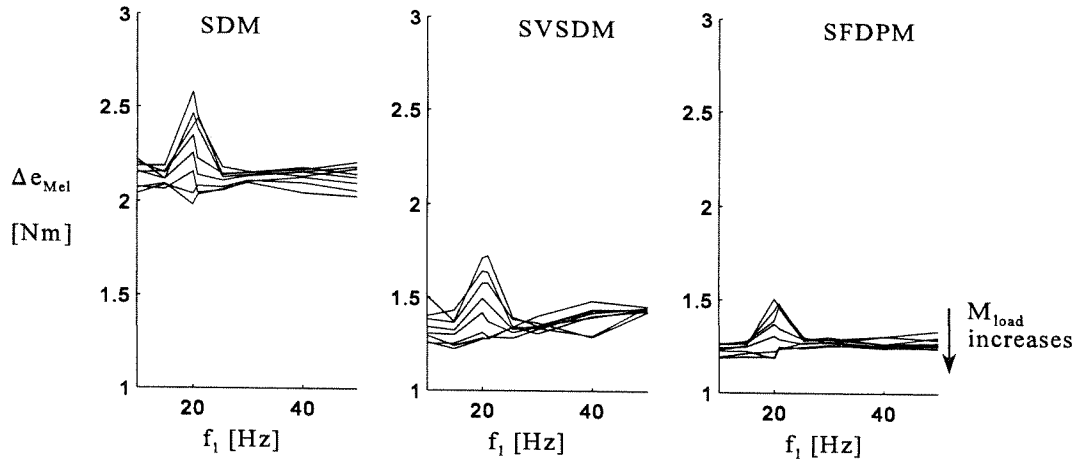

Fig. 4.20 Evaluation of three modulators, peak-peak torque ripple Δe_{Mel} versus fundamental frequency, f_1 and load torque M_{load}.

For every single modulator, the average $\Delta e_{Mel}(f_1)$ is calculated, the result is 8 numbers, then the average of the 8 numbers is calculated. This number represent the torque ripple performance of the modulator and the number is named: $Avg\_\Delta e_{Mel\_Xmodulator\ name}$. The ratio of two modulators is named: Q_{Mel} and defined:

$$Q_{Mel} = \frac{Avg\_\Delta e_{Mel\_Xmodulator}}{Avg\_\Delta e_{Mel\_SFDMP}} \qquad \textbf{(4.39)}$$

Xmodulator	SDM	SVSDM	SFDMP
Q_{Mel}	1.7	1.1	1.0

Table 4.6 Xmodulaor is either SDM, SVSDM or SFDMP, Q_{Mel} a measure of relative torque ripple produced by the modulators.

An evaluation of current THD is also made.

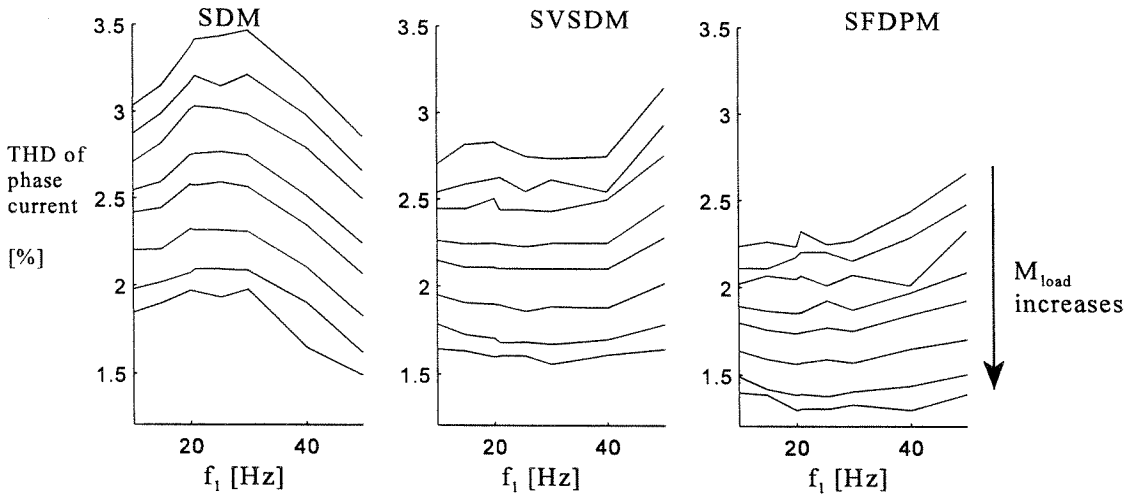

Fig. 4.21 Evaluation of three modulators, THD of phase current versus fundamental frequency, f_1 and load torque M_{load}.

For every single modulator, the average THD(f_1) is calculated, the result is 8 numbers, then the average of the 8 numbers is calculated. This number represent the current THD performance of the modulator, the number is named: $Avg\_THD_{\_Xmodulator\ name}$. The ratio of two modulators is named: Q_{Mel} and defined:

$$Q_{THDi} = \frac{Avg\_THD_{Xmodulator}}{Avg\_THD_{SFDMP}} \qquad \textbf{(4.40)}$$

Xmodulator	SDM	SVSDM	SFDMP
Q_{THDi}	1.4	1.2	1.0

Table 4.7 Xmodulator is either SDM, SVSDM or SFDMP, Q_{THDi} a measure of relative current THD produced by the modulators.

In this paragraph is concluded that the THD analysis of the phase current show SFDMP compared to SFDMP and SDM is better. It can also been seen that the flux amplitude error has dominating influence on the current THD.

The torque ripple analysis of the phase current shows that the SFDMP compared to SFDMP and SDM better. There was a reason to expect this since the SFDMP was designed with the purpose to minimize the torque ripple. And it was also assumed that flux angle error has dominating influence on the torque ripple.

The implementation of SDM and SFDMP is simpler than SFDMP. SFDMP relative performance to SVSDM measured by Q_{Mel} and Q_{THD} is below 20 % better. The simpleness of the SVSDM is ranked higher than the reduced performance compared to SFDMP. Therefore the SVSDM is selected to be implemented in the laboratory.

4.7 Conclusion

Three modulators are described:

- Sigma Delta Modulator, SDM /1/,/5/
- Space Vector Sigma Delta Modulator, SVSDM /5/,/6/,/15/,/16/
- Stator Flux orientated Discrete Pulse Modulator, SFDPM

The modulators are controlled either by voltage or flux references, the modulators only need an internal feedback loop. The voltage SDM, SVSDM and the flux controlled modulator SFDPM are compared by a simulation study. The SFDPM is not seen reported in any paper and is considered new. It is shown that the flux controlled modulator, performs better than the voltage controlled sigma delta modulator on the following points.

1: The THD analysis of the phase current shows that the SFDMP compared to SVSDM produce a current with 20% lower THD. The SFDMP compared to SDM produce a current with 40% lower THD.

2: The torque ripple shows that the SFDMP compared to SVSDM produce a torque with 10% lower ripple. The SFDMP compared to SDM produce a torque with 70% lower ripple.

The performance of SFDMP and SVSDM are quite close and the implementation of SVSDM is more simple. Therefore SVSDM is selected for implementation in the realized resonant converter.

Experimental results are shown, they verify the converter is able of working at DC link voltages of 300 V and 500 V.

5

The Voltage Peak Control strategy, VPC

Control of the resonant link voltage peak is a challenge that can, and has been, attached, in many ways. Five approaches used in parallel resonant converters are:

- Passive clamp circuit /2/, /3/
- Active clamp circuit /4/
- Non clamped, increased resonant inductor current approach /7/,/14/
- Link current initialization approach using auxiliary circuit /8/,/9/
- Link current initialization approach without using auxiliary circuit /10/,/11/,/12/

Except the active clamp circuit the link voltage peak is ideally controlled to twice the DC link voltage level or a bit higher. Using an active clamp, voltage peaks are around 1.3 times the DC link voltage. The voltage peak control strategy dealt with here is described in /10/,/11/,/12/ and is called VPC. It is first described in /12/ and in this report the dervison of the VPC strategy is described more matematical precisely. The dervison is made using a loss less resonant circuit. Then VPC is impemented in a real resonant converter where it is concluded the resonant circuit loss cannot be ignored. An extened discussion of the VPC strategy is done, where the effect of ohmic losses, load current changes during a resonant period and delay in the control electronics are included.

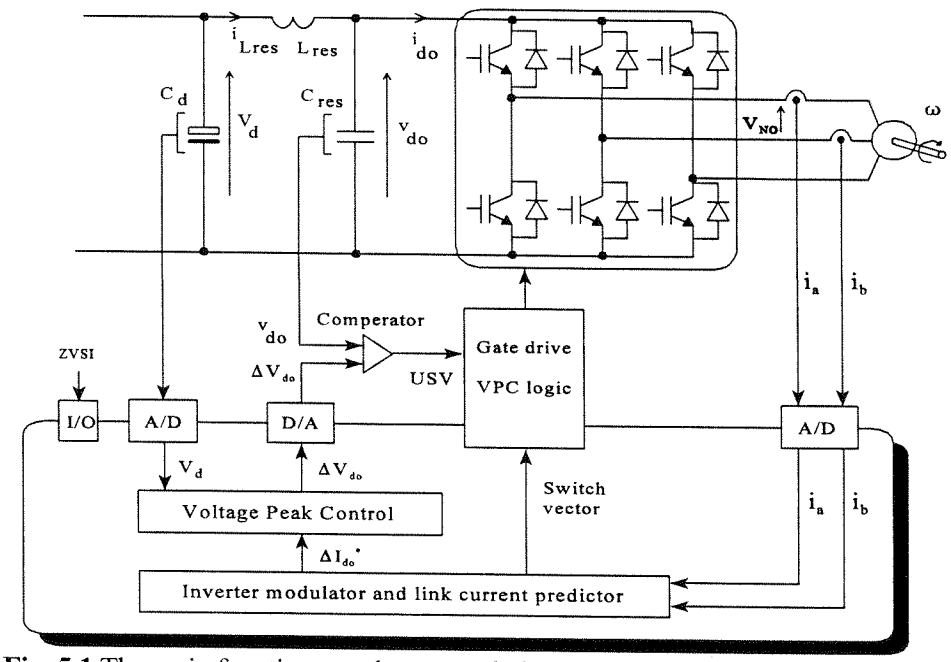

Fig. 5.1 The main functions used to control the resonant peak link voltage in resonant

The increased complexity due to many parameters makes it necessary to use a numerical solution. For real time application, the results from the numerical solution are used to make a VPC function table. The VPC table is implemented in the ADSP 21020 DSP system. Finally, experimental results are shown using the short circuit method and the non-short circuit method shown in chapter 3. The main VPC circuit is shown in Fig. 5.1.

5.1 Link Voltage Peak Control

The parallel RDCL converter proposed in /1/ has an oscillating link voltage due to the resonant link circuit, L_{res} and C_{res}. It is shown in Fig. 5.2.

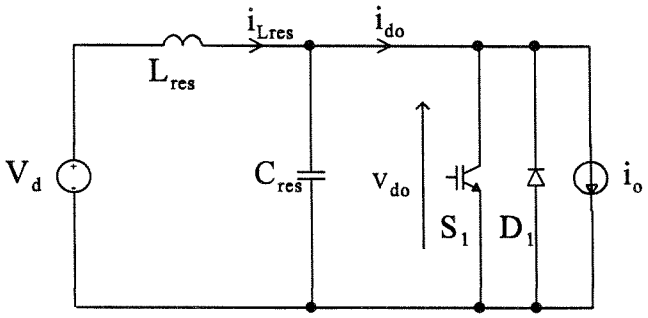

Fig. 5.2 Ideal resonant inverter.

If the circuit is considered ideal and unloaded, the link voltage v_{do} is given by

$$v_{do} = V_d\left(1 - \cos\left(2\pi f_{res} t\right)\right)$$

$$f_{res} = \frac{1}{2\pi}\,\frac{1}{\sqrt{L_{res}\,C_{res}}} \qquad \textbf{(5.1)}$$

where

V_d : DC-link voltage
L_{res} : Resonant inductor
C_{res} : Resonant capacitor
f_{res} : Resonant frequency

From eq. 5.1 it is seen that the link peak voltage is $2V_d$ and the minimum voltage is zero. The equation of the resonant link voltage v_{do} is shown in eq. 5.2 and based on Fig. 5.2

$$v_{do} = \underbrace{Z(i_{L(0)} - m)\sin(\omega t)}_{\text{part one}} + \underbrace{V_d + (v_{do(0)} - V_d)\cos(\omega t)}_{\text{part two}} \qquad \textbf{(5.2)}$$

where:

$i_{L(0)}$: initial resonant inductor current
$v_{do(0)}$: initial resonant capacitor current
m : load current equal to i_o in Fig. 5.2, m = constant
ω : angular frequency = $2\pi f_{res}$
Z : resonant impedance = $\sqrt{L/C}$

Eq. 5.2 describes the behaviour of the resonant link voltage and a discussion of voltage limiting methods derived from this equation is carried out.

The amplitude of the sine function in eq. 5.2 part one is $Z(i_{L(0)} - m)$, due to the fact the sine function is phase shifted 90 ° relative to $V_d+(v_{do(0)} - V_d) \cos(\omega t)$ both a positive and a negative amplitude would increase the peak value of v_{do}. But for a zero value of $Z(i_{L(0)} - m)$ the peak value of v_{do} is limited to $2V_d$, assumed $v_{do(0)} =0$. One way of link voltage control is therefore to ensure that $(i_{L(0)} - m)$ always is zero. This method is described in /9/, but unfortunately this control requires an initial current that increases the number of power electronic components.

If part one of eq. 5.2 is assumed to be zero, it is seen that the peak value of v_{do} can be limited below $2V_d$ by choosing a positive value of $v_{do(0)}$. Unfortunately is the zero voltage interval lost both at the beginning of the resonant period and the end of the resonant period, because v_{do} is oscillating between $v_{do(0)}$ and $2Vd-v_{do(0)}$.

If part one of eq. 5.2 is not zero the peak value of v_{do} is increased but this increase could be eliminated by selection a proper value of $v_{do(0)}$. It is well known that the addition of two trigonometric function with same argument can be rewritten to just one trigonometric function. This is done in order to get an idea of how to derive a control equation. Eq. 5.2 is rewritten to eq. 5.3.

$$v_{do} = V_d - \sqrt{Z^2(i_{L(0)} - m)^2 + (v_{do(0)} - V_d)^2} \cos(\omega t + \delta) \qquad \textbf{(5.3)}$$

where

$$\delta: \operatorname{atan}\left(\frac{Z(i_{L(0)} - m)}{V_d - v_{do(0)}}\right)$$

The amplitude of the cos function in eq. 5.3 must be V_d to ensure the v_{do} reaches zero voltage at the end of the resonant period. This is the background for eq. 5.4.

$$V_d = \sqrt{Z^2(i_{L(0)} - m)^2 + (v_{do(0)} - V_d)^2} \qquad \textbf{(5.4)}$$

With a proper selection of the initial conditions $i_{L(0)}$ and $v_{do(0)}$ it is possible to control the peak value of v_{do} to 2 V_d.

In order to derive the voltage peak control equation and give an overview of the control principle the analysis is extended to include the resonant-link current shown in eq. 5.5.

$$i_L = (V_d - v_{do}) \sin(\omega t) + Zi_{L(0)} \cos(\omega t) + Zm(1 - \cos(\omega t)) \qquad \textbf{(5.5)}$$

The current equation is rewritten to contain a single trigonometric function.

$$Zi_L = Zm + \sqrt{Z^2(i_{L(0)} - m)^2 + (V_d - v_{do(0)})^2} \sin(\omega t + \delta) \qquad \textbf{(5.6)}$$

Equations 5.3 and 5.6 are used to describe the behaviour of the resonant link circuit in a phase plane plot. The phase plane plot equation is

$$(v_{do},Zi_L) = V_d + jZm + \sqrt{Z^2(i_{L(0)} - m)^2 + (v_{do(0)} - V_d)^2}\ (-\cos(\omega t + \delta) + j\sin(\omega t + \delta)) \quad (5.7)$$

Eq. 5.7 is a very useful equation and it is explained in more details. A phase-plane plot is shown in Fig. 5.3

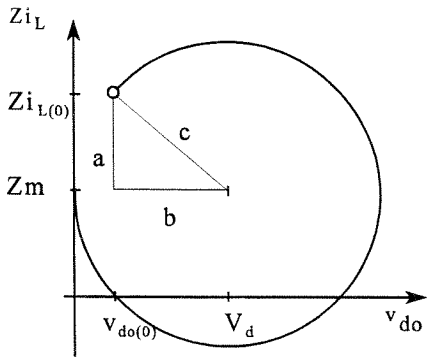

Fig. 5.3 Phase-plane plot of steady-state situation where:
$a = Z(i_{L(0)}-m)$, $b = V_d - v_{do(o)}$, $c = Vd$

From Fig. 5.3 and eq. 5.7 it is seen that the trajectorie has the following properties.

1. The center of the circle is (V_d, Z_m)
2. The distance from the coordinate giving by the initial values $(v_{do(0)}, Zi_{L(0)})$ and the center of the circle is the radius of the circle.

It is now possible to draw two circles with different m, where m is the current flowing through the inverter, and from simple geometric calculation determine a control equation that ensures the resonant link voltage peak to be limited to $2V_d$.

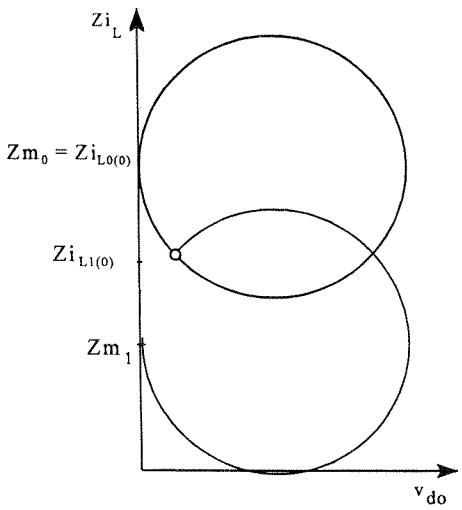

Fig. 5.4 A link current step from m_0 to m_1.

Under the assumption that the resonant circuit is ideal the VPC equation derived

$$v_{do(0)} = V_d(1 - \cos(\text{asin}\left(\frac{Z(m_1 - m_0)}{2V_d}\right))) \qquad \textbf{(5.8)}$$

where

m_0	:	link load current before change
m_1	:	link load current after change
V_d	:	DC link voltage
Z	:	resonant impedance
$v_{do(0)}$	:	initial resonant capacitor voltage

Using eq. 5.8 it is ensured the resonant circuit initial conditions that limit the resonant voltage v_{do} to 2 V_d are present.

It is possible to derive the initial condition $v_{do(0)}$ from eq. 5.4 directly.

If $m_1 - m_0$ is larger than 2 V_d/Z_{res}, the two trajectories do not collide. The current $m_1 - m_0$ must be less than 2 V_d/Z_{res} to ensure the VPC strategy works.

The eq. (5.8) is derived with the conditions that the three arguments V_d, Z_{res} and i_{do} are constant during the resonant period and the resonant circuit is without loss. The conditions are discussed in the following:

V_d To reduce the error the DC voltage, V_d , can be measured directly and this is quite simple because the dynamical change of V_d is small compared with the resonant link frequency.

Z_{res} The impedance Z_{res} is determined by the component values of C_{res} and L_{res}. The capacitance could change significantly by capacitive load of the inverter. In the following it is assumed that the load capacitance is zero. The inductance changes if saturation of the inductor core occurs. Measurements have been carried out in /13/ and an aproximated function of the inductance is:

$$L_{res} = 150 - 0.015 i_{Lres} \quad [\mu H] \qquad \textbf{(5.9)}$$

An inductance of 148 [µH] is used in the following. A quality factor of Q=110 was measured for the actual resonant circuit with C_{res} = 100 [nF].

i_{do} During one resonant cycle it is assumed that the DC link current i_{do} is constant.
The i_{do} changes due to the non-infinite value of the load inductance. The effect of the resonant link is a change of the circuit energy. If the resonant energy is decreased or increased too much during one resonant period this has a substantial negative influence on the VPC ability to control the resonant DC link voltage peak. The change of i_{do} is considered in the following.

5.2 Analysis of DC link with losses

The equivalent circuit in Fig. 5.2 is extended to include the equivalent serial resistor R. The circuit is shown in Fig 5.5.

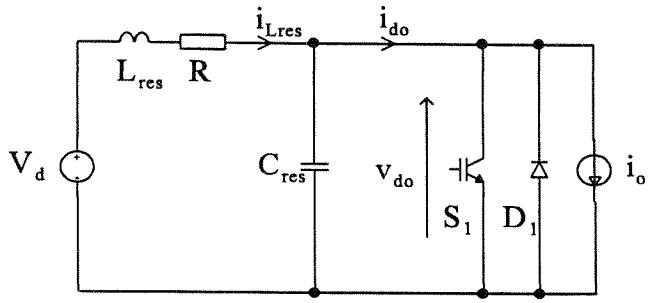

Fig. 5.5 Equivalent circuit of a resonant DC link converter, with resonant link losses concentrated in R.

The load is modelled by a current generator i_o

$$i_o = kt + m \qquad \textbf{(5.10)}$$

where

k : di_{do}/dt

m : DC value

Often the link current can be considered constant in the time interval of interest, but with a resonant period of approximately 20 [μs] the current can change several amperes and the influence is discussed in the following.

The change of i_o has significant influence on the resonant circuit. Here the influence of a fast change and a slow change is discussed.

A negative $\Delta i_{do} = i_{do\_old} - i_{do}$ during the zero voltage period generates an increase of the zero voltage period, and a positive Δi_{do} step during the zero voltage period generates an excessive link voltage peak.

A physical description of the resonant circuit behaviour is used to explain the influence of i_{do} when it is not a step function but a ramp function as kt in eq.5.10. The slope k can be both positive and negative, eg. if the load is a RL load, the slope is positive, but k is negative in the case of the turn off tail current of an inverter IGBT.

The V_d-L_{res}-R part of the resonant circuit is a low impedance path for low frequency signals, and C_{res} is a low impedance path for high frequency signals. In the case of a current step that generates an infinite high di/dt, the current is flowing through the low impedance path provided by C_{res}.

For a low di/dt signal only a fraction of the current flows through C_{res}. Simulation studies of k = 0.05..0.25 [A/μs] show that L_{res} carries most of the current and the change of the resonant circuit energy is small.

It is noticed that a k=0.25 [A/μs], which is equal to a ramp current peak of 5 [A] during a 20 [μs] period, has little influence on the energy change of C_{res}, but it has a huge influence on the voltage peak control strategy. This is seen in Fig. 5.6 by using a phase plane plot. In the plots the resonant inductor current i_{Lres} is plotted versus the resonant link voltage v_{do}.

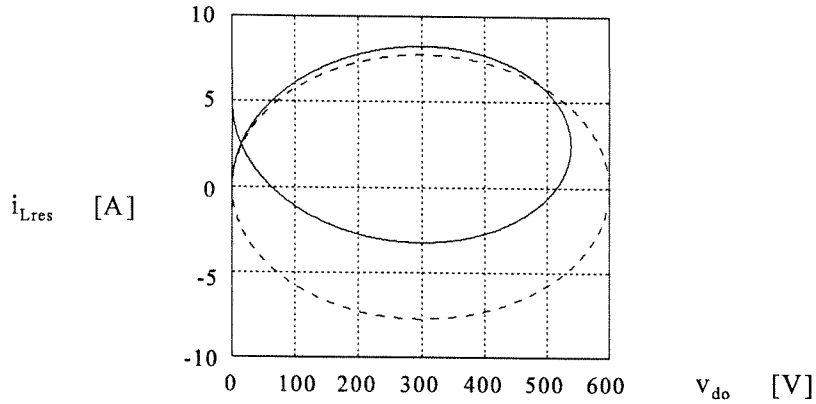

Fig. 5.6 Phase plane plot showing the influence of current i_{do} change, i_{do}=kt, during the resonant period. The dashed curve is with no current change ,k=0, and the full curve shows the influence of a current change of k=DI·f_{res} k=0.21 [A/μs], V_d=300 [V].

The voltage drop due to kt, where DI = 5 [A] and f_{res} = 42 [kHz] in Fig. 5.6, is explained by the v_{do} equation for the circuit shown in Fig.1. The whole equation, including the effect of R, is shown later. Here it is assumed that R,$v_{do(0)}$ are zero and $i_{L(0)}$=m=0.

$$v_{do} = (V_d - kL)(1 - \cos\omega t) \qquad \textbf{(5.11)}$$

The factor kL is the reason why the full curve showing v_{do}, only reaches approx. 538 [V]. The voltage drop is

$$\Delta V(k) = 2kL_{res} = \frac{1}{\pi} DI\,Z \qquad \textbf{(5.12)}$$

Using k=DI·f_{res} and L_{res} = 142 [μH] , f_{res} = 41 [kHz] , DI = 5 [A] is ΔV(k) = 62 [V]. In case k was negative, the peak voltage increase would be 62 [V]. A limitation of ΔV(k) can be done by a decrease of the resonant impedance or DI.

Now an estimate is made of the link current change DI during a resonant period using the induction machine parameters and the dynamic equivalent circuit shown in App. B. It is, however, assumed that:

R_s, R_r = 0
$j\omega\Psi_r$ = 325 [V]
Lss+Lsr = 21 [mH]

and the average of $\mathbf{V}_s$ during the resonant period is $V_s = -{}^2/_3 V_d$. V_d = 550 [V.] The current rate is then

$$k = \frac{j\omega\Psi_r - V_s}{L_{ss} + L_{sr}} \qquad \textbf{(5.13)}$$

The value of k is calculated to 32.32 [kA/s], from this DI is found to be DI=0.8 [A] for f_{res}=41 [kHz]. The k value is used in the calculation of the VPC table.

In Fig. 5.7 the influence of the resistor R is shown. The resistor causes an energy loss that results in a decrease of the voltage amplitude.

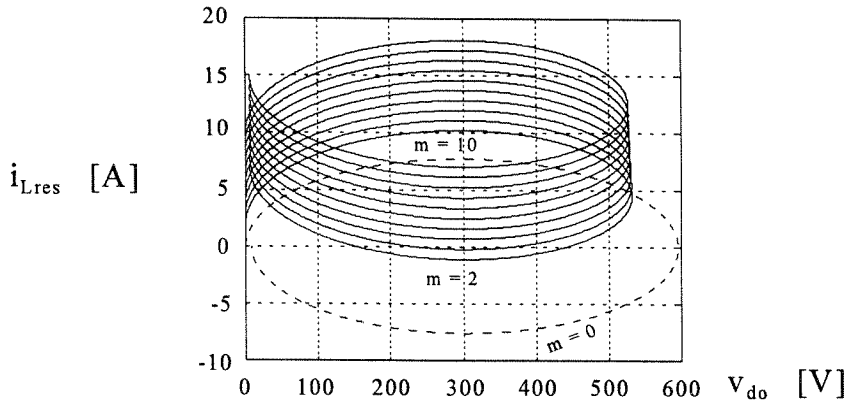

Fig. 5.7 Phase plane plot showing the influence of the resistor R and the current i_{do} changing during a resonant cycle. The full lines are for increasing m = [2..10] values and DI = 5 [A] the dotted line is for m=0 and DI =0. In all cases R = 0.35 [Ω].

The link voltage equation is:

$$\begin{aligned} v_{do} = &(L_{res}\omega^2(i_{Lres(0)} - m) + RC\omega^2 v_{do(0)})\frac{1}{\beta}e^{-\alpha t}\sin\beta t + v_{do(0)}e^{-\alpha t}(\cos\beta t - \frac{\alpha}{\beta}\sin\beta t) \\ &+ (V_d - mR - kL_{res})(1 - e^{-\alpha t}(\cos\beta t + \frac{\alpha}{\beta}\sin\beta t)) \\ &- kRt + kR\frac{2\alpha}{\omega^2} - \frac{kR}{\beta}e^{-\alpha t}\cos(\beta t + \phi) \end{aligned} \qquad \textbf{(5.14)}$$

and the current equation for i_{Lres} is:

$$\begin{aligned} i_{Lres} = &\frac{V_d - v_{do(0)}}{L_{res}\beta}e^{-\alpha t}\sin\beta t + i_{Lres(0)}e^{-\alpha t}(\cos\beta t - \frac{\alpha}{\beta}\sin\beta t) \\ &+ m(1 - e^{-\alpha t}(\cos\beta t + \frac{\alpha}{\beta}\sin\beta t)) \\ &+ kt - \frac{2\alpha k}{\omega^2} + \frac{k}{\beta}e^{-\alpha t}\cos(\beta t + \phi) \end{aligned} \qquad \textbf{(5.15)}$$

and the constants used are:

Constant name	Constant expression
α	$\frac{R}{2L_{res}}$
ω	$\frac{1}{\sqrt{L_{res}C_{res}}}$
β	$\sqrt{\omega^2 - \alpha^2}$
ϕ	$\tan^{-1}(\frac{\beta^2 - \alpha^2}{2\alpha\beta})$

The eq. (5.14) and eq. (5.15) are derived in App. A.

In Fig. 5.7 the v_{do} does not resonate down to zero voltage because there is not compensated for the loss in R. The loss compensation can be done by initiating the resonant period with $i_{Lres(0)} = \Delta I_{Lres} + m$. Where ΔI_{Lres} is the current used to overcome losses in the resonant circuit and this value is calculated from eq. 3.1.

Before using eq. 5.14 and eq. 5.15 for analysis of the resonant link is a verification of their validality done. In Fig. 5.5 the equivalent circuit of the resonant link simulated in PSpice is shown and in Fig. 5.8 is the simulation result compared with the curves obtained from eq.5.14 and eq.5.15.

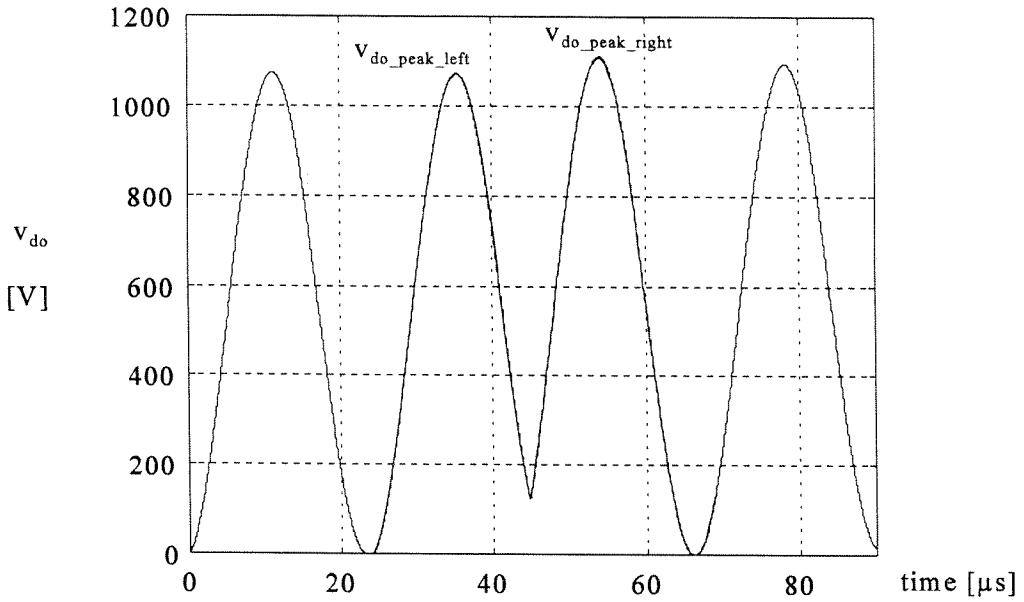

Fig. 5.8 Verification of eq.5.14 and eq.5.15. Here the simulated v_{do} from PSpice and v_{do} from eq. 5.14 are shown.

Notice that the value of ΔV_{do} is calculated using both eq. 5.14 and eq. 5.15. The calculation of ΔV_{do} is described in the next paragraph. The calulated and simlated curves agree very well and eq. 5.14 and eq. 5.15 are used for further work. Table 5.1 shows some characteristic values.

	i_{Lres} at ΔV_{do}	ΔV_{do}	v_{do} peak left side ΔV_{do}	v_{do} peak right side ΔV_{do}
PSpice simulation	9.72	122.5	1072	1110.6
eq.5.5 and eq.5.6	9.63	122.7	1073	1107.3
Deviation [%]	-0.9	0.2	0.1	-0.3

Table 5.1 characteristic values from Fig. 5.8.

In the following it is described how ΔV_{do} is calculated and how to deal with parameter variations.

The change of link current m, to a lower value, generates a current step that generates a link voltage peak above twice V_d, if the current change is sufficient large. In Fig. 5.9 five full circles are shown and one dashed circle. A jump from one of the full circles to the dashed circle is done by a step decrease of link current m.

According to the idea of the voltage peak control, is the excessive voltage peak avoided if the change from a full circle to the dashed circle happens at the intersection point marked by a small circle in Fig. 5.9. The value of v_{do} at the intersection point is equal to ΔV_{do} and ΔV_{do} is the voltage level where the current change $\Delta i_{do} = i_{doold} - i_{do}$ must happen to ensure a voltage peak limitation to $2V_d$.

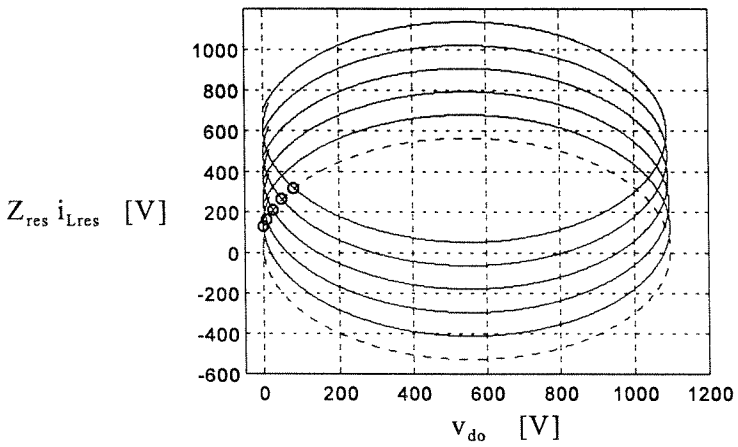

Fig. 5.9 Phase plane plot based on i_{Lres} (eq.5.15) and v_{do} (eq.5.14). The value of v_{do} at points of intersection is the $\Delta V_{do}=f(V_d,m,k,R,I_{Lres(0)},v_{do(0)},L_{res},C_{res})$, the intersection points of interests are marked by circles. The link current m is m=0..15 [A], the other parameters are constant.

The intersection points marked by circles in Fig. 5.9 are found by iteration. Finding an analytical equation, like eq.5.8, has not been possible. The values of ΔV_{do} calculated from Fig. 5.9 are plotted as a function of m in Fig. 5.10. The Δi_{do} is equal to m in this case since $\Delta i_{do} = i_{doold} - i_{do}=m-0$.

When parameters change, the change is most visible on the last half of the phase plane plot. Since the intersection points of the dotted line, Fig. 5.9, are between zero and $\pi/2$ [rad], the parameter changes have relatively small influence on the location of the intersection points.

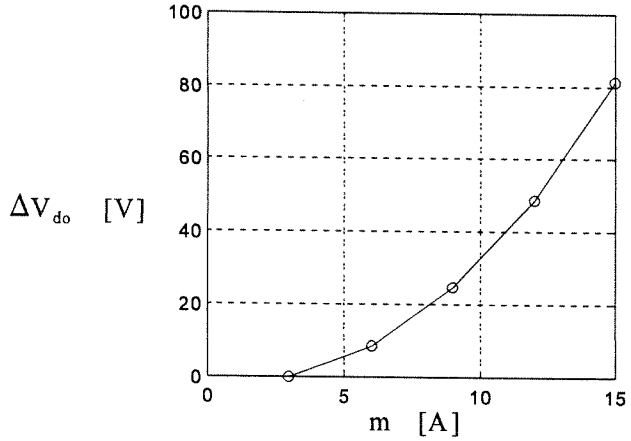

Fig. 5.10 Link voltage values ΔV_{do} as a function of link current change m. V_d=550 [V],m=3..15 [A], k=33.1[kA/s],R=0.35 [Ω],$I_{Lres(0)}$=3.4 [A],$v_{do(0)}$ = 0, L_{res}=148[μH],C_{res}=100 [nF].

Some parameters are used to calculate ΔV_{do} change significantly, and the influence of the parameters is considered in the following. The parameters looked at are V_d, m, k, $I_{Lres(0)}$ and t_d. Where t_d is the delay in electronics. To compensate the delay t_d, the signal that updates the switch vector and generates the link current change, must be generated earlier. ΔV_{do} is calculated for m= 2..15 [A] and for a fixed value of DI, $i_{Lres(0)}$,V_d,t_d.

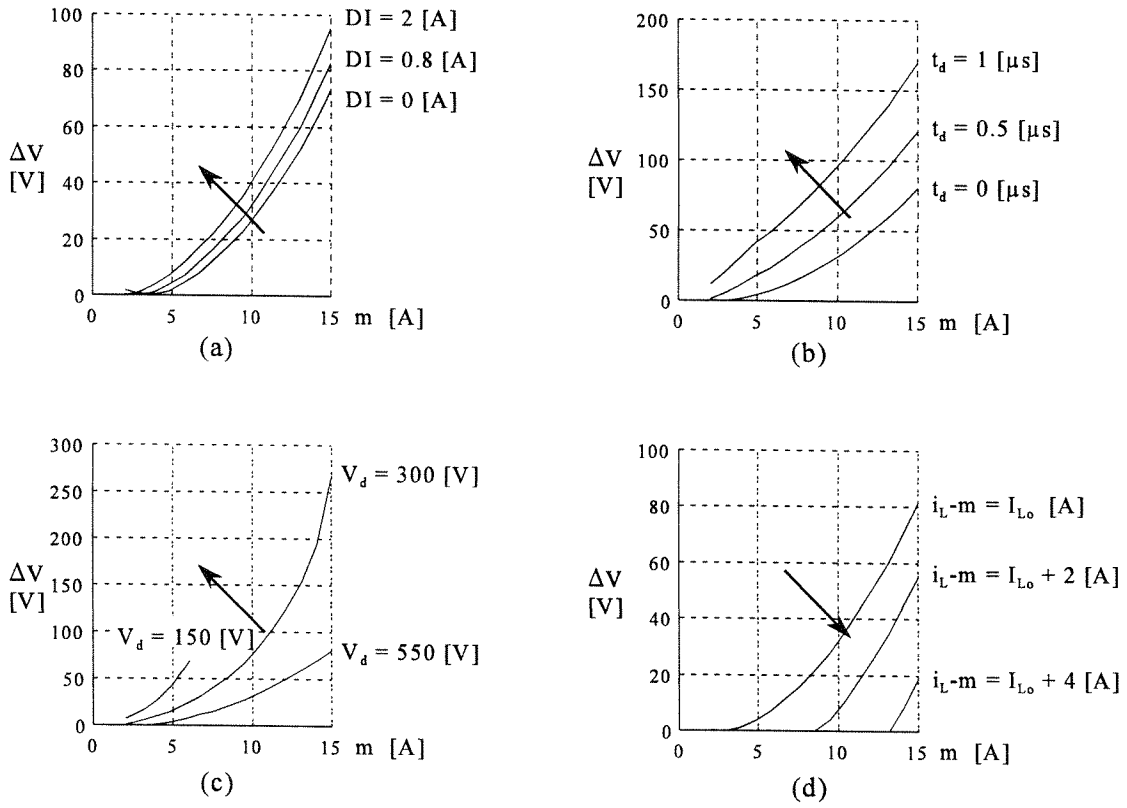

Fig. 5.11 The influence of parameter changes in four cases
a) Different DI b) different t_d c) different V_d d) different (i_{Lres}-m)

It is clear by looking at Fig. 5.11.a to Fig. 5.11.c that an increase of DI, t_d and decrease of V_d leads to an increase of ΔV_{do}. What is the effect of this on a resonant converter?. Clearly, if

ΔV_{do} is not increased, in the nine cases shown in the three figures, there is more than adequate energy in the resonant link to ensure that the resonant voltage reaches zero voltage and keeping the resonance on going. A second effect of keeping ΔV_{do} smaller than required is the link voltage peak is increased. Unfortunately, there is a situation where too much energy in the resonant link can cause a zero voltage failure. This is explained from Fig. 5.12.
The dashed lines show that an increased resonant circuit energy can lead to a zero voltage failure. The failure is avoided if the ΔV_{do} is lowered.

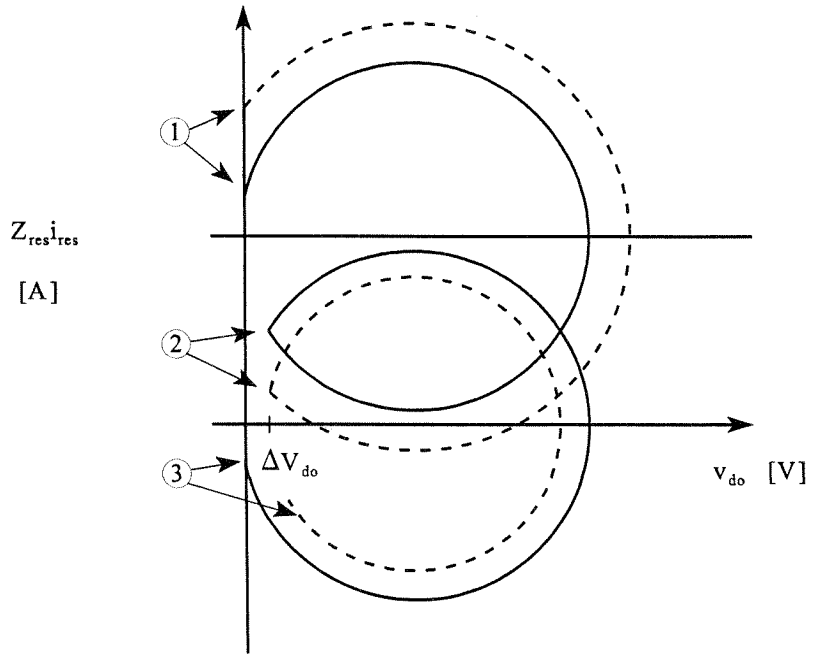

Fig. 5.12 The dotted line show an initalisation error leading to zero voltage failure.

When ΔV_{do} is calculated and the switch vector is updated, as shown in Fig. 5.12, wrong initial conditions cause zero voltage failure. A problem occurs if VPC is used, as in point 2. If ΔV_{do} is calculated for the full line situation, but due to initial current error in point 1, is used for the dashed line situation an error occur. The link voltage $v_{do}$is not resonating to zero voltage as shown in point 3.

In Fig. 5.12 is shown that ΔV_{do} needs to be deceased at increased resonant circuit energy. To compensate this problem the ΔV_{do} must be decreased by eg. 20 V depending on the level resonant circuit energy. Subtracting 20 V from ΔV_{do} sets a minimum ΔV_{do} where the VPC can not be used. As shown later in this chapter this problem is only serious using the short circuit method described in chapter 3. When using the non-circuit method the problem is reduced.

A result of the analysis of the parameters variations, is that a change of
DI : to a higher value
t_d : to a higher value
V_d : to a lower value
does not cause zero voltage failure but an increase of the resonant peak voltage. It is considered possible to choose DI, t_d and V_d in such a way, the operation conditions newer change them to values that cause zero voltage failure. From experimental experience it is known that increased resonant circuit energy, due to initial conditions,is a problem and causes zero voltage failure. The most serious initial condition errors occur if two succeeding VPC turn-off happen.

5.3 Implementation of the VPC principle using short circuit method

It is very important to know the resonant circuit state to ensure correct operation. In last paragraph was discussed how initial errors lead to zero voltage failure. Already in Chapter 3 was the problem of proper initialization of the resonant circuit discussed and a circuit, that ensured the ongoing resonance, was described and tested. The four different initial conditions are shown in Fig. 5.13.

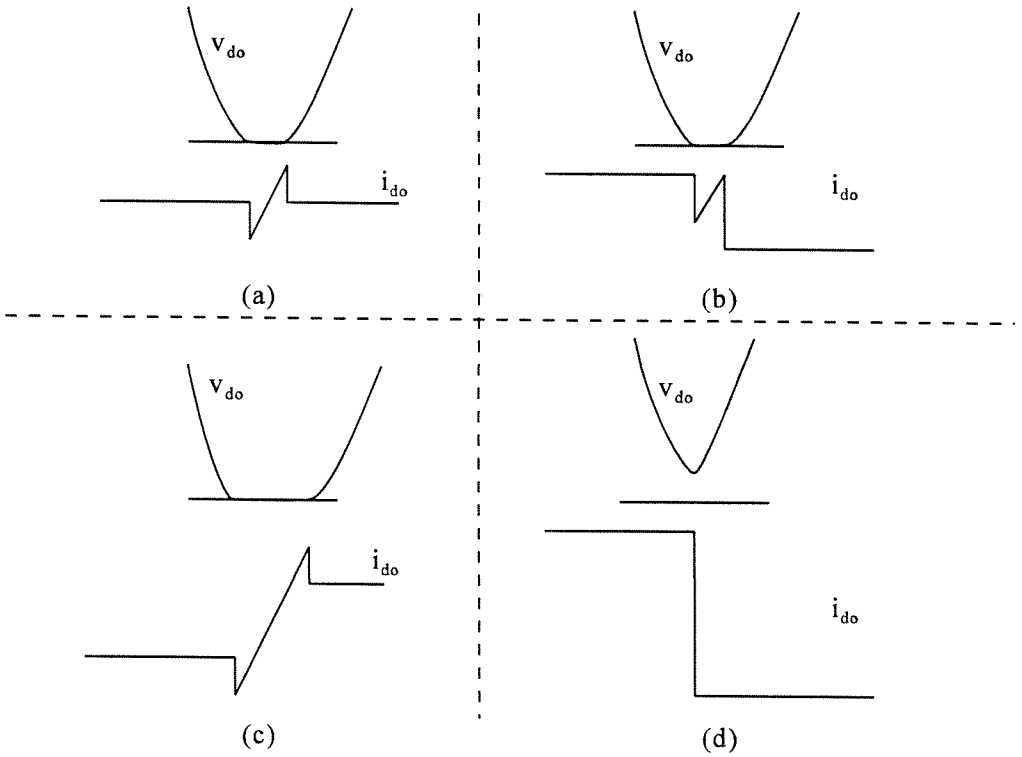

Fig. 5.13 Four situations of resonant circuit initial conditions.
a: No link current change. b: A link current change where VPC in not used.
c: Link current change. d: Link current change with VPC.

Here it is discussed what type of initialization circumstances that can create problems for the function of the VPC.

Fig. 5.13.a and Fig. 5.13.c. show two situations where the initial conditions of the beginning resonant period is well defined. The initial link voltage $v_{do(0)}$ is zero and the initial link current is $i_{Lres} = i_{do}$-m. The two situations are well suited for a VPC turn off at the next switch vector update. Circumstances shown in Fig. 5.13.b are more critical and a VPC turn off can fail here. The problem is that the switch vector update causes a link current change that is relative small. The link current change is not large enough for a VPC turn off, which is explained later on. It is explained in chapter 3, that there are circumstances where the resonance is lost if there is no short circuit of the link. As a consequence a short circuit is always done even if the link current change itself is sufficient to maintain the resonance, as in Fig. 5.13.b. The resonant energy is therefore in some cases larger than required and the initial conditions are not well defined. This situation is not good if a VPC turn off happens at next switch vector update, and a loss of resonance may happen.

Fig. 5.13.d shows a link current change where VPC is used. If two succeeding VPC turn-off's happen, where the first VPC turn off results in an increase of the resonant circuit energy, this would lead to a zero voltage failure.

A conclusion to the discussion of initial conditions is that the preferable initial state are shown Fig. 5.13.a and Fig. 5.13.c. The two states are preferred since the dominant parameter changes increase the resonant circuit energy. It is therefore desirable to avoid initial conditions that give unpredictable increase of the resonant circuit energy. Such a state is shown in Fig. 5.13.b.

A simple way to ensure only the state shown Fig. 5.13.a is used, before a VPC turn off is done by updating the switch vector every second time and not every time there is a zero voltage interval. Unfortunately this decreases the converter output voltage quality and it decreases the switching frequency. With a decreased switching frequency is the acoustic noise level increased.

Updating the switch vector every second time is only necessary using the short circuit method described in chapter 3. If the non-short circuit method is used the switch vector can be changed at every zero voltage interval.

Calculation of the VPC function

The resonant converter is working with a maximum DC link voltage of 300 [V] if the short circuit method is used.

In Fig. 5.1 is shown where the calculation of ΔV_{do} is done in the resonant converter. There is a functionally block and the input is the link current change Δi_{do}. Eksperimental testing of the VPC principle is made with following parameters

V_d	= 350	[V]
L_{res}	= 148	[μH]
C_{res}	= 100	[nF]
t_{delay}	= 500	[ns]
R	= 0.35	[Ω]
DI	= 0	[A]
$i_{Lres(0)}$ - m	= 3	[A]
m	= 4..11	[A]

A zoom of the phase plane plots showing the intersection points used in the determination of the VPC function is shown in Fig. 5.14.

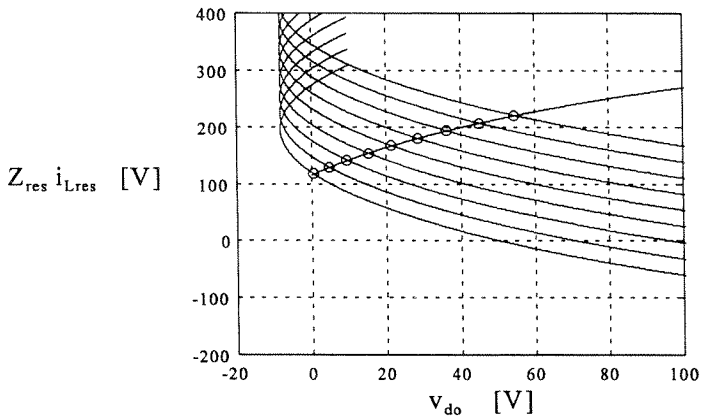

Fig. 5.14 The intersection points in the phase plane is used in the calculation of the VPC function

From the intersection points in Fig. 5.14 is ΔV_{do} found and plotted as function of m which is the same as Δi_{do} in this case.

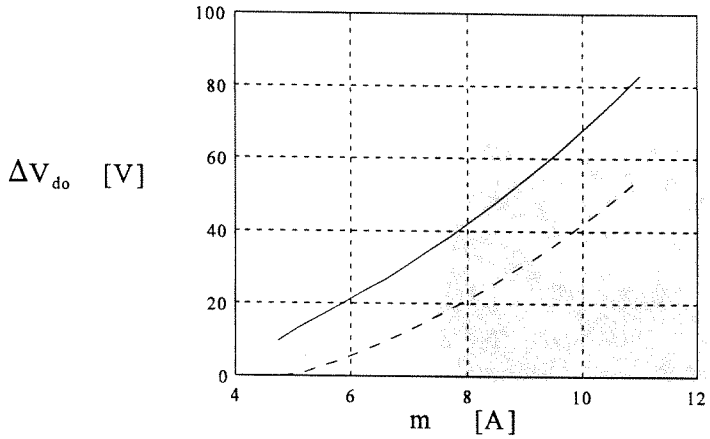

Fig. 5.15 ΔV_{do} as function of m. The dotted line is found from the intersection points in Fig 5.14. The full line includes the time delay t_d = 500 [ns].

The VPC function is a second order polynomial approximation to the full line curve shown in Fig. 5.14. The function is:

$$\Delta V_{do} = 0.49\,\Delta i_{do}^2 + 3.96\,\Delta i_{do} - 20.51 \qquad \textbf{(5.16)}$$

If ΔV_{do} is small enough there is a risk that the VPC control action happens at the same time the circuit that maintain the resonance is active. As a consequence the resonance is lost. To avoid this situation there is used a minimum limit of ΔV_{do}. The limit is ΔV_{do}= 30 [V] and from Fig. 5.14 or eq. 5.16 it is found that Δi_{do} = 6.9 [A]. This current is sufficient high to generate a significant voltage overshoot. The eq.5.16 is programmed into the digital signal processor and the verification of the VPC strategy is made.

5.4 Experimental verification of the VPC strategy using short circuit method.

A test of the resonant converter loaded with an induction machine is carried out. The resonant converter has a DC link voltage of 300 [V] and the nominal phase current of the induction machine is 6.9 [A]. A constant V/f control described in chapter 4 is used. With 300 [V] it is possible to magnetize the machine fully up to 30 [Hz]. Test is carried out at full load current, 10 [A] peak, and with a fundamental frequency of 30 [Hz].

First measurement of the link voltage v_{do} and phase current is shown in Fig. 5.16. The two upper pictures are without VPC and there is a peak voltage of v_{do} = 780 [V]. The two lower pictures are with VPC active and the peak voltage here is v_{do} = 683 [V]. It is shown later on that the relative high peak voltage occur because the VPC strategy had to be turned off for ΔV_{do}<30 [V]. The voltage peaks where the VPC is active are controlled very close to twice the DC link voltage. The experimental results of v_{do} agree with the simulated results shown in the first report /12/ chapter 4.

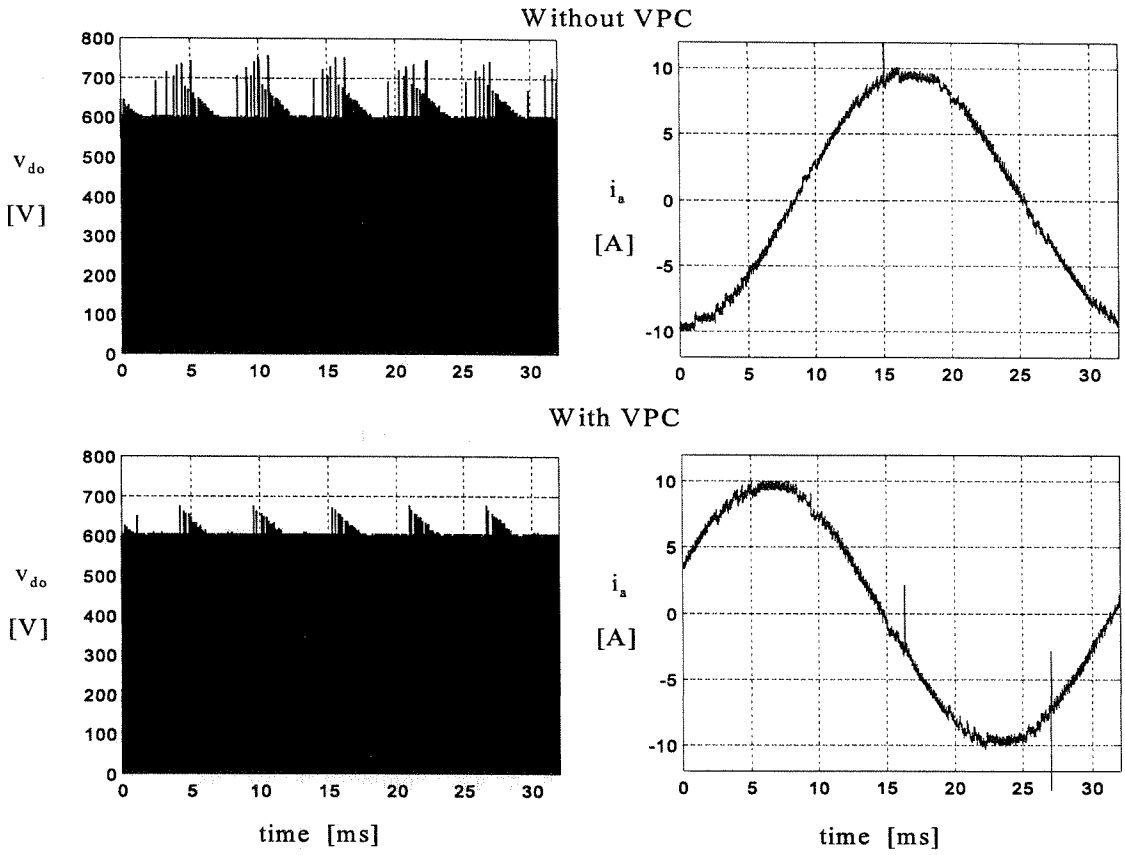

Fig. 5.16 Experimental results. Left side is resonant link voltage v_{do} and right side is induction machine phase current. The two upper pictures are without the use of VPC and two lower pictures is with the VPC activated.

A zoom of the link voltage v_{do} and link current i_{do}, is shown in Fig. 5.17.

Fig. 5.17a show a link current change of 10 [A] at point 1, for a DC link voltage of $V_d = 300$ [V] without using VPC. The link current change causes a transfer of energy. The stored energy in L_{res}, $e_{Lres} = {}^1/_2 L_{res} \Delta i_{do}{}^2$, is transferred to C_{res} and in the next zero voltage interval, point 2, transferred back to the DC voltage source.

In Fig. 5.17b is the VPC used, the link current change is 10 [A] at point 1. The inverter switches are turned off at non zero voltages, and turn off voltage is 45 [V]. As result is the link peak voltage controlled close to twice the DC link voltage, here 610 [V]. If VPC were not used the peak voltage was 780 [V].

It should be noticed the measurement of v_{do} is sensitive to probe adjustments. The probe was calibrated before the measurements, but with no accurate reference it is difficult to be precise. The oscilloscope has a resolution of 8 bit and with 200 [V/div] there is an distortion of 6.3 [V]. The measurements must be considered in the light of these errors.

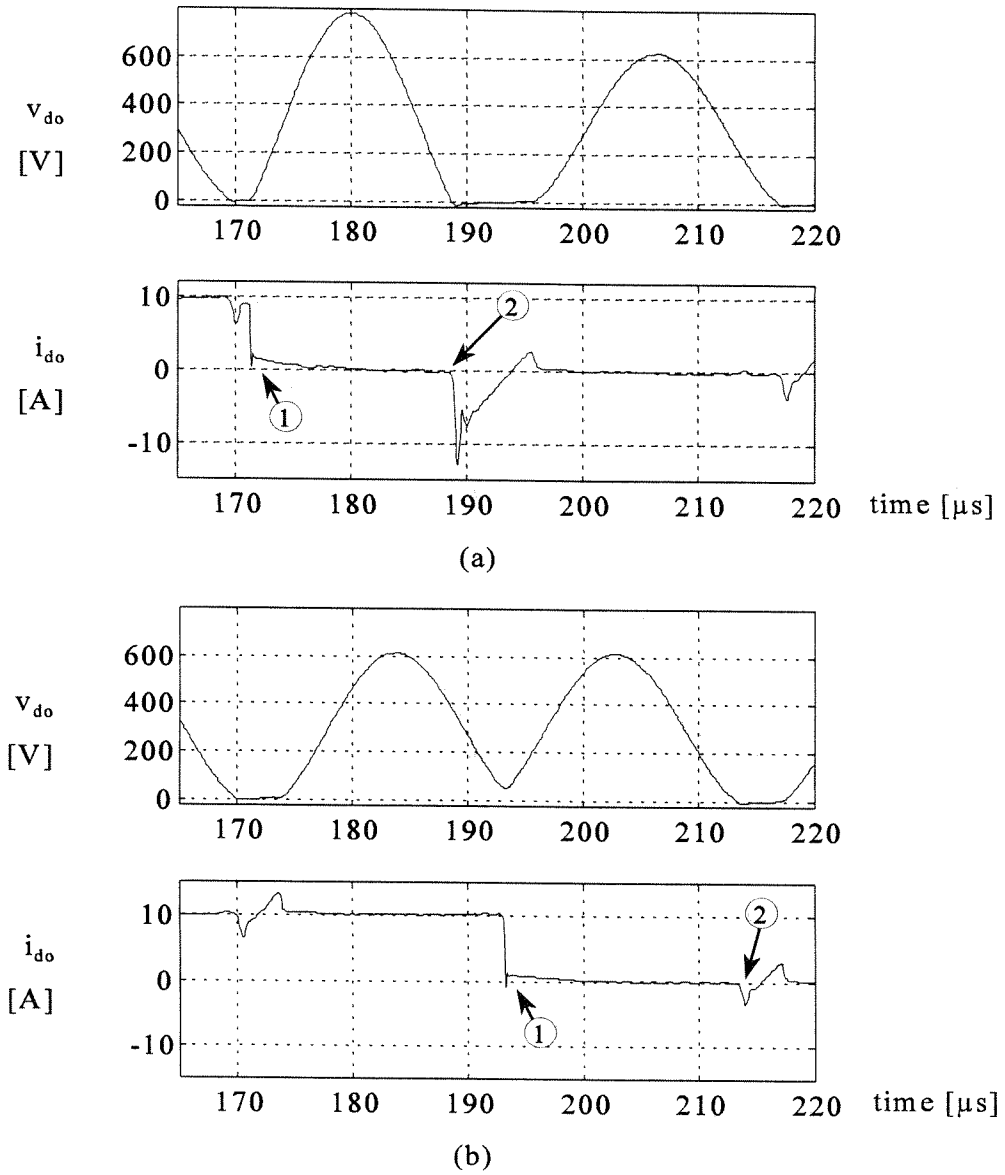

Fig. 5.17 Experimental results.
a) Link current change without VPC
b) Link current change with VPC

In table 5.2 is shown calculated peak values and measured peak values of v_{do}. It is interesting to notice that with a DC voltage of 550 [V] the v_{do_peak} excess the limit of 1300 [V], discussed in the first report, at $\Delta i_{do} = 14$ [A]. The converter apparent power at this current is approx. 6.7 [kVA].

Z=38.47 [Ω]	$v_{do\ peak} \sim \sqrt{V_d^2 + (\Delta i_{do} Z)^2}$							
Δi_{do} [A]	7	10	12	14	7	10	12	14
V_d [V]	300	300	300	300	550	550	550	550
v_{do_peak}	703	788	851	917	1162	1221	1268	1320
$v_{do\_peak\_measured}$	682	780	-	-	-	-	-	-

Table 5.2 Peak link voltage as function of link current change.

In Fig. 5.18 is shown the resonant link voltage v_{do} and the link current i_{do}. Link current changes of 10 [A], 7.3 [A] and 7.0 [A] are shown. A link current change at 10 [A] and 7.3 [A] happen using VPC but at a link current change smaller than 7.3 [A] happens without VPC. An increased link voltage peak of 682 [V] is observed.

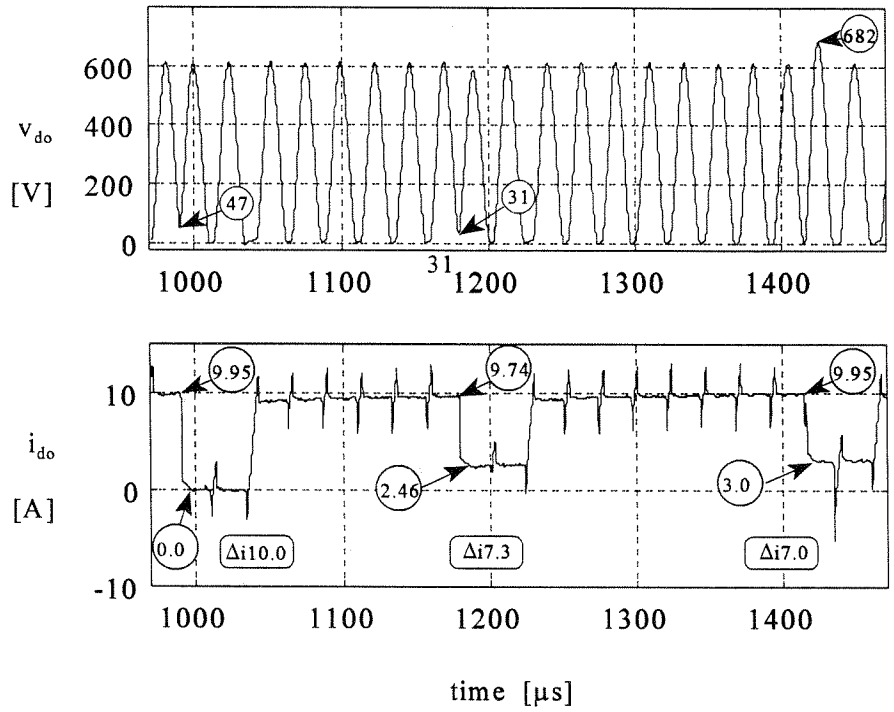

Fig. 5.18 Experimental results. Link voltage v_{do} and link current i_{do}.

Chapter 3 described how the resonance was maintained by a short circuit interval. The short circuit was initiated if the resonant link voltage v_{do} became smaller than 10 [V]. A VPC turn off below 10 [V] do not have any effect since the short circuit of the inverter is initiated. There is a 10 [V] minimum limit for ΔV. In Fig. 5.15 is ΔV shown as function of m (= Δi_{do}), from the dashed line is seen that a ΔV = 10 [V] is for a m= 7 [A]. When ΔV is calculated from the VPC equation (eq. 5.16) it is necessary to compensate the delay in the electronics. If the delay is 500 [ns] the minimum ΔV is 30 [V], as shown in Fig. 5.15. It is a very unpleasant problem since it no matter how good the VPC strategy works, when it is used, there is a significant over voltage because it has to be turned off in some cases.

5.5 Implementation of the VPC principle using Non-short circuit method

Using the non-short circuit method proposed in in chapter 3, then the problemes of implementation described in paragraph 5.3, 5.4 and 5.5 reduces. If the non-circuit method is used and the link is not loaded and one is able to use the theorical minimum compensation current $\hat{\imath}_s$ shown in eq. 3.6 the link equaions eq.3.3 and eq. 3.4 are reduced to

$$i_{Lres} = \frac{V_d}{Z}\sin(\omega t) \tag{5.17}$$

$$v_{do} = V_d(1 - \cos(\omega t)) \tag{5.18}$$

This is the equations of the loss less resonant link circuit. The $\hat{\imath}_s$ must however be increased to obtain a stable converter operation. The energy of the resonant circuit is therefore increased. This situaion is descirbed in Fig. 5.12. The influence of excessive energy in the resonant circuit can cause zero voltage failure but compared to the short circuit method the voltage is distorted less and the problem is therefore reduced. The increase of resonant voltage is low and do not posses a serious disadvantage.

Based on the analysis in 5.2 the only parameter that needs to be compensated is the turn off delay t_d of the control circuit and inverter switch. It is simple to make a new equation eq.5.16 and this equation is implemented in the resonant converter. In general it is much simpler to realize VPC using the non-shorting method compared to the short circuit method.

5.6 Experimental verification of the VPC strategy using Non-short circuit method.

All the figures shown in this paragraph are measured results. Notice, that all measurements are done with a sample rate of 1 MSPS or 0.5 MSPS. Any resonant transient is therefore shown. The resonant frequency of the converter is 41 [kHz] and the DC link voltage is either $V_d = 300$ [V] or $V_d = 500$ [V].

The VPC strategy is now used together with the non-short circuit method. At first Fig. 5.19 a measurement of resonant link voltage v_{do}, link current i_{do} and line voltage is shown, there is not used VPC.

In Fig. 5.20 VPC is turned on, a measurement of link voltage v_{do}, link current i_{do} and the ΔV are shown. The ΔV is the voltage calculated by the DSP and converted to an analog value by an D/A converter. This is shown in Fig. 5.1.

Comparing Fig. 5.19 and Fig. 5.20 it is concluded that the VPC startegy works, the converter operation was stable and therefore extensive efficient measurement was possible and the results are presented in chaper 6. The current stress of the inverter diodes are reduced using VPC one can observe that the non-short circuit is used by comparing Fig. 5.18 with Fig. 5.20. No short circuit current pulses are present in the link current shown Fig. 5.20.

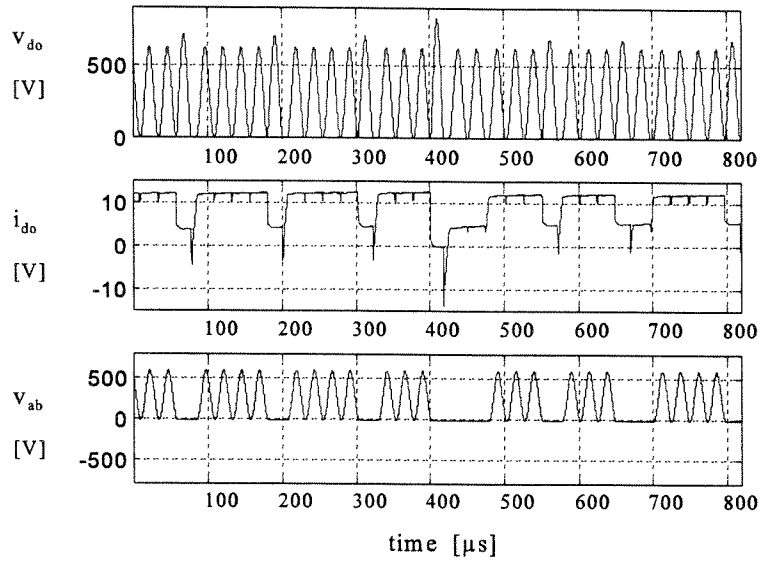

Fig. 5. 19 Experimental results of the RDCL converter. DC link voltage V_d = 300 [V].

The problem shown in Fig. 5.18 where there is a lower limit of ΔV which generates an increased voltage peak is not present here, since the short circuit of the inverter bridge is not necessary.

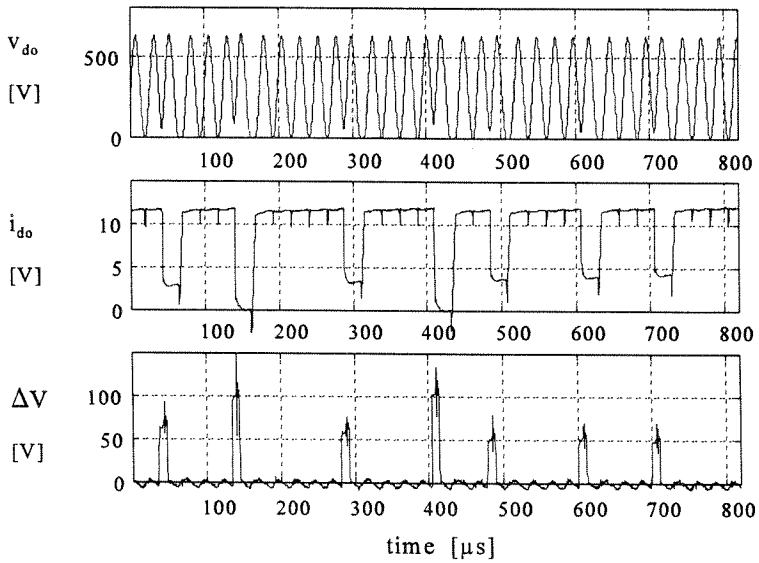

Fig. 5.20 Experiment results of the RDCLVPC converter. DC link voltage V_d=300 [V]

Now is looked at a whole fundamental period of the phase current.

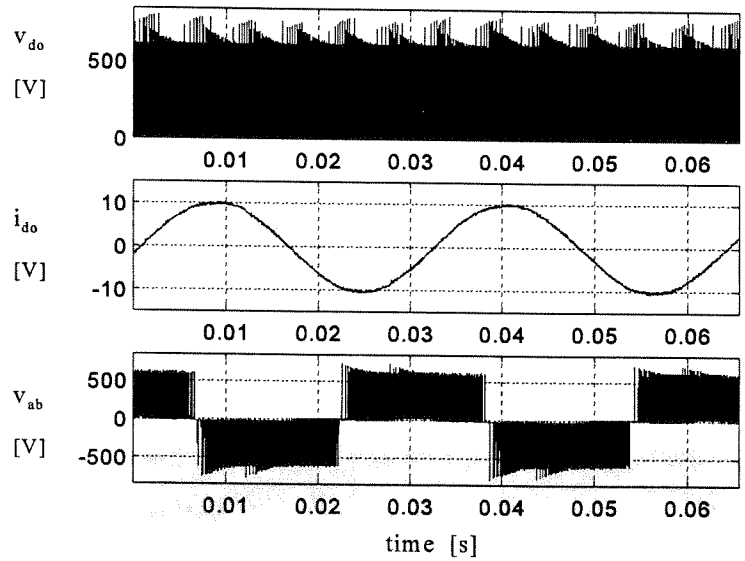

Fig. 5.21 Experimental results of the RDCL converter. $V_d = 310$ [V]

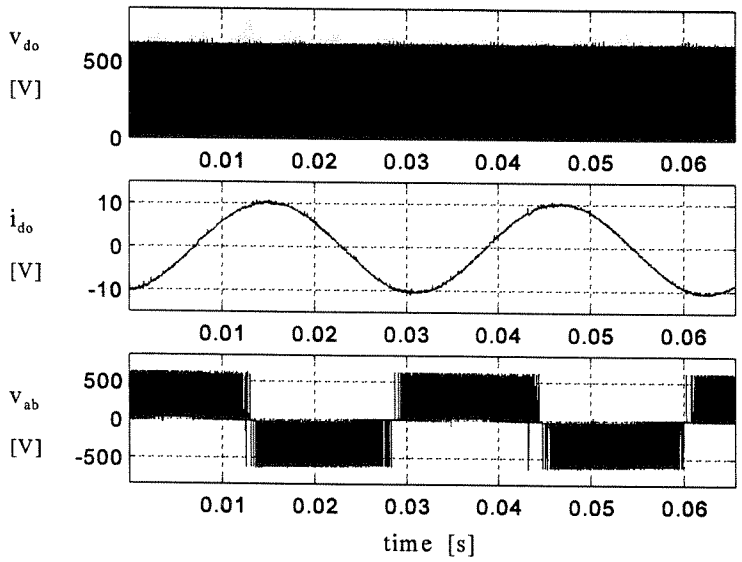

Fig. 5. 22 Experimental results of the RDCLVPC converter. $V_d = 310$ [V]

A comparison of the voltage peaks with and without VPC is shown in Table 5.3.

VPC status	peak link voltage $\hat{v}_{do}$ [V]	$\hat{v}_{do}/V_d$ ratio
turned off	813	2.6
turned on	650	2.1

Table 5.3 Comparison of resonant link voltage peak with and with-out VPC. The DC link voltage is 310 [V].

In /10/ a simulation is made showing the ΔV for a fundamental period of the current. A measurement in Fig. 5.23 of the ΔV show a nice agreement.

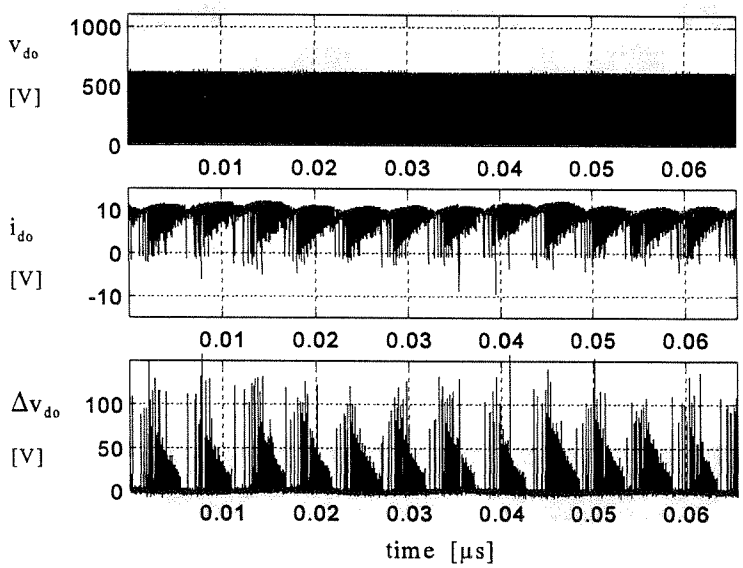

Fig. 5.23 Experimental result of the RDCLVPC converter. $V_d = 310$ [V].

In Fig. 5.23 VPC is turned on, a measurement of link voltage v_{do}, link current i_{do} and the ΔV shown. Some of the high ΔV_{do} peaks are noise, which is shown on Fig. 5.20.

Experimental results for a DC link voltage of 500 [V] is shown in chapter 6.

5.7 Conclusion

The Resonant DC Link Voltage Peak Controlled, RDCLVPC Converter is loaded with an induction machine and the voltage peak control and the VPC is tested. For an ideal converter the VPC strategy limits the resonant link voltage to twice the DC link voltage, which is equal to a clamp factor of 2.0. In the real converter parasitic losses, changes in DC link voltage, changes of link current, time delay in component and changes of components characteristics due to non-linearitis and temperature changes are present.

The influence of the parasitic losses, changes in DC link voltage, changes of link current, time delay in components are taken into account. A numerical solution is used to calculate the VPC function, the analytical solution was not obtainable. The VPC function is approximated by a second order polynomial. The polynomial is implemented in the laboratory prototype of the

RDCLVPC converter.

First experimental results are shown with and without the VPC strategy using the short-circuit method described in chapter 3.

With the VPC control active the link voltage peak is limited to 610 [V] for a DC link voltage of 300 [V] and link current change of 10 [A]. The clamp factor is 2.1. Under the same conditions, without VPC is the resonant link voltage peak 780 [V].

Unfortunately it is necessary to turn the VPC strategy off, if the resonant link voltage is below 30 [V]. As a consequence the resonant link voltage peak is not controllable for link current changes below 7.3 [A]. A link current change of 7.3 [A] generates a voltage peak of 684 [V]. There is an excess voltage of 84 [V]. and the clamp factor is 2.3.

The described situation is unpleasant since no matter how good the VPC strategy works, there is an over voltage, because it is necessary to turn the VPC off under a certain link voltage level.

The above problem is solved using the non-short circuit method proposed in chapter 4. A clamp factor of 2.1 is always obtained using the non-short circuit method.

One disadvantage of the VPC is a measurement of v_{do} is needed. The non-soft switching of the inverter switchings happens at a relative low voltage. Experimental work in chapter 6 show the influence of VPC on the inverter losses and resonant link losses.

6

An experimental test of the resonant converter

The RDCLVPC resonant converter was build over a period of one and a half year. This chapter show some test results. Since the RDCL converter is the fundamental part of the RDCLVPC, test results of the RDCL is also shown. Tests shown in this chapter are done at a DC link voltage level of 300 [V] or 500 [V]. The test period lasted from 25/07-1996 to 5/08-1996, more than one week was the converter was running 5-10 h every day without problems. It did also function afterwards, but it has not been operating a whole day as required during efficiency measurements. The voltage peak control strategy was tested and extensive measurements of the inverter losses were made. The behaviour of the converter loaded with a 300 m long cable and machine was also measured. The converter and test setup are shown Fig. 6.1.

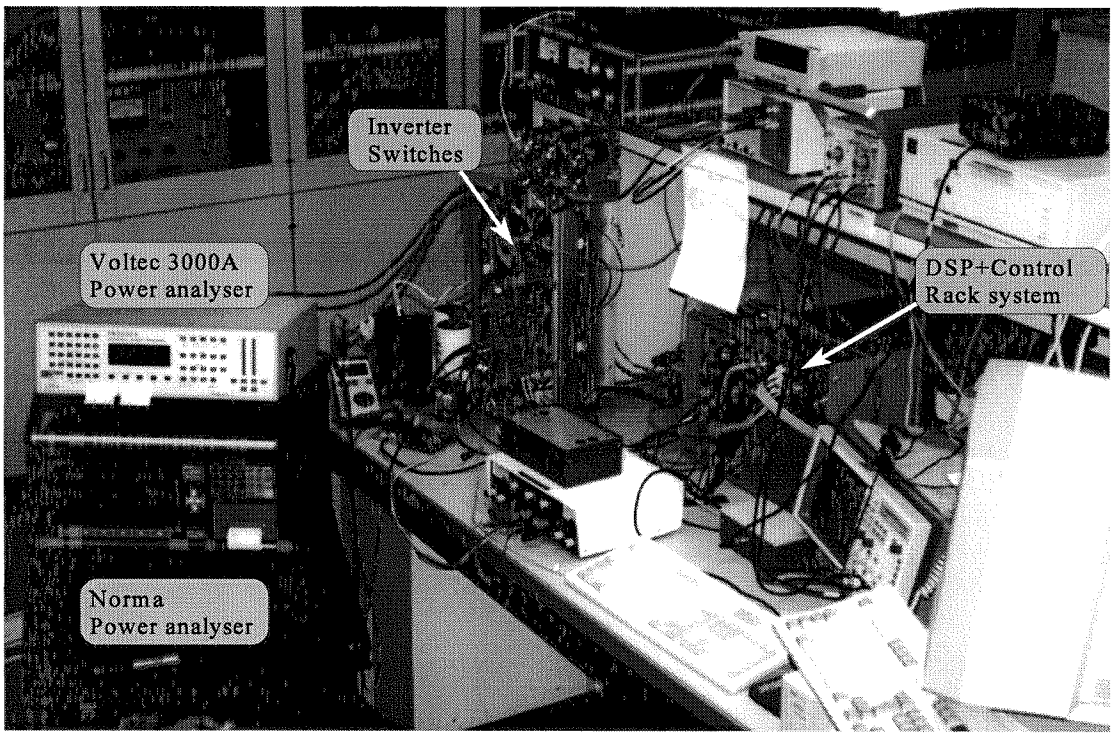

Fig. 6.1 Resonant converter and measurement equipment in the laboratory.

The load system consists of an induction machine loaded by a DC machine. The test bench is shown in Fig. 6.2.

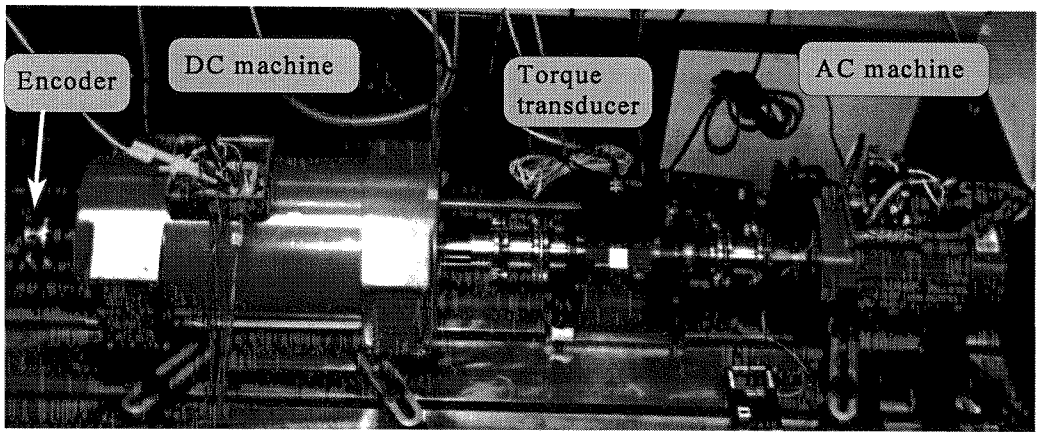

Fig. 6.2 Machine bench with a 3.0 [kW] ABB induction machine and a DC machine load.

The induction machine is star connected and to detect the working points of the induction machine the torque is measured by a torque transducer. The rotor speed was also measured using an encoder. In Fig. 6.3 the main power electronic circuit is shown. A secondary winding was applied to the resonant inductor as described in chapter 3. The secondary winding is the dark wire, and the primary winding is white in Fig. 6.3. The primary winding numbers are 45 and the secondary winding numbera are 14.

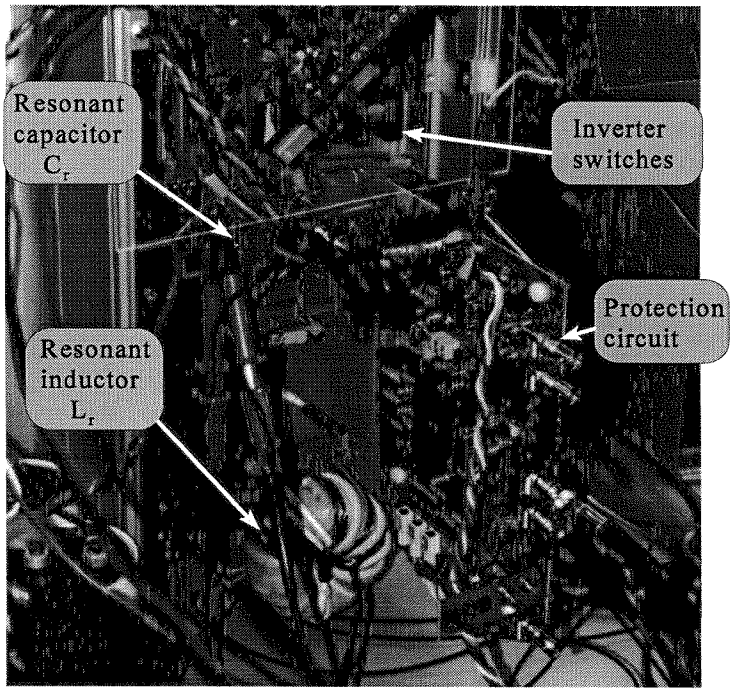

Fig. 6.3 Inverter bridge and resonant link circuit

When the VPC strategy is used, a resonant link voltage measurement is required, which is done with one of the Tektronix x100 voltage probes as shown Fig. 6.3. The large vertical PCB shown is a protection circuit and it generates the zero voltage synchronisation signal ZVSI. Hidden behind the two voltage probes is the rectifier and DC filter.

Note, that all measurements are done with a sample rate of 1 Mega Samples Per Second, MSPS or 0.5 MSPS. Any resonant transient is therefore always shown. The resonant frequency of the converter is 41 [kHz] when it is not loaded with a cable.

6.1 Test of V/f control

The Space Vector Sigma Delta Modulator,SVSDM as described in chapter 4 is implemented with a V/f, control.

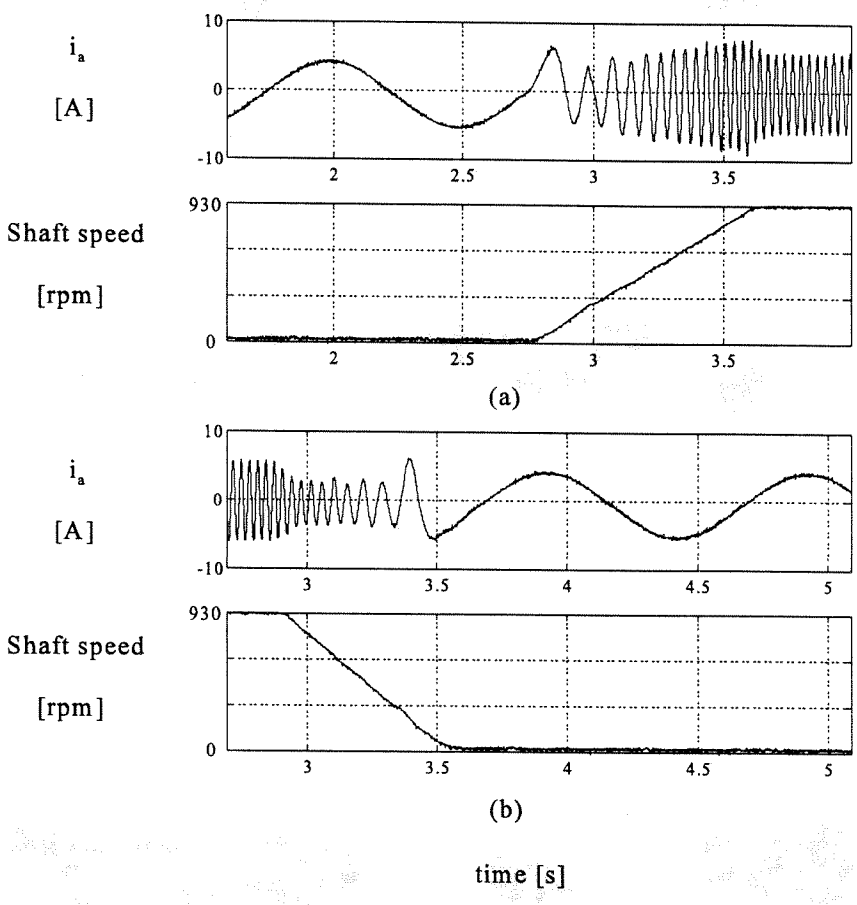

Fig. 6.4 Phase current and induction machine shaft speed at run up (a) and run down (b).

In Fig. 6.4 is the reference frequency at the top changed from 1 [Hz] to 32 [Hz], and at the two traces at the bottom the reference frequency is changed from 32 [Hz] to 1 [Hz]. The shaft speed changes during 0.7 [s]. The machine was not loaded during the test. It is concluded that the V/f control is working with a resonant converter. The DC link voltage was $V_d = 300$ [V].

6.2 Test of VPC principle.

In this paragraph the effect of the voltage peak control is shown. First measurements at 300 [V] DC link voltage for different power loads are shown and then measurement at 500 [V] are made.

In Fig. 6.5 left side the converter output power is 188 [W], $I_{RMS} = 2.5$ [A] and the machine is not loaded. Right side of the converter output power is 2.2 [kW], $I_{RMS} = 6.4$ [A]. The modulation index is 1.0 and the frequency $f_1 = 32$ [Hz]. The VPC is not activated and it seen that large excessive link voltage peaks at no load are not present, but at 2.2 [kW] the voltage peak increased about 120 [V] beyond twice V_{dc}.

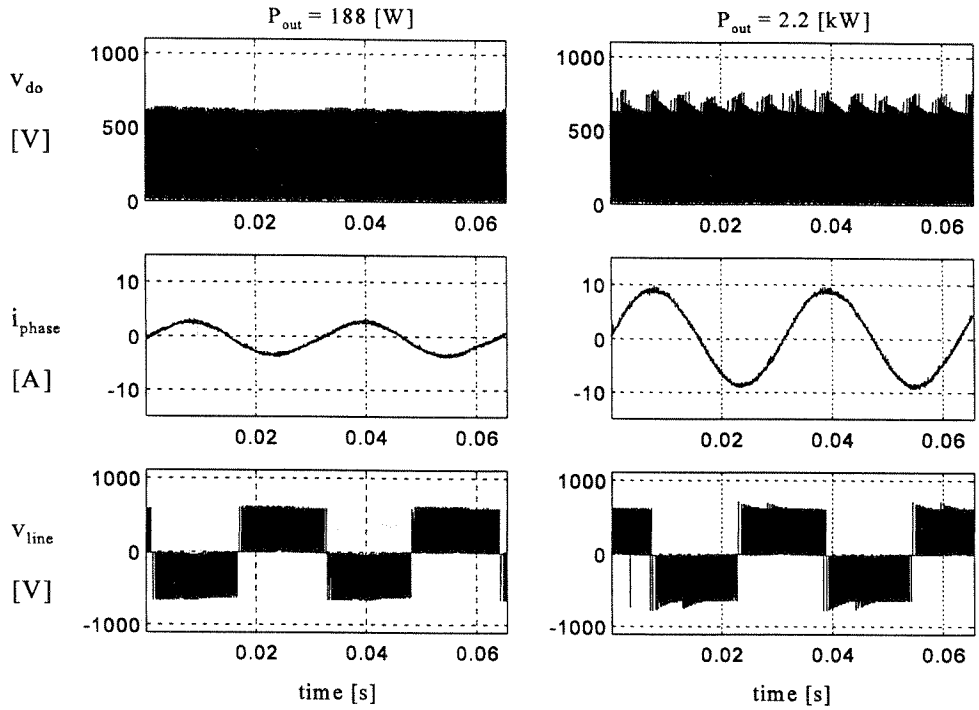

Fig. 6.5 RDCL converter. DC link voltage V_{dc} = 300 [V], link voltage v_{do}, phase current i_{phase}, line voltage v_{line}.

In Fig. 6.6 a comparison of the RDCL and RDCLVPC converter is made. In left side the VPC is not active and the voltage peak increases to 161 [V]. If the VPC is turned on the voltage peaks are reduced to 34 [V].

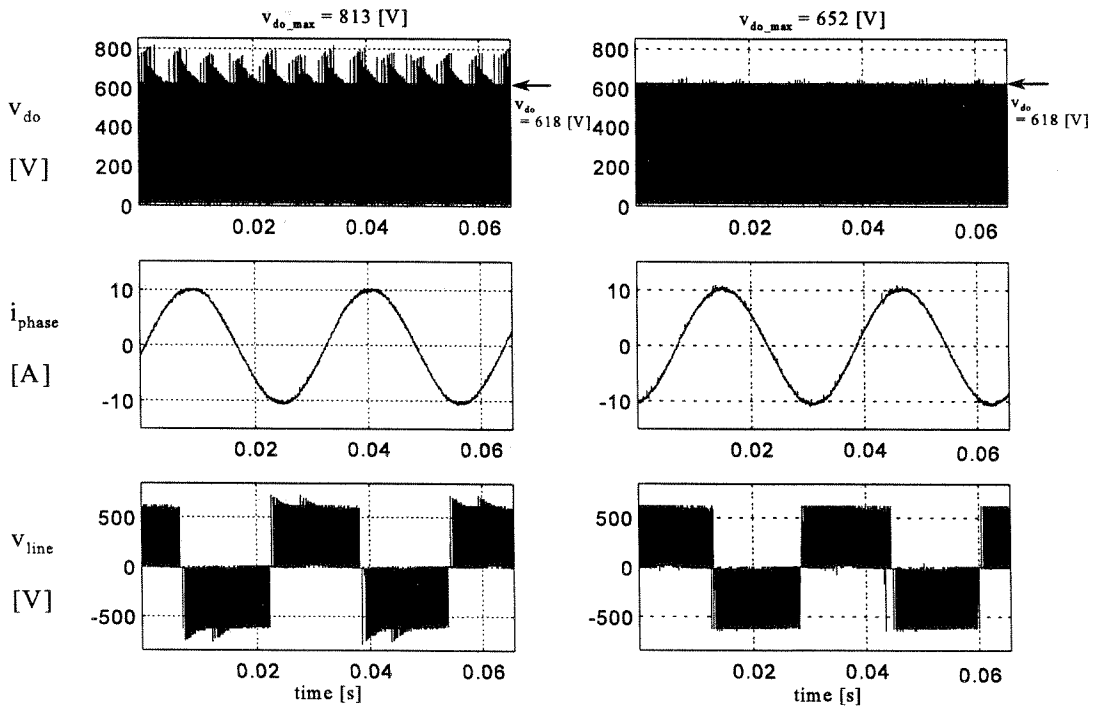

Fig. 6.6 Left side RDCL without VPC. Right side RDCLVPC with VPC.V_d = 310 [V]

The VPC strategy is able of eliminating excessive voltage peaks of the RDCL converter.

In Fig. 6.7 is a fast fourier tranformation, fft, spectrum plot of phase current and line voltage shown.

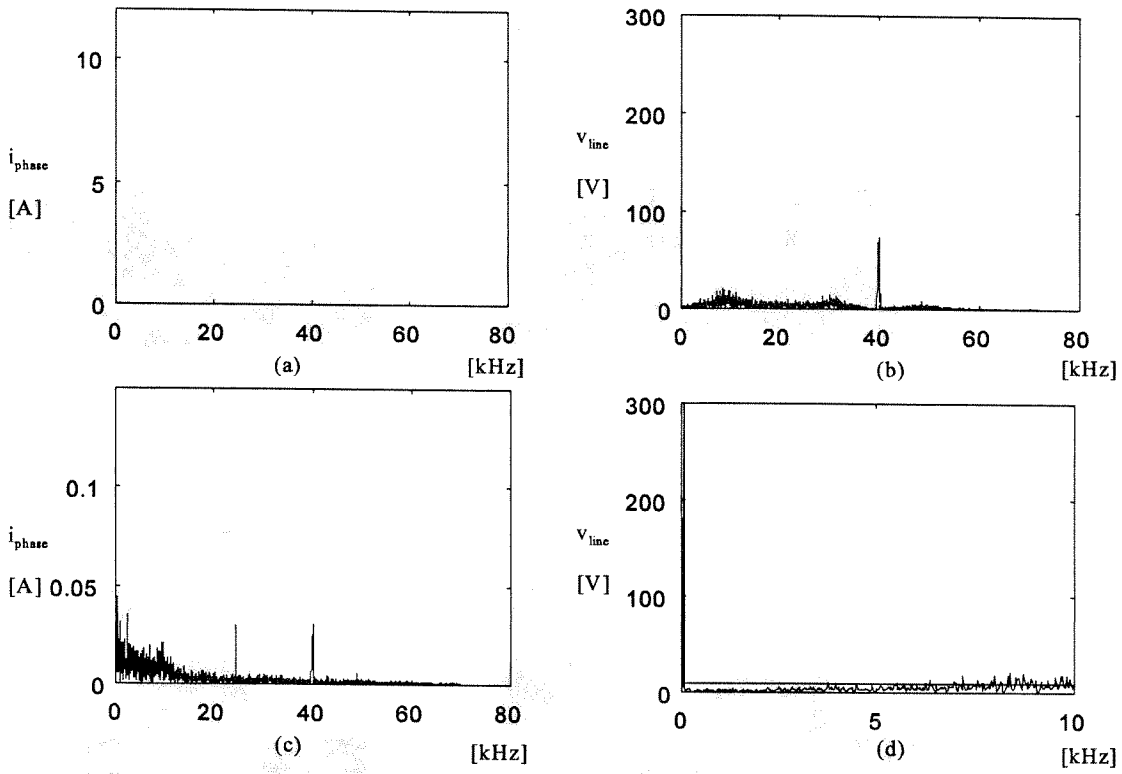

Fig. 6.7. RDCLVPC converter. Fft of phase current i_{phase} and fft of line voltage v_{line}. $f_1 = 32$ [Hz].
a) i_{phase} harmonics from DC to 70 [kHz] b) v_{line} harmonics from DC to 70 [kHz]
c) i_{phase} harmonics from 100 [hz] to 70 [kHz] d) v_{line} harmonics from DC to 10 [kHz]

The fft spectrum of the RDCL and RDCLVPC is quit similar, and only the plot from the RDCLVPC is shown. In Fig. 6.7.d, the vertical full line indicates 10 [V]. The time domain curves used in the fft calculation are the curves shown in Fig. 6.6 right side.

The DC link voltage is increased to 500 [V].

In Fig. 6.7 left side the converter output power is 385 [W], I_{RMS} = 2.8 [A] and the machine is not loaded. Right side the converter output power is 1.9 [kW], I_{RMS} = 4.1 [A]. The modulation index is 1.0 and the frequency f_1 = 50 [Hz].

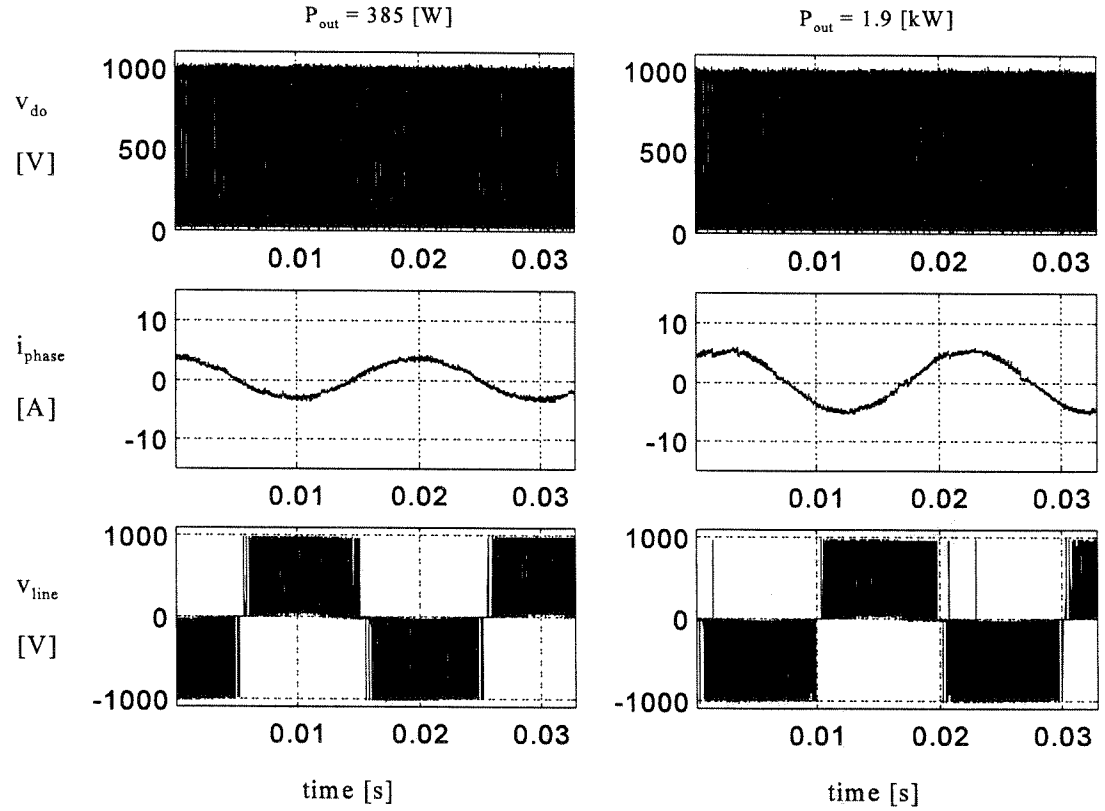

Fig. 6.7 RDCL converter. DC link voltage V_d = 500 [V]. Resonant link voltage v_{do}, phase voltage i_{phase}, line voltage v_{line}.

There is only a small over voltage present, in Fig. 6.8 this is even more clear.

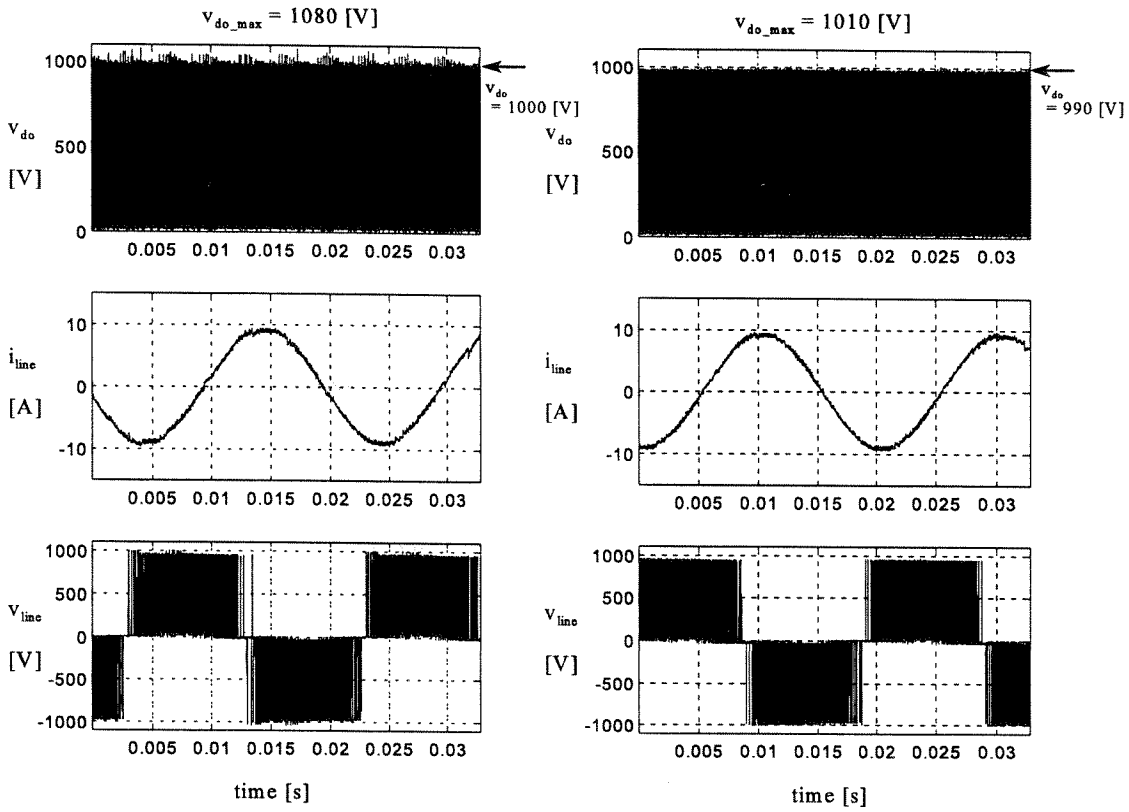

Fig. 6.8 Left side VPC is not active. Right side VPC is active. V_d = 500 [V]

Compared with Fig. 6.6 where the VPC strategy reduces the resonant peaks to 161 [V] the VPC strategy only reduces the peaks with 70 [V] in Fig. 6.8. This is explained by the increase of DC link voltage. From eq. 5.7 a general relation k_0 between resonant voltage peak and DC link voltage is found.

$$k_0 = \frac{\hat{v}_{do}}{V_d} = \sqrt{\frac{Z^2 m^2}{V_d^2} + 1} + 1 \qquad \textbf{(6.1)}$$

where: Z = resonant impedance
V_d = DC link voltage
$\hat{v}_{do}$ = resonant peak voltage
m = fundamental of phase current.

Using the actual parameter values, Table 6.1 is calculated:

Z [Ω]	V_d [V]	m [A]	k_o	$\hat{v}_{do}$ calculate [V]	$\hat{v}_{do}$ measured [V]
38.5	310	10.2	2.6	810	813
38.5	500	9.3	2.2	1115	1080

Table 6.1 Calculated and measured resonant link voltage peaks $\hat{v}_{do}$ for the RDCL converter.

The calculated and measured $\hat{v}_{do}$ agrees well. The damping effect of increasing V_d is shown, k_0 decreases from 2.6 to 2.2 increasing V_d from 310 [V] to 500 [V] .
It is concluded, based on Fig. 6.7, that the VPC strategy is able to limit the resonant link voltage peaks close to the theoretical value of $2V_d$.

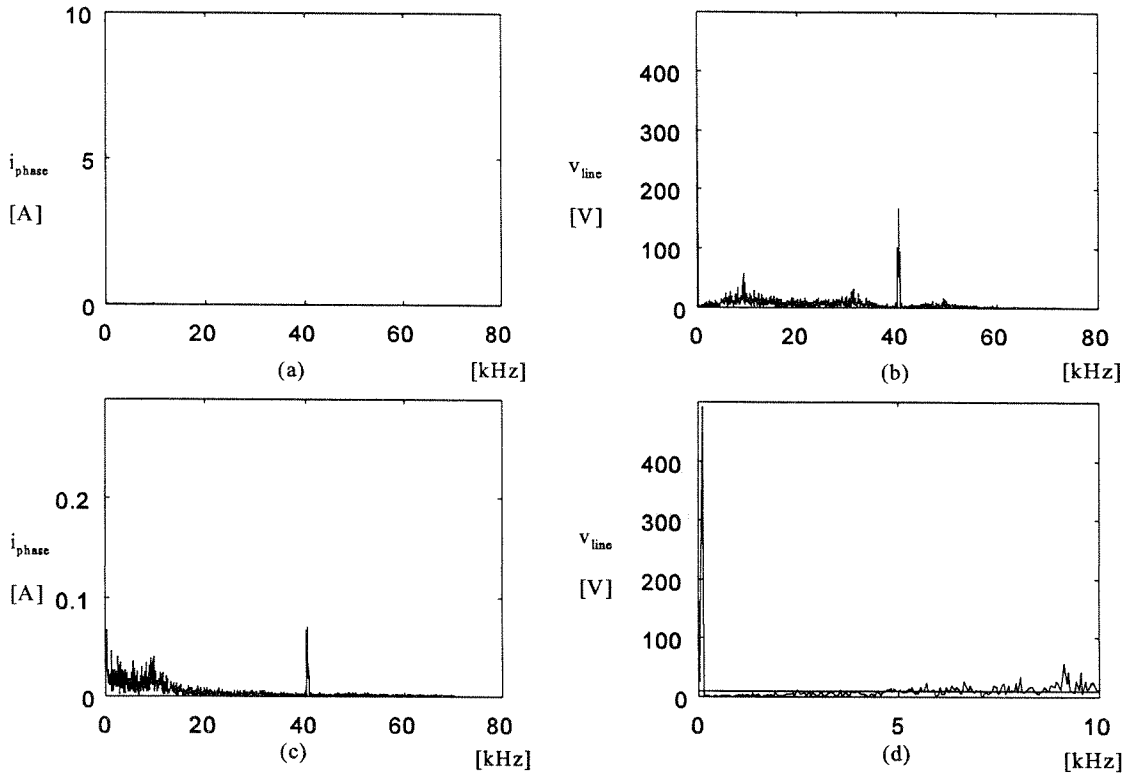

Fig. 6.9. RDCLVPC converter. Fft of phase current i_{phase} and fft of line voltage v_{line}. $f_l = 50$ [Hz].
a) i_{phase} harmonics from DC to 70[kHz] b) v_{line} harmonics from DC to 70 [kHz]
c) i_{phase} harmonics from 100 [Hz] to 70 [kHz] d) v_{line} harmonics form DC to 10 [kHz].

The fft spectrum of the RDCL and RDCLVPC is quit similar, and only the plot using the RDCLVPC is shown. In Fig. 6.9.d, the vertical full line indicate 10 [V]. The time domain curves used in the fft calculation are the curves shown in Fig. 6.8 right side.

6.3 Resonant converter efficiency

The resonant converter efficiency is measured using the two power analyzers shown in Fig. 6.1. The power is measured in six different points. This is shown in Fig. 6.9.

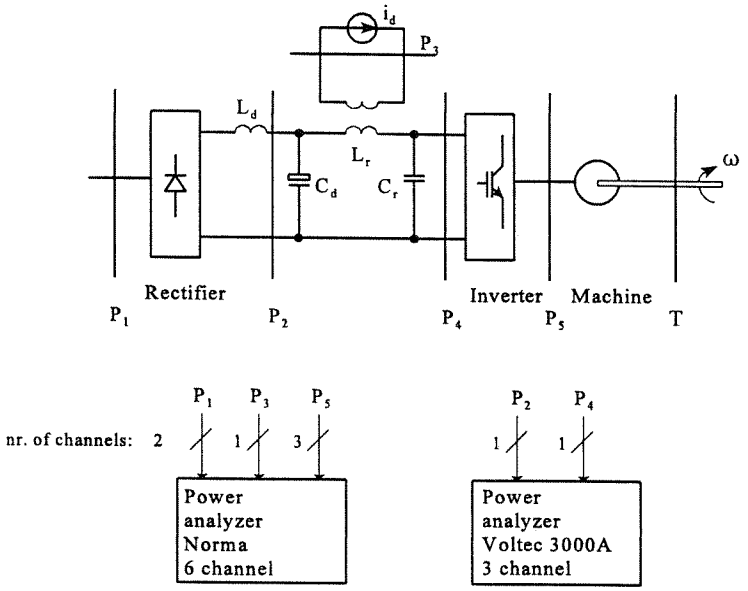

Fig. 6.9 The power is measured in five points. This enable measurement of the loss distribution inside the resonant converter.

First is shown the measurement of power losses from input P_1 to output P_5. This is shown in Fig. 6.10.

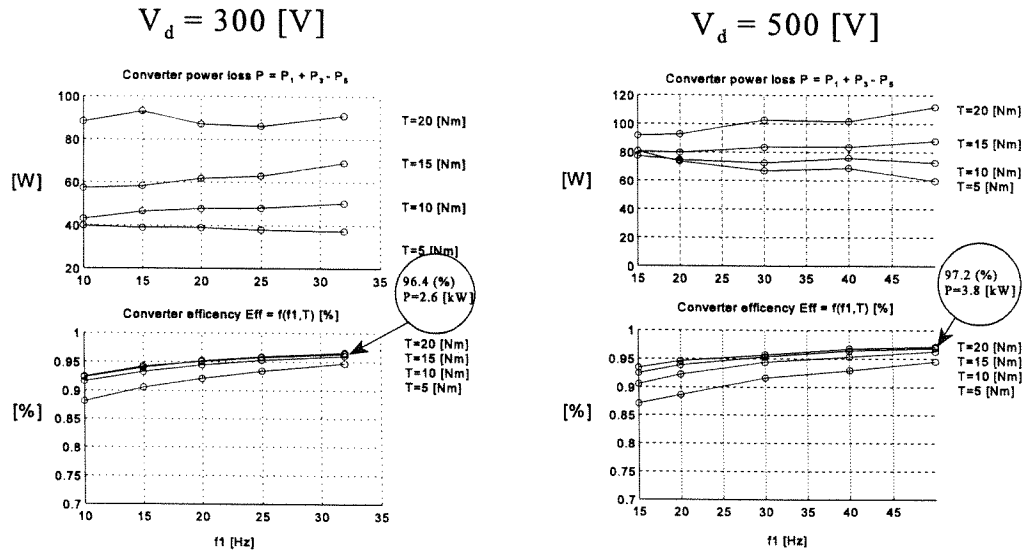

Fig. 10. Overall RDCL converter efficiency, without VPC, using the new non-short circuit method, load machine nominal output power 3.0 [kW]:
Left: DC link voltage V_d = 300 V
Right: DC link voltage V_d = 500 V

The power loss of the resonant converter is calculated from the measured values in P_1,P_3 and P_5. The power loss in the control circuit and driver circuit are not included. There is a little difference in the efficiency of the two converters RDCL and RDCLVPC. An explanation of this is shown when the loss distribution in the converters is measured. Fig. 6.11 shows the loss distribution of the RDCL and the RDCLVPC converter.

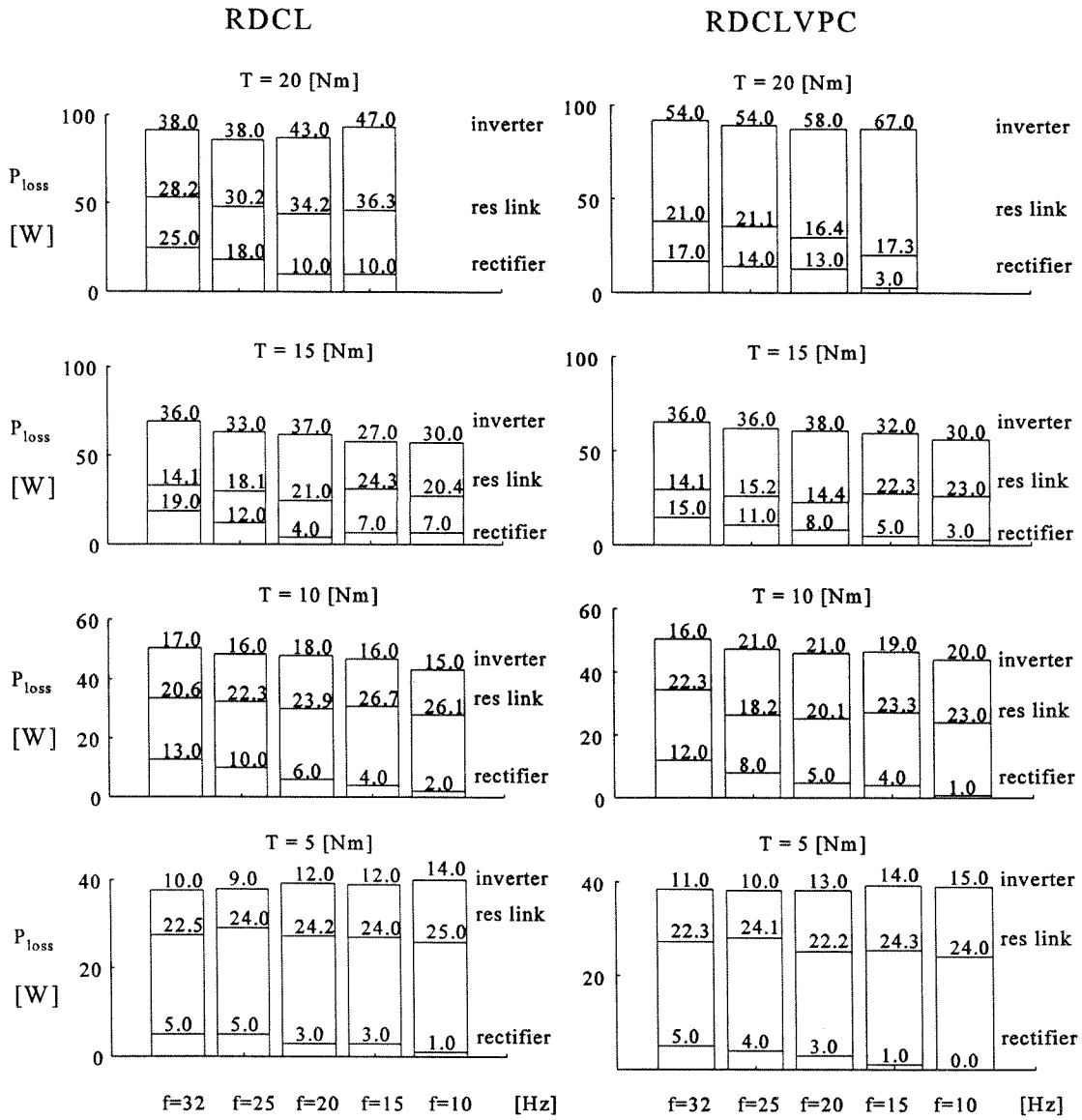

Fig. 6.11 Loss distribution inside the RDCL and RDCLVPC converter at different load situations. Load torque = 20 [Nm] is the nominal torque of the induction machine. V_d = 300 [V].

The use of the VPC strategy decreases the reactive power of the circuit compared with the RDCL converter. Transfer of energy due to link current changes are reduced, and the current stress of resonant inductor and antiparallel diodes are lower. On the other hand, is the inverter switch loss increased using the VPC strategy. The loss is moved from the resonant link to the inverter switches using VPC. This effect is only significant at torque of 20 [Nm] where the link current is large. If the torque is 15 [Nm] or below there is no difference of in the losses. Increasing the DC link voltage, it is lightly that there is no

difference of the loss distribution at 20 [Nm]. Naturally the losses were measured using a link voltage of Vd = 500 [V], but the Voltech 3000A then shifted voltage range from 500 [V] to 1000 [V]. This caused the error of the measured power to increase, and getting a reasonable measurement of losses was not possible. This is therefore not shown. The Norma power analyzer continued to give reasonable measured values and therefore calculating the overall converter losses was possible. Shown in Fig. 6.10.

It is concluded that the VPC increases the inverter switch losses but at the same time reduces the resonant link current stress.

6.4 Converter loaded with a long cable

The resonant converter is loaded with a 300 [m] cable and the induction machine. The DC link voltage was 300 [V] and the VPC strategy was not used, the cable changes the resonance capacitance and no new VPC table was made.

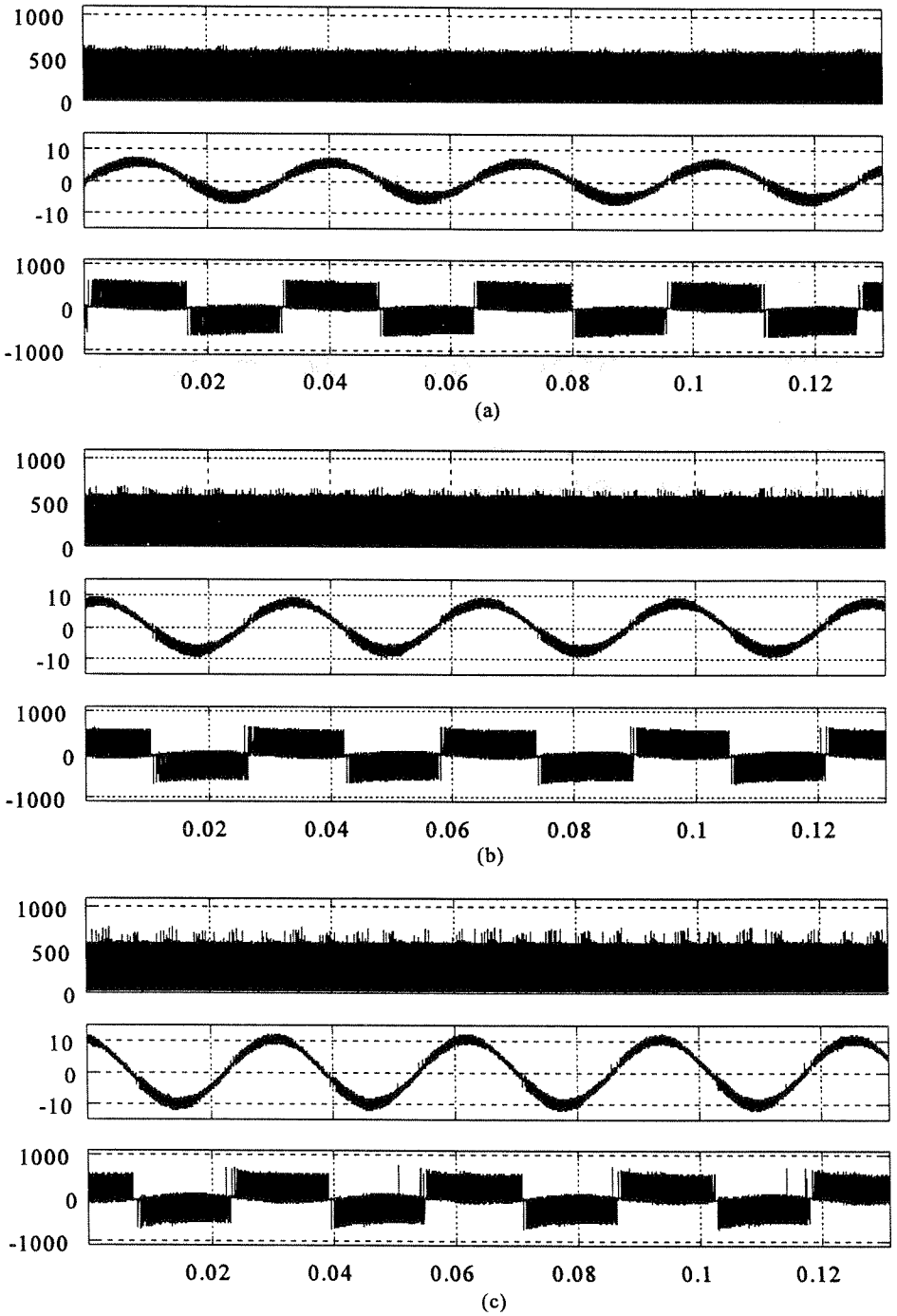

Fig. 6.12 In (a), (b) and (c) the load of the machine is increased to nominal load torque T=20 [Nm] using the RDCL converter and a $V_d = 300$ [V].

The 300 [m] cable was put on the roof of the laboratory. To ensure the stability of the resonant converter the energy supplied to compensate resonant circuit losses was increased. It was not expected that the current source delivering the energy would survive a test using a DC voltage of 500 [V]. A detailed look at Fig. 6.13 showing the resonant link current i_{do} and voltage v_{do} is quit interesting.

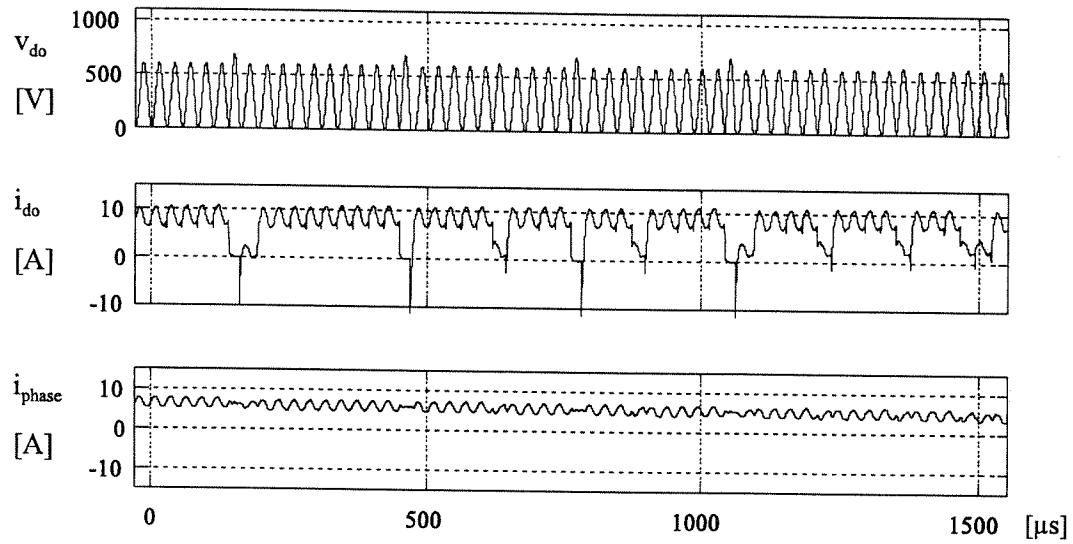

Fig. 6.13 RDCL converter loaded with 300 [m] cable and induction machine. V_d = 300 [V]

The resonant frequency is decreased due to the cable capacitance. Without cable the resonant frequency is 41 [kHz,], with the cable the resonant frequency is 35 [kHz]. During the resonant period the cable is charged and discharged without the transients known in PWM-VSI converters. It is expected that the EMI level is lower using the resonant converter compared with a hard switched converter.

6.5 Conclusion

The Resonant DC Link Voltage Peak Controlled, RDCLVPC Converter proposed in the first report /12/ and the RDCL /1/ converter has been realized and tested. The DC link voltages were 300 [V] and 500 [V]. It is shown that the converters are able of operating stable at both voltages. This is due to the proposed non-short circuit method described in chapter 3. The test period lasted more than one week and the converter was running 5-10 h every day. Based on the laboratory experience with the converter there is found no reason the resonant converters should not operate at higher DC link voltages as 600 [V].

The voltage peak strategy, is tested and proven to be able to limit the resonant voltage peaks below 2.1 times the DC link voltage.

Limiting the resonant voltage peaks using VPC introduces inverter switch turn off at non zero voltages. This increases the inverter switch losses but at the same time the resonant link current stress is reduced. Measurement show the inverter switches and resonant link total losses are almost the same comparing the RDCL and RDCLVPC converter.

A converter efficiency of 96.4 [%] at P_{out} = 2.6 [kW] using a DC link voltage of 300 [V] was measured and a converter efficiency of 97.2 [%] at P_{out} = 3.8 [kW] was measured using a DC link voltage of 500 [V].

During the development of the resonant converter many fault situations arrived, but none of them was able to kill the inverter switches rated 1700 [V] and 30 [A]. This is due to the current slope limitation of the resonant inductor. The resonant converter is also in this way robust.

Test with a 300 [m] long cable and an induction motor load was carried out at a DC link voltage of 300 [V]. The VPC and long cable condition were not tested. The cable does not generate high frequency current oscillation known from PWM-VSI converters but a super imposed sinusoidal current with the frequency of the resonant circuit.

It is concluded the RDCLVPC and the RDCL converters first described by analysis and simulation is successfully tested in the laboratory.

7

Conclusion

The desire of reducing switching loss and high dv/dt in the hard switched PWM-VSI are significant reasons for working with the three-phase resonant converter. The converter ideally eliminates the switching loss and generates an output voltage with a very low dv/dt or low di/dt. Attractive abilities of the PWM-VSI as simple power circuit and high output voltage quality should also be resonant converter properties. In the first Ph.D. report an investigation of resonant converters is carried out, and one resonant converter was selected for realization in this report.

The selected resonant converter uses a parallel resonant link and basically this type of converter generates high voltage peaks beyond twice the DC link voltage. This drawback can be solved by using a clamp circuit, but the power circuit simplicity of the converter is lost. With a new way to control the resonant peak is the additional clamp circuit avoided and the simpleness of the power electronic parallel resonant converter, RDCL /1/ is kept. The proposed converter is named Resonant DC Link Voltage Peak Control (RDCLVPC) converter. It is a modification of the RDCL converter and it is natual to work with both the RDCL and the RDCLVPC. Therefore this report treats both converters.

7.1 Summary of the Report

Resonant link circuit:

The first problem realizing parallel resonant converters is to make them stable in operation. When the converters are simulated it is quite easy to make them stable, due to ideal circuit components. In the laboratory electrical noise, and limited bandwidth on the components may create difficulties, that can make an apparently good design to a bad choice.

The resonance of the converter must be initiated and then the resonance must be maintained. If the resonant circuit was loss less, the resonance would continue forever. A key point here is that the resonance make the resonant link voltage oscillate down to zero, for every resonant cycle. During the zero voltage interval the inverter switches can be turned on and off with low losses and zero dv/dt. The real resonant circuit has losses that must be compensated to ensure the resonant oscillation has a zero voltage interval. The resonant circuit losses is compensated by adding energy that are equal to or larger than the energy lost during one resonant cycle. Resonant circuit loss compensation can be made by a short circuit of the inverter switches during the zero voltage inverval. During the short circuit, energy is stored in the resonant link inductor and after a few micro seondes the short circuit is turned off and the resonance commence.

It is necessary with a short circuit at every zero voltage interval, if it does not happen the inverter stops and the resonance must be restated. Realizing a circuit which is, able to generate a short circuit interval, that ensures the ongoing resonance can be very difficult. Another problem of the short circuit method is the duration of the short circuit interval. If the DC link voltage increases from eq. 100 [V] to 500 [V] the length of the necessary short circuit interval decreases, because the compensation energy in the resonant inductor is obtained faster. In the used inverter, switches and control electronics have a time delay of more than a micro second. The short circuit

pulse duration value is at minimum equal to the time delay. At a DC link voltage of 300 [V] the required short circuit time is shorter than the minimum obtainable short circuit time. Higher current circulations are then generated and the converter tends to be unstable. At higher DC link voltages than 300 [V] the converter cannot operate longer than a few minutes before it stops. If the electronic control circuit is improved, the DC voltage limit can be raised, still to long short circuit intervals are used.

Based on the gained experience with the short circuit method a new method, called non-short circuit method is proposed. This method transfers power to the resonant circuit inductively, this is done by a secondary winding on the resonant coil and it then becomes a transformer. The secondary side power source is a current generator that produces a pulsating train with a frequency of the resonant circuit. This method is easy to implement and makes the resonance stable. Using the non-short circuit method, the converter can operate at higher DC link voltages as 500 [V] without problems.

Resonant converter modulator:

Three modulators are described and investigated, Sigma Delta Modulator, SDM /1/,/5/, Space Vector Sigma Delta Modulator, SVSDM /5/,/15/,/16/ and Stator Flux oriented Discrete Pulse Modulator, SFDPM.

The modulators are controlled either by voltage or flux references. The modulators only need an internal feedback loop. The voltage SDM, SVSDM and the flux controlled modulator SFDPM is compared by a simulation study.

The SFDPM is not seen reported in any paper and is considered new. It is shown that the flux controlled modulator, performs better than the voltage controlled sigma delta modulator.

The THD analysis of the phase current shows that the SFDMP compared with SVSDM produce a current with 20% lower THD. The SFDMP compared with SDM produce a current with 40% lower THD.

The torque ripple shows that the SFDMP compared with SVSDM produce a torque with 10% lower ripple. The SFDMP compared with SDM produce a torque with 70% lower ripple.

The performance of SFDMP and SVSDM is quit close and the implementation of SVSDM is simpler. Therefore SVSDM is selected for implementation in the realized resonant converter.

Resonant VPC control:

Third stage is realization of the Voltage Peak Control (VPC) principle. The idea of the principle is to control the resonant link voltage peak by proper switching of the inverter switches. Mathematical is the VPC strategy explained from phase plane plots. The phase plane plot makes it possible to obtain an overview of the differential equation solutions that describe the resonant link current and voltage. Looking at the phase plane plots, it is seen that the link voltage peak can be controlled by changing the inverter switch state before the zero level of the resonant voltage is reached.

In the first report a control equation is derived using idealized condition. Including real life conditions, the link voltage peak control is not efficient using the simple VPC equation. In this report link component losses and many other factors are included. Including all the factors, it is not possible to expressing the VPC in one simple analytical equation. The calculation effort is now quite huge and it is not possible to do on-line with the used digital signal processor. An off-line calculated look up table is generated. The VPC control is negative affected by the short-circuit method. Significant better results were obtained using the non-short circuit method.

Measurements on the RDCL and RDCLVPC converter:

A 5 [kW] Resonant DC Link Voltage Peak Controlled, RDCLVPC converter and the RDCL converter have been realized and tested. The DC link voltages were 300 [V] and 500 [V]. It is shown that the converters are able to operating stable at both voltages. This is due to the proposed

non-short circuit method. The test period lasted more than one week and the converter was running 5-10 hours every day. Based on the laboratory experience with the converters there is found no reason that the resonant converters should not operate at higher DC link voltages as 600 [V].

The voltage peak strategy, is tested and proven to be able to limit the resonant voltage peaks below 2.1 times the DC link voltage.

Limiting the resonant voltage peaks using VPC introduces inverter switch turn off at non zero voltages. This increases the inverter switch losses but at the same time the resonant link current stress is reduced. Measurements show that the total inverter switch loss and resonant link loss are almost the same comparing the RDCL and RDCLVPC converter.

A converter efficiency of 96.4 [%] at P_{out} = 2.6 [kW] using a DC link voltage of 300 [V] was measured and a converter efficiency of 97.2 [%] at P_{out} = 3.8 [kW] was measured using a DC link voltage of 500 [V].

During the development of the resonant converter many fault situations arrived, but none of them was able to destroy the inverter switches rated 1700 [V] and 30 [A].This is due to the current slope limitation of the resonant inductor. The resonant converter is also in this way robust.

Test with a 300 [m] long cable and an induction motor load was carried out at a DC link voltage of 300 [V]. The VPC and long cable condition were not tested. The cable does not generate high frequency current oscillations known from PWM-VSI converters but a super imposed sinusoidal current with the frequency of the resonant circuit.

It is concluded that the RDCLVPC and the RDCL converter first described by analysis and simulation have been successfully tested in the laboratory.

7.2 Conclusion

Aim of the report:

In this report analysis, realization of the RDCL and RDCLVPC converter are described, and experimental tests are carried out.

The main aim was to realize the RDCLVPC and the RDCL converters to get practical experience and secondly measure the performance.

There were several sub-aims of the report:

1: In the first report the link voltage peak control, VPC, principle is derived using highly idealized conditions. To increase the efficiency of the VPC control the influence of the converter loss elements and the DC link current changes is incorporated in this report.

2: To build a converter which is able to operate stable at higher DC link voltages as 500 [V].

3: Measuring the efficiency of the RDCLVPC converter.

4: Test the resonant converter ability to drive a long cable and a motor.

The resonant converters are realized and their performances concerning switching losses and dv/dt are tested. The converters have a high switching frequency and a high efficiency. To show

the benefit of low dv/dt, the RDCL converter was loaded successfully with a 300 [m] long cable and induction machine. Both converters are able of operating stable at a DC link voltage of 500 [V].

It is concluded that the aim of the report is fulfilled.

During the work with the resonant converter's three ideas are proposed, which are considered new.

1: A principle that controls the resonant link voltage peaks using the inverter switches and by that avoiding additional clamp circuit components. The principle is named Voltage Peak Control, VPC.

2: A modulator that generates low current harmonics and low torque ripple. The modulator is named Stator Flux oriented Discrete Pulse Modulator, SFDPM.

3: A method that make the resonance of the resonant circuit robust. This method is named 'non-short circuit' method.

7.3 Future work

The following topics are considered interesting to work further on:

- Protection against load and line faults.

- Measurement of sound pressure level from an induction machine when it is fed by the resonant converter. Work should be put in an investigation of a particular application eg. a pump system.

- In this work no particular effort is made to optimize the resonant converter efficiency. Particular the design of the resonant inductor/transformer could be optimized.

- Designers of switches could concentrate of developing a switch particular suited for softswitching. The properties should be low delay, very fast switching and low on state voltage.

- The resonant converter doubles the output voltage amplitude compared with the PWM-VSI. The effect on standard induction machine insulation must be investigated.

Before the resonant converter is going into production, cost considerations must also be made. This is of major importance, and is clear that the cost of the resonant circuit is a disadvantage. On the other hand the resonant circuit eliminates the need of snubber circuits, and properly reduces the EMI input/output filter size required in the PWM-VSI.

Bibliography

/1/ "The Resonant DC-Link Inverter - A New Concept in Static Power Conversion" IEEE-IAS 1986, Conference Record, pp. 648-655
D.M. Divan.

/2/ "The design and implementation of a passsive clamp resonant dc link inverter for high power applications"
Ph.D thesis, University of Wisconsin-Madision, 1992
G. L. Skibinski.

/3/ "Topology, Analysis and Control of a Resonant DC Link Power Converter"
Ph.D thesis, University of Wisconsin-Madision, 1992
V. G. Vekataramanan.

/4/ "A High Frequency Resonant DC Link Inverter Using IGBTs"
IPEC 1990, pp. 152-160
A. Mertens, D.M. Divan.

/5/ "Preformance Characterization of A New Discrete Pulse Modulated Current Regulator"
IEEE-IAS Annual Meeting 1988, pp. 395-405
T. G. Habetler, D.M. Divan.

/6/ "Analyse des Oberschwingungsverhaltens von taktsynchronen Delta Modulations-verfahren zur Steuerung von Pulsstromrichtern bei hoher Taktzahl"
Ph.D. thesis, 1992, University of Aachen, ISBN 3-86073-069-X
A. Mertens.

/7/ "A Resonant Link Brushless D.C. Drive"
ICEM 1992, pp. 254-258
D.A. Stone, P.H.Mellor, N.Schofield.

/8/ "Efficient Snubbers for Voltage Source GTO Inverters"
IEEE PESC Rec. 1990, pp. 20-27
W. McMurray.

/9/ "An Improved High Frequency Resonant DC Link Inverter For Induction Motor Drives"
IEEE-IAS Rcc. 1988, pp. 742-748
J.-S. Lai, B.K. Bose.

/10/ "Link voltage Peak Control of Parallel Resonant Converter by Control of the Converter Switching Instant"
Proceed. of IEEE PESC 1995, Vol. 2, 1995, pp. 929-935
S. Munk-Nielsen, F. Blaabjerg, J. K. Pedersen.

/11/ "A new Parallel Converter Link voltage Control"
Proceed. of PEDES'96, Vol.1, 1996, pp.27-32
S. Munk-Nielsen, F. Blaabjerg, J. K. Pedersen, F. F. Protiwa, O. Apeldoorn.

/12/ "Resonant Converters - Analysis and Simulation"
1. part of Ph.D thesis, Aalborg University 1996
S. Munk-Nielsen.

/13/ "Verificering af nyt styreprincip for en resonans DC-link inverter"
M.Sc project 1995, Aalborg University 1995
Sigurdur Sigurjónsson, Klaus Sloth Jensen.

/14/ "A Control Technique to Eliminate Irregular Current and Voltage Pulses in Resonant DC Link Power Conmverters"
Proceed. of PESC 1994, pp. 671-676
R.C. Castanheira, B.J.C. Fo, F.R. Menezes, P.D. Garcia, and A.F.Moreira.

/15/ "Performance Characterization of a New Discrete Pulse Modulated Current Regulator "
IEEE PESC 1987, pp. 271-278
T.G. Habetler, D.M. Divan.

/16/ "Performance Analysis of Three Phase Inverters controlled by Synchronous Delta-Modulation Sytstems"
IEEE Industry Applications JULY/AUGUST 1994, pp. 779-788, Vol. 30, Nr. 4
Axel Mertens.

/17/ "Statorflux-orienteret asynkron vektor-modulering til trefasede AC-drevsystemer"
P. Thøgersen, Ph.d thesis in Danish.

/18/ "The Use of Harmonic Distorsion to Increase the Output Voltage of a Three-Phase PWM-inverter"
p. 1224 - 1228 IEEE Transactions On Industry Applications, Vol IA-21, NO. 1. JAN/FEB 1985
J. A. Houldsworth, D. A. Grant.

/19/ "Analysis and realization of a pulse width modulator based on voltage space vectors"
IEEE-IAS Conf. Rec., 1986, pp. 244-251
H. Van Der Broeck, H.Skudelny, G. Stanke.

/20/ "The Field Orientation Principle in Control of Induction Motors"
Book publised at Kluwer academic publishers, 1994, ISBN 0-7923-9420-8
A. M. Trzynadlowski.

/21/ "Hastighedsservo"
9.th semester report 1990, Aalborg University
L.S. Pedersen, A. Rebsdorf, B. Rønn, J. Jensen, S.Munk-Nielsen.

/22/ "Automatic Control of Converter-Fed Drives"
Book publised 1994, ISBN 0-444-98660-X
M.P. Kaźmierkowski, H. Tunia.

/23/ "Stromrichtergespeiste Drehfeldmaschinen"
Book publised 1980, Springer Verlag, ISBN 3-211-81565-1
H. Kleinrath.

/24/ "Advanced Engineering Mathematics"
Book publised 1979, Fourth Edition J.Wiley & Sons, ISBN 0-471-04271-4
E. Kreyszig.

/25/ "Static Power Conversion Method and Apparatus Having Essentially Zero Switching Losses and Clamped Voltage Levels"
US-patent, Sept. 5, 1989
D.M Divan.

/26/ "Power Electronics"
Book publised 1985, Chalmers University of Technology, No ISBN
K. Thorborg.

/27/ "Development and Control of A Resonant DC-Link Converter For Multiple Motor Drives"
Ph.D. thesis, 1992, University of Trondheim, ISBN 82-7119-359-7
A. Petterteig.

/28/ "Resonant Power Converters"
Book publised 1995, ISBN 0-471-04706-6
M. Kazimerczuk.

/29/ "Stator Flux Orientated Asynchrous Vector Modualtion for AC-drives"
PESC 1990, pp. 641-648
P. Thøgersen , J.K. Pedersen.

App. A

Resonant circuit equations for a lossy resonant circuit

In this appendix is derived an equation of resonant inductor current i_L and link voltage v_{do} of the circuit shown Fig A.1. The losses are concentrated in R, the value of R is determined by a measurement of the Q-factor. The resonant circuit is loaded by a current source, i_{do}, that serves as an equivalent of the inverter switches and load. The inverter switches are assumed loss less and the load current shape are limited to a step with a superimposed ramp. The current shape i_{do} is given by (A.3).

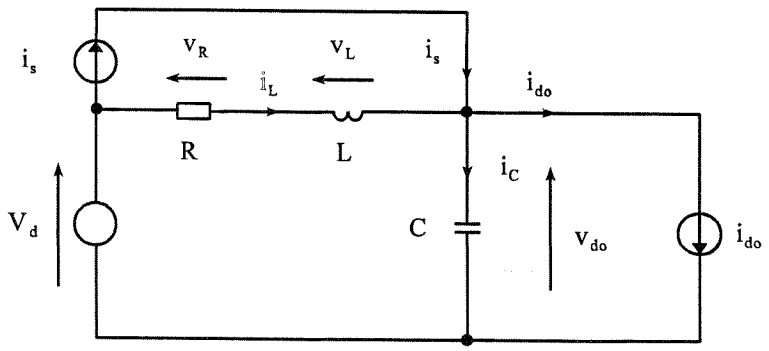

Fig. A.1 Equivalent model of RDCLVPC converter

$$0 = V_d - v_R - v_L - v_{do} \quad \textbf{(A.1)}$$

$$0 = i_L - i_C - i_{do} + i_s \quad \textbf{(A.2)}$$

$$i_{do} = m + kt \quad \textbf{(A.3)}$$

$$i_s = \hat{i}_s \cos(\beta t) \quad \textbf{(A.4)}$$

$$i_C = i_L - m - kt + i_s \quad \textbf{(A.5)}$$

The elements in equation (A.1) are shown in Table A.1, as function of time and with their Laplace transformation. In (A.6) is the Laplacian of I_L shown

f(t)	F(s) = $\mathcal{F}$(f)
$v_L = L\frac{di_L}{dt}$	$V_L = sL I_L - L i_{L(0)}$
$v_{do} = \frac{1}{C}\int i_L - i_{do} + i_s\, dt + v_{do(0)}$	$V_{do} = \frac{1}{sC}(I_L - \frac{m}{s} - \frac{k}{s^2} + \hat{i}_s \frac{s}{s^2+\beta^2}) + \frac{v_{do(0)}}{s}$
$v_R = R i_L$	$V_R = R I_L$
V_d	$\frac{V_d}{s}$

Table A.1

The laplace transform of (A1) is

$$0 = \frac{V_d}{s} - RI_L - sLI_L + Li_{L(0)} - \frac{1}{sC}(I_L - \frac{m}{s} - \frac{k}{s^2} + \hat{i}_s \frac{s}{s^2+\beta^2}) + \frac{v_{do(0)}}{s}) - \frac{v_{do(0)}}{s} \qquad \textbf{(A.6)}$$

Then I_L is

$$I_L = \frac{V_d - v_{do(0)}}{L}\frac{1}{(s+\alpha)^2+\beta^2} + i_{L(0)}\frac{s}{(s+\alpha)^2+\beta^2} + m\omega^2\frac{1}{s((s+\alpha)^2+\beta^2)} + k\omega^2\frac{1}{s^2((s+\alpha)^2+\beta^2)} - \hat{i}_s s\omega^2\frac{1}{(s^2+\beta^2)((s+\alpha)^2+\beta^2)} \qquad \textbf{(A.7)}$$

Resonant current i_L is found using Table A.2 Assumed $R<2Z$

$F(s) = \mathcal{F}(f)$	$f(t)$
$\frac{V_d - v_{do(0)}}{L} \frac{1}{(s+\alpha)^2 + \beta^2}$	$\frac{V_d - v_{do(0)}}{L\beta} e^{-\alpha t} \sin \beta t$
$i_{L(0)} \frac{s}{(s+\alpha)^2 + \beta^2}$	$i_{L(0)} e^{-\alpha t} (\cos \beta t - \frac{\alpha}{\beta} \sin \beta t)$
$m \omega^2 \frac{1}{s((s+\alpha)^2 + \beta^2)}$	$m(1 - e^{-\alpha t}(\cos \beta t + \frac{\alpha}{\beta} \sin \beta t))$
$k \omega^2 \frac{1}{s^2((s+\alpha)^2 + \beta^2)}$	$kt - \frac{2\alpha k}{\omega^2} + \frac{k}{\beta} e^{-\alpha t} \cos(\beta t + \phi)$
$\hat{i}_s \omega s \frac{1}{(s^2 + \beta^2)((s+\alpha)^2 + \beta^2)}$	$\hat{i}_s \frac{((\frac{\alpha^2}{\beta^2} + 2) e^{-\alpha t} - 2) \sin(\beta t) + (\frac{\alpha}{\beta}(e^{-\alpha t} - 1)) \cos(\beta t)}{\frac{\alpha}{\beta}((\frac{\alpha}{\beta})^2 + 4))}$

Table A.2

$$
\begin{aligned}
i_L = {} & \frac{V_d - v_{do(0)}}{L\beta} e^{-\alpha t} \sin \beta t + i_{L(0)} e^{-\alpha t} (\cos \beta t - \frac{\alpha}{\beta} \sin \beta t) + m(1 - e^{-\alpha t}(\cos \beta t + \frac{\alpha}{\beta} \sin \beta t)) \\
& + kt - \frac{2\alpha k}{\omega^2} + \frac{k}{\beta} e^{-\alpha t} \cos(\beta t + \phi) \\
& - \hat{i}_s \frac{((\frac{\alpha^2}{\beta^2} + 2) e^{-\alpha t} - 2) \sin(\beta t) + (\frac{\alpha}{\beta}(e^{-\alpha t} - 1)) \cos(\beta t)}{\frac{\alpha}{\beta}((\frac{\alpha}{\beta})^2 + 4))}
\end{aligned}
\qquad \textbf{(A.8)}
$$

Constants used are given by

Constant name	Constant
α	$\frac{R}{2L}$
ω	$\frac{1}{\sqrt{LC}}$
β	$\sqrt{\omega^2 - \alpha^2}$
ϕ	$\tan^{-1}(\frac{\beta^2 - \alpha^2}{2\alpha\beta})$

Table A.3

A link voltage equation is derived. Equation (A.2) is used, the time functions of i_L, i_C,i_s, and i_{do} are shown in Table A.4 left side and in the right side are the Laplace transformation of the functions shown.

f(t)	$F(s) = \mathcal{F}(f)$
$i_L = \frac{V_d}{R} - \frac{L}{R}\frac{di}{dt} - \frac{V_{do}}{R}$	$I_L = \frac{1}{sL+R}(\frac{V_d}{s} + Li_{L(0)} - V_{do})$
$i_C = C\frac{dv_{do}}{dt}$	$I_C = sCV_{do} - Cv_{do(0)}$
$i_{do} = m + kt$	$I_{do} = \frac{m}{s} + \frac{k}{s^2}$
$i_s = \hat{i}_s \cos(\beta t)$	$i_s = \hat{i}_s \frac{s}{s^2 + \beta^2}$

Table A.4

$$0 = \frac{1}{sL+R}\left(\frac{V_d}{s} + Li_{L(0)} - V_{do}\right) - sCV_{do} + Cv_{C(0)} - \frac{m}{s} - \frac{k}{s^2} + \hat{i}_s \frac{s}{s^2+\beta^2} \qquad \textbf{(A.9)}$$

$$\begin{aligned} V_{do} = {} & \frac{(L\omega^2(i_{L(0)} - m) + RC\omega^2 v_{do(0)})}{(s+\alpha)^2+\beta^2} + \frac{v_{do(0)}s}{(s+\alpha)^2+\beta^2} \\ & + \frac{(V_d - mR - kL)\omega^2}{s((s+\alpha)^2+\beta^2)} - \frac{kR\omega^2}{s^2((s+\alpha)^2+\beta^2)} \\ & + \frac{\hat{i}_2\omega^2 L}{s^2+\beta^2} - \frac{\hat{i}_2\omega^2(\omega^2 L - Rs)}{(s+\alpha)^2+\omega^2} \end{aligned} \qquad \textbf{(A.10)}$$

$F(s) = \mathcal{F}(f)$	$f(t)$
$(L\omega^2(i_{L(0)} - m) + RC\omega^2 v_{do(0)})\frac{1}{(s+\alpha)^2+\beta^2}$	$(L\omega^2(i_{L(0)} - m) + RC\omega^2 v_{do(0)})\frac{1}{\beta}e^{-\alpha t}\sin\beta t$
$v_{do(0)}\frac{s}{(s+\alpha)^2+\beta^2}$	$v_{do(0)}e^{-\alpha t}(\cos\beta t - \frac{\alpha}{\beta}\sin\beta t)$
$(V_d - mR - kL)\omega^2\frac{1}{s((s+\alpha)^2+\beta^2)}$	$(V_d - mR - kL)\omega^2\frac{1}{s((s+\alpha)^2+\beta^2)}$
$(V_d - mR - kL)\omega^2\frac{1}{s((s+\alpha)^2+\beta^2)}$	$kRt - kR\frac{2\alpha}{\omega^2} + \frac{kR}{\beta}e^{-\alpha t}\cos(\beta t + \phi)$
$\frac{\hat{i}_2\omega^2 L}{s^2+\beta^2} - \frac{\hat{i}_2\omega^2(\omega^2 L - Rs)}{(s+\alpha)^2+\omega^2}$	$\hat{i}_s\omega\frac{1}{2}((L+tR)\sin(\omega t) + tZ\cos(\omega t))^*$ *assumed $R \ll Z$

$$
\begin{aligned}
v_{do} = & (L\omega^2(i_{L(0)} - m) + RC\omega^2 v_{do(0)})\frac{1}{\beta}e^{-\alpha t}\sin\beta t + v_{do(0)}e^{-\alpha t}(\cos\beta t - \frac{\alpha}{\beta}\sin\beta t) \\
& + (V_d - mR - kL)(1 - e^{-\alpha t}(\cos\beta t + \frac{\alpha}{\beta}\sin\beta t)) \\
& - kRt + kR\frac{2\alpha}{\omega^2} - \frac{kR}{\beta}e^{-\alpha t}\cos(\beta t + \phi) \\
& + \hat{i}_s\,\omega\frac{1}{2}((L + tR)\sin(\omega t) + tZ\cos(\omega t))
\end{aligned}
\qquad \textbf{(A.11)}
$$

App. B

Induction machine data and equations

Electrical and mechanical parameters for the induction machine used in the testing of the resonant converter is shown. The machine equations used in the simulation program is shown.

The load used is an induction machine, MT 100 Lb 28-4 from ABB. Nominal data are:

• Phase current	I_{NO}	= 6.9 [A]
• Phase-phase voltage	V_{NO}	= 400 [V]
• Output power	P_{NO}	= 3.0 [kW] with load cos(ϕ)=0.8
• Speed	n	= 1430 [rmp]

Measured electrical and mechinical parameters /21/

• stator resistance	r_s	= 1.8 [Ω]
• rotor resistance	r_r	= 1.8 [Ω]
• stator lekage inductance	l_s	= 165 [mH]
• rotor lekage inductance	l_r	= 172 [mH]
• Magnetizing inductance	l_h	= 158 [mH]
• stator lekage inductance	l_{ss}	= 7 [mH]
• rotor lekage inductance	l_{rs}	= 14 [mH]
• Inertia	J_{ASM}	= 9.6e-3 [kgm^2]
• pole pair	p	= 2

Machine equations are from /17/ they are originally described in /23/.

System matrixes and equations for electrical machine model in the fixed stator coordinate system.

Resistance matrix

$$R_s = \begin{bmatrix} r_s & 0 & 0 & 0 \\ 0 & r_s & 0 & 0 \\ 0 & 0 & r_s & 0 \\ 0 & 0 & 0 & r_s \end{bmatrix} \quad \textbf{(B.1)}$$

Inductance matrix nr. 1

$$L_1 = \begin{bmatrix} l_s & 0 & l_h & 0 \\ 0 & l_s & 0 & l_h \\ l_h & 0 & l_r & 0 \\ 0 & l_h & 0 & l_r \end{bmatrix} \quad \textbf{(B.2)}$$

Inductance matrix nr. 2

$$L_2 = \begin{bmatrix} 0 & 0 & 0 & 0 \\ 0 & 0 & 0 & 0 \\ 0 & l_h & 0 & l_r \\ -l_h & 0 & -l_r & 0 \end{bmatrix} \quad \textbf{(B.3)}$$

Unity matrix

$$E = \begin{bmatrix} 1 & 1 & 1 & 1 \\ 1 & 1 & 1 & 1 \\ 1 & 1 & 1 & 1 \\ 1 & 1 & 1 & 1 \end{bmatrix} \quad \textbf{(B.4)}$$

Input voltage vector

$$u = \begin{bmatrix} \text{real}(V_{inv}) \\ \text{imag}(V_{inv}) \\ 0 \\ 0 \end{bmatrix} \quad \textbf{(B.5)}$$

where:

V_{inv} : stator voltage, the rotor voltages are zero.

Current vector:

$$x = \begin{bmatrix} \text{real}(I_s) \\ \text{imag}(I_s) \\ \text{real}(I_r) \\ \text{imag}(I_r) \end{bmatrix} \quad \textbf{(B.6)}$$

where:

I_s : Stator current
I_r : Rotor current

Electrical machine equations using bilinear transformation /17/:

$$A = -(-L_1^{-1}R + L_1^{-1}\omega p L_2) \tag{B.7}$$

$$B = -L_1^{-1} \tag{B.8}$$

$$x = (E - \frac{h}{2}A)^{-1}((E + \frac{h}{2}A)x + \frac{h}{2}B(u + u_{old})) \tag{B.9}$$

where:

ω : synchronous rotor speed
h : simulation time step

update voltage:

$$u_{old} = u \tag{B.10}$$

Electrical torque calculation:

$$M_{el} = -\frac{3}{2}l_h(\text{real}(i_s)\text{imag}(i_r) - \text{imag}(i_s)\text{real}(i_r)) \tag{B.11}$$

Rotor speed calculation:

$$M_{asm} = M_{el} - M_{load} \tag{B.12}$$

$$\omega = \omega + \frac{1}{J}\frac{h}{2}(M_{asm} + M_{asm\_old}) \tag{B.13}$$

update torque:

$$M_{asm\_old} = M_{asm} \tag{B.14}$$

In the simulation program equation B.7 to B.14 is a single function, called at every simulation time step. Two other integration methods were tested, the Runge-Kutta /24/ and Forward Euler /24/ method. The Runge-Kutta method is more complex and provide high accuracy at relative

large time steps, h.

The time step, h was determined by the resonant frequency. About 10 to 20 steps during every resonant period is necessary. The Runge-Kutta method is therefore forced to use small time steps and is not efficient. The opposite, was the case of the Forward Euler the time step was not small enough to obtain sufficient accuracy. A bilinear/24/ integration method is a reasonable choice, it is accurate and is not as complex as the Runge-Kutta integration method.

Danish summary

Dette er et referat af den anden af to rapporter, som udgør Ph.D projektet. Den valgte konverter fra første rapport 'Resonant DC Link Voltage Peak Control', RDCLVPC konverter realiseres i denne nummer to rapport. Baggrunden for valget af RDCLVPC er ønsket om høj virkningsgrad, lav dv/dt i konverterspænding, simpelt effektkredsløb og mulighed for at kontrollere mellemkreds-peakspændingen. RDCLVPC er en modificeret 'Resonant DC Link', RDCL konverter, hvor 'Voltage Peak Control', VPC kontrollerer mellemkreds-peakspændingen.

Da den ene konverter er en mindre modifikation af den anden, beskrives realiseringen af begge konvertere i denne rapport.

I løbet af realiseringen af resonanskonverterne opstod der behov for re-design. Tilsyneladende gode ideer viste sig ved realiseringen i laboratoriet at være uhensigtsmæssige. Et væsentligt praktisk problem med resonanskonverterne er at opretholde den resonanssvingning, der giver 'zero voltage switching' ZVS for effekttransistorerne. Den i forvejen kendte metode opretholder resonansen ved at tænde for konvertertransistorerne under ZVS tilstanden således, at konverterbroen er kortsluttet nogle få mikro sekunder. Under kortslutningen oplagres der energi i resonanskredsen, denne energi sikrer at resonansen opretholdes. Kortslutningsmetoden er uhensigtsmæssig fordi den nødvendiggør, at effekttransistorerene i et meget kort tidsinterval skal tænde og slukke. Tidsintervallet er væsentligt kortere end selve resonansperioden. Det ønskede kortslutningstidsinterval er i praksis kortere end den korteste tid transistoren kan nå at tænde og slukke på. Dette er uheldigt og betyder forøget tab, desuden er det meget svært at realisere en konverter, som har en mellemkredsspænding højere end 300 [V]. En ny metode som ikke involverer en kortslutning af konverterbroen er foreslået i denne rapport. Metoden kaldes 'ikke kortslutnings' metoden og påvises ved laboratorieforsøg at være meget fordelagtig at bruge som følge af simpel realisereing og en robust konverter driftstilstand ved spændinger også over 300 [V], metoden er testet ved 500 [V].

Der foretages en analyse af tre forskellige modulationstyper, som anvendes ved åben loop kontrol af den asynkronmaskine, der er tilkoblet frekvensomformeren, en ny modulator foreslås og sammenlignes med de to andere. Den har en bedre performance mht. strømripple og momentripple, men den er mere komplex at realisere.

Den foreslåede VPC metode i første rapport, realiseres efter yderligere analyse som inkluderer tabselementer og andre faktorer. Målinger viser at VPC er i stand til at kontrollere mellemkreds-peakspændingen inden for 2.1 gange mellemkredsspændingen. Dette er tæt på den teoretiske værdi på to gange mellemkredsspændingen.

En 5 [kW] resonant RDCLVPC og RDCL konververter er realiseret og testet. Mellemkredsspændingen var 300 [V] og 500 [V], konverteren arbejder stabilt ved begge spændinger. Test perioden varede mere end en uge. Der blev målt en konverter virkningsgrad på 96.4 [%] ved P_{out} = 2.6 [kW] og mellemkredsspændingen lig 300 [V]. Med en mellemkredsspænding på 500 [V] blev virkningsgraden målt til 97.2 [%] ved P_{out} = 3.8 [kW].

En test med 300 [m] kabel og en asynkronmaskine som last blev udført med succes. Under laboratoriearbejdet blev der ikke ødelagt en eneste effekttransistor, dette skyldes den dæmpning af strømmen resonansinduktoren giver ved fejl.

Det konkluderes at RDCL og RDCLVPC konverterne først beskrevet ved analyse og simulation er sucesfuldt testet i laboratoriet.

Nomenclature

α	$R/(2L_{res})$	[Ω/H]
α_s	phase shift of two link currents eq. i_c and $-i_c$	[°]
ΔI_{Lres}	initial resonant inductor current to overcome losses in res. cir.	[A]
ΔV_{do}	turn-off voltage calcultated by the VPC algorithm	[V]
ΔV_{max}	maximum allowed turn-off voltage of IGBT	[V]
ω_{res}	angular resonant frequency $1/(\sqrt{(LresCres)})$	[rad/s]
a	complex operator $\exp(j2\pi/3)$	[ ]
C_{res}	resonant circuit capacitor	[F]
$\cos(\phi)$	phase displacement of output voltage and current	[rad]
DI	current change during a resonant period	[A]
f_{res}	resonant frequency $1/(2\pi\sqrt{(L_{res}C_{res})})$	[Hz]
g_a,g_b,g_c	gate signals to the inverter branches	[ ]
k	current change rate	[A/s]
m	equivalent DC load current source	[A]
M_{el}	electrical torque	[Nm]
M	park's transformation vector, defined page 34	[ ]
L_{res}	resonant circuit inductor	[µH]
i_a,i_b	phase currents	[A]
i_o	DC side inverter current calculated from phase current and switch vector.	[A]
i_{do}	resonant link current	[A]
I_{do}	average DC link current	[A]
i_{Lres}	resonant inductor current	[A]
$i_{Lres(0)}$	initial resonant inductor current	[A]
I_{NO}	converter output phase current	[A]
Q	quality factor, Z_{res}/R	[ ]
R	equivalent serial resistor of resonant circuit	[Ω]
S	switch vector	[ ]
T	measured mechanical torque	[Nm]
t_{delay}	time delay in low voltage electronic and inverter IGBT	[s]
T_{res}	resonant periode time $1/f_{res}$	[s]
V_d	DC link voltage	[V]
v_{ax},v_{bx},v_{cx}	branch voltage(x=0) or (x=N) or phase voltages(x=n)	[V]
v_{do}	resonant link output voltage, equal to resonant capacitor voltage	[V]
$v_{do(0)}$	initial resonant capacitor voltage	[V]
V_{NO}	converter output link voltage	[V]
$\mathbf{v_{ave}}$	average output voltage vector, defined page 35	[V]
$\mathbf{v_s}$	complex voltage vector, defined page 34	[V]
$\mathbf{v_n}$	complex voltage vector, defined page 34	[V]
$\mathbf{v_0}$	complex voltage vector, defined page 34	[V]
$\mathbf{v_N}$	complex voltage vector, defined page 34	[V]
VPC	Voltage Peak Control	
Z_{res}	resonant impedance $\sqrt{(L_{res}/C_{res})}$	[Ω]
ZVSI	control signal generated when v_{do} reach zero voltage	[ ]

List of publications

1. Frede Blaabjerg, John K. Pedersen, Johnny W. Jensen, Stig Munk-Nielsen."A Compact High Performance 16-Bit Microprocessor Controlled AC-servodrive". Symposium on Industrial Electronics IEEE. 1992. pp. 146-150.

2. Frede Blaabjerg, Ulrik Jaeger, Stig Munk-Nielsen, John K. Pedersen. "Comparison of NPT and PT IGBT-devices for Hard Switching Applications". Proceed. of IAS'94/IEEE. 1994, Vol. 2, pp. 1174-1181.

3. Frede Blaabjerg, Ulrik Jaeger, Stig Munk-Nielsen, John K. Pedersen. "Power Losses in PWM-VSI Inverter Using NPT or PT IGBT Devices". Proceed. of PESC '94. 1994, Vol. 1, pp. 434-441.

4. Frede Blaabjerg, Ulrik Jaeger, Stig Munk-Nielsen, John K. Pedersen. "Power Losses and Short Circuit behaviour of PT and NPT IGBT". Proceed. of PEMC '94. 1994. Vol. 2, pp. 799-807.

5. Frede Blaabjerg, Stig Munk-Nielsen, John K. Pedersen. "An Advanced Measurement System for Verification of Models and Data-sheets". Proceed. IEEE 1994, PELS Workshop on Computers in Power Electronics. 1994, pp. 234-239.

6. Stig Munk-Nielsen, Frede Blaabjerg, John K. Pedersen. "Link voltage Peak Control of Parallel Resonant Converter by Control of the Converter Switching Instant". Proceed. of PESC'95, Vol. 2, 1995, pp. 929-935.

7. Frede Blaabjerg, Ulrik Jaeger, Stig Munk-Nielsen, John K. Pedersen. "Power Losses in PWM-VSI Inverter Using NPT or PT IGBT Devices". IEEE Trans. on Power Electronics, Vol. 10, No. 3, May 1995, pp. 358-367.

8. Stig Munk-Nielsen, Frede Blaabjerg, John K. Pedersen, Franz F. Protiwa, Oscar Apeldoorn. "A new Parallel Converter Link voltage Control". Proceed. of PEDES '96. Vol. 1, 1996, pp.27-32.

9. Stig Munk-Nielsen, Frede Blaabjerg, John K. Pedersen. "Link voltage Peak Control of Parallel Resonant Converter by Control of the Converter Switching Instant". IEEE Trans. on Power Electronics.

10. Stig Munk-Nielsen, Frede Blaabjerg, John K.Pedersen. "Ny frekvensomformer reducerer stress på motoren". Elteknik nr.8, 1996, pp. 12-15. (In Danish)

11. Stig Munk-Nielsen, Frede Blaabjerg, John K.Pedersen. "An Efficiency Study of a Robust and Simple Three Phase Resonant Converter". EPE'97.

12. Stig Munk-Nielsen, Frede Blaabjerg, John K.Pedersen. "A New Robust and Simple Three Phase Resonant Converter". IAS'97.